DOTTORATO DI RICERCA
IN INGEGNERIA CIVILE E
INDUSTRIALE

University of Calabria

DIMEG –Department of Mechanical, Energy and Management Engineering

Ph.D.Thesis

XXXVI Cycle

Ph.D.in Civil and Industrial Engineering

Materials, Processing and Assessment for Bioengineering Applications

Candidate

Michela Sanguedolce

Michela
Sanguedolce
09.02.2024
09:11:46
GMT+00:00

Ph.D.Coordinator:

Prof. Domenico Mundo

Mundo
Domenico
12.02.2024
11:37:38
GMT+01:00

Supervisor:

Prof. Luigino Filice

LUIGINO FILICE
12.02.2024 10:04:24
GMT+00:00

TABLE OF CONTENTS

ABSTRACT (ITA)

Le leghe di titanio, in particolare la lega *Ti6Al4V*, sono correntemente lo "standard of care" per gli impianti ortopedici, in particolare la generalmente soddisfacente risposta biologica. Nonostante ciò, problemi quali l'insorgenza di infezioni, il cedimento dell'impianto a causa della scarsa osteointegrazione ed il fenomeno dello stress shielding sono frequenti. Inoltre, le infezioni legate agli impianti ortopedici risultano difficili da diagnosticare e, talvolta, le cure antibiotiche a livello sistemico sono poco efficaci. Alla luce di ciò, risulta essenziale la realizzazione di impianti dotati di proprietà antibatteriche a scopo di prevenire lo sviluppo di infezioni e della antibiotico-resistenza ma al contempo atti a promuovere l'integrazione con i tessuti circostanti, al fine di ridurre l'insorgenza delle chirurgie di revisione. Le interazioni biomateriale-tessuto all'interfaccia hanno un ruolo chiave nel buon funzionamento degli impianti: non solo influenzano la connessione con i tessuti circostanti ma anche il comportamento di eventuali batteri patogeni e la formazione di biofilm. Essendo la relazione fra composizione del biomateriale, design dell'impianto e risposta biologica all'interno del corpo umano molto complessa, predire la buona riuscita dell'impianto nel breve e lungo termine non risulta al momento fattibile. I metodi di analisi *in vitro* sono di rilievo in questo campo ma hanno numerose limitazioni, inclusa l'assenza di una risposta immunitaria, presente nelle condizioni *in vivo*. Ciò porta quindi ad una maggiore spinta verso lo sviluppo e miglioramento di modelli predittivi. Il focus del presente lavoro è la modifica superficiale della lega di titanio *Ti6Al4V*, comunemente impiegata per la manifattura di fissatori ossei, al fine di affrontare i più frequenti problemi di scarsa osteointegrazione, infezione e sensibilizzazione ai metalli. Sono a tal fine esplorate le tecniche di modifica superficiale basate su meccanismi meccanici e termici, per la creazione di linee guida ai fini della regolazione della risposta biologica. Le tecniche studiate includono la sabbiatura, la fresatura, l'elettroerosione, la texturizzazione laser e la deposizione di rivestimenti. L'obiettivo è quello di approfondire l'effetto che le proprietà superficiali di un impianto hanno sulla risposta biologica con un approccio multi-livello: (i) modulazione dell'integrazione dell'impianto con il tessuto osseo circostante agendo direttamente sulle proprietà superficiali (i.e. rugosità, microstruttura, composizione chimica, angolo di contatto) impiegando tecniche di

deformazione e rimozione di materiale e studiando la risposta *in vitro* di cellule ossee; (ii) migliorare l'adesione di rivestimenti a base di biopolimeri, in particolare il chitosano, che ad oggi risulta essere di qualità insufficiente per l'applicazione, modificando le proprietà del rivestimento tramite diverse tecniche di deposizione, la composizione del rivestimento stesso e le proprietà del substrato; (iii) svolgere un'analisi preliminare degli effetti delle modifiche superficiali sulla risposta *in vitro* di batteri patogeni.

ABSTRACT (ENG)

Titanium alloys, in particular *Ti6Al4V*, are the current standard of care for orthopedic implants due to their good biological response. But issues such as infection susceptibility and implant failure due to poor osteointegration and stress shielding persist. Furthermore, orthopedic implant infections are challenging to detect and not always completely solved by systemic antibiotic delivery. Thus, it is essential to develop implants with antibacterial properties to prevent infections and antibiotic resistance due to frequent antibiotic delivery, while promoting integration with surrounding tissues and reducing the revision surgeries rate. Biomaterial-tissue interactions at the implant interface play a crucial role in its operation, influencing tissue attachment. The surface of an implant also affects how bacterial pathogens interact and create biofilms. The complexity of the relationship between biomaterial composition, device design, and biological response in living organisms presents challenges in predicting the outcome of the implant. *In vitro* methods are valuable but have limitations, necessitating the improvement of predictive models. The focus of this work is modifying the surface of the *Ti6Al4V* titanium alloy, commonly used in skeletal fixation devices. The goal is to address issues related to poor integration, infection, and metal sensitivity. Surface modification techniques, involving mechanical and thermal mechanisms, are herein explored to provide some guidelines for the prediction and modulation of performance. The studied techniques include grit blasting, milling, electrical discharge machining, laser texturing, and coating deposition. The aim is to deepen the influence of implant surface properties on its performance and biological response, with a multi-level approach: (i) modulate the integration of the implants with surrounding bone tissues by acting on surface properties (i.e. surface roughness, microstructure, chemistry, contact angle), employing material deformation and removal techniques, and studying the effects on *in vitro* bone cells response; (ii) improve the to date insufficient adhesion of biopolymer coatings made of chitosan by: tuning film properties through different deposition techniques, coating composition, and substrate properties; (iii) preliminary analyze the effect of surface modification techniques on *in vitro* bacterial response.

INTRODUCTION

"Wellbeing is a positive state experienced by individuals and societies. Similar to health, it is a resource for daily life and is determined by social, economic, and environmental conditions. Wellbeing encompasses quality of life, as well as the ability of people and societies to contribute to the world in accordance with a sense of meaning and purpose."

- World Health Organization

The importance of wellbeing as a holistic health-related state emerged in 1948 when the World Health Organization [1] expanded the definition of health from a physical state to a psycho-physical one. Since then, wellbeing has been considered part of the right to health that should be guaranteed to any human being.

The increasing number of orthopedic operations, demand for bone implants and prostheses, and hospitalizations and the surge in chronic disorders of longer living patients are one of the clear signs that population wellbeing is being negatively affected.

The majority of artificial joints and other implants sufficiently performs its functions and frequent technical and/or manufacturing modifications and new implant designs aim to improve function and longevity. But more than often, these devices, do not work as expected and might require early revision surgery, while others must be recalled and taken off the market immediately. The need for implantable devices is increasing day by day due to sudden changes in the age structure of the world population. Also, the percentage of the population comprising the age group of 60 years and above is increasing drastically, and elderly patients are more likely to suffer from bone fractures and bone implant revisions for poor osteointegration, and from a disease-related poor quality of life. Estimations by experts have predicted that the need for medical implants will grow by at least 39% by 2050 [2]. To counteract this trend, research has been encouraged to develop sustainable technologies to decrease devices and implants production costs, to enable treatments to minimize implant rejection and revisions and to maximize the therapeutic efficacy of medical treatments. Substantial research has been carried out over the last decade to develop medical implants for bone regeneration and healing body tissues [3]. Recent advancements in materials and manufacturing techniques are revolutionizing the

field of medical implants, offering the development of materials with an improved biological response, since those implants still fail due to infection and other body environment related conditions.

By carrying out a review of the research papers published on the manufacturing of biomedical implants [4], [5], the factors playing a role in their development and innovation were evaluated. The *WordCloud* plot in Figure 1 generated through a tool for bibliometric analysis (*Bibliometrix,* K-Sinth Srl, Italy [6]) schematically shows the most relevant keywords introduced by the authors (*Author's Keywords*) of research papers concerning the manufacturing of biomedical devices for bone and joints functionality restoration.

Over the years, the characterization of the features related to surface properties and bulk mechanical properties, fatigue and corrosion resistance and the bodily/biological response in contact with materials and prostheses (i.e., biocompatibility, osteointegration, etc.) - and how to modulate them - have drawn the greatest attention and have played a relevant role. They were followed by material choice (e.g., titanium alloys), manufacturing processes, and the final application (e.g. bone regeneration).

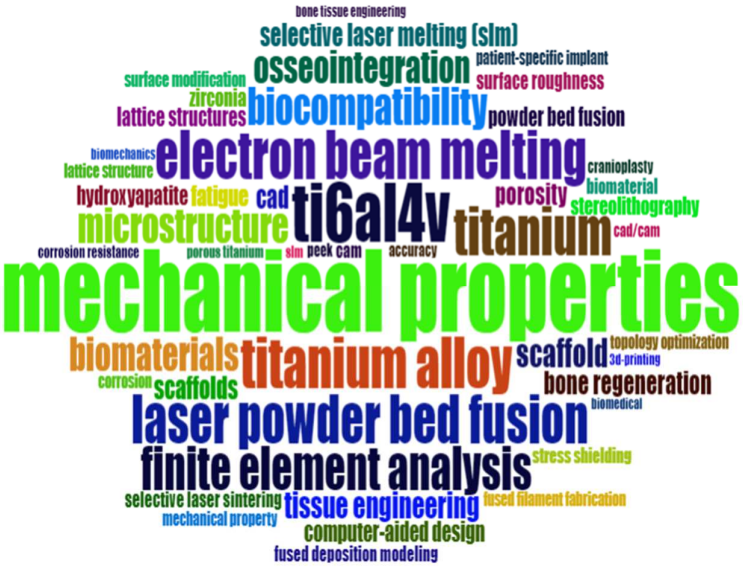

Figure 1. WordCloud mapping *Author's Keywords*. Images were generated through the Bibliometrix tool.

The bibliometric tool permitted the analysis of the literature cited in each paper and the extraction, not only of the *Author's Keywords*, but also the so-called *Keywords Plus*, that

is the keywords used in the reference papers, which express the research trends in a more objective fashion [7]. Figure 2 shows the network of relationships among the *Keywords Plus* which gives information about the relevance (i.e., the number of interconnections between the different topics), and the number of co-occurrences (i.e., how many times the considered topics/words appear together), with the bubble size being proportional to the occurrence of those words. A central position of the topic/word in the plot indicates the importance of the topic, and the tie density measures the topic's development in time.

The analysis confirms that design and fabrication are central research topics to the development of bone contacting implants and that the outcome of the design is mainly assessed by characterizing the mechanical and morphological properties of the implant/prosthesis and other performance indicators (i.e., porosity, surface roughness, corrosion behavior, fatigue etc.). A relevant role is also played by the *in vitro* and *in vivo* biological performance of the implant/prosthesis (i.e., its response to contact with tissues or cells, like cell differentiation) in terms of bone ingrowth, biocompatibility, and cell behavior. Taken together, the bibliometric analysis confirms the increasing relevance assumed by design parameters for biomedical implants like geometric features, mechanical properties, surface properties (e.g. roughness and microstructure), and the pursuit of their correlation to the clinical performance through *in vitro* and *in vivo* studies.

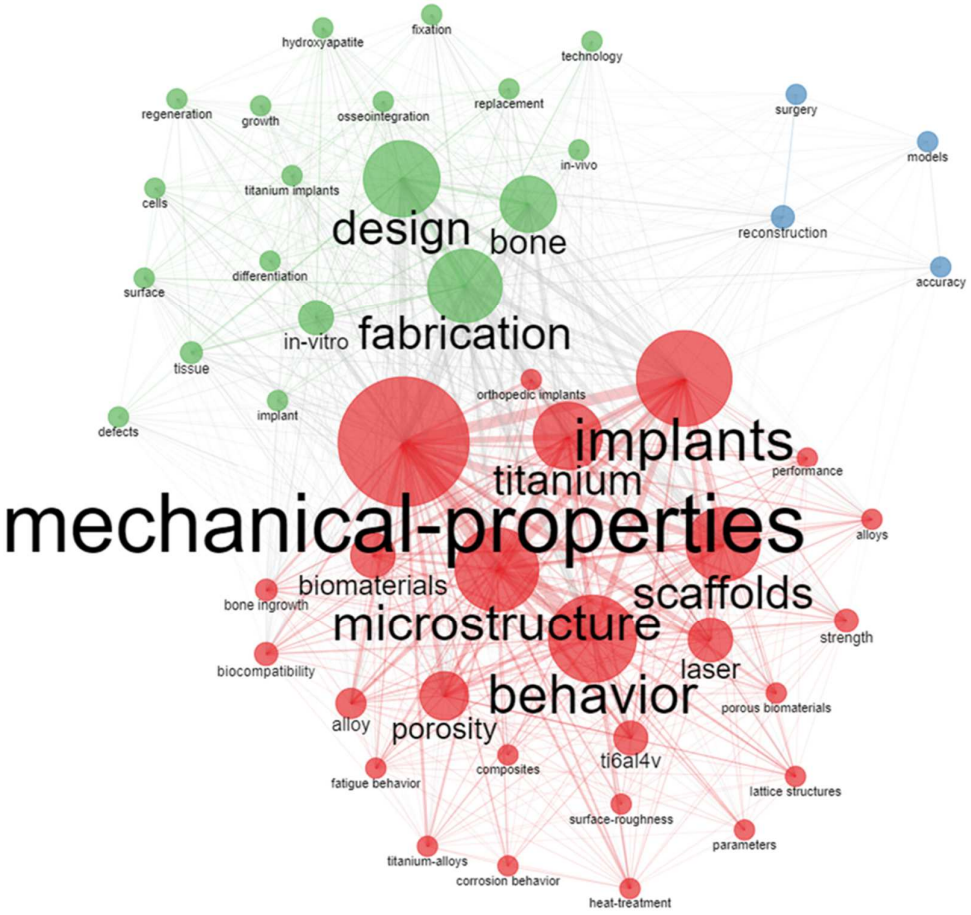

Figure 2. Co-occurrence network of *Keywords Plus* (i.e., keywords used in the references cited in the papers included in the analysis). Images were generated through the Bibliometrix tool.

MOTIVATION OF HE WORK AND APPLICATION

Within the implants and prostheses development, surface modification employing different classes of processes, singularly or combined, might enable specific function supply to these devices. Also, in certain cases, the combination of different materials to create a substrate-coating system represents an advisable solution to alter surface properties of a device without modifying the bulk properties. In the biomedical field, where titanium alloys play a central role, complications arise such as high bacterial proliferation within implants, poor integration, infection, metal sensitivity [8].

The starting point is that surface properties dictate the interactions between a biomedical device and the body environment. Some limitations are still found in the

available literature regarding a systematic study of processes able to tune the surface accommodating different needs, according to the specific application. Also, a drive towards improvement of *in vitro* testing procedures exists for the prediction of biomedical devices performance.

The objective of this work is that of opportunely modify the surface of the *Ti6Al4V* titanium alloy to address its current issues when applied to skeletal fixation devices, where this alloy plays the role of standard of care. The issue will be approached from different but interrelated points of view:

1. It is possible to modulate the integration of the implants with surrounding bone tissues by acting on implant/prosthesis surface properties. Surface deformation and removal techniques like grit blasting and milling under different conditions will be applied to study the effect of surface processing conditions and features (i.e. surface texture, microstructure, composition, contact angle) on preliminary *in vitro* cell response.

2. Engineered natural materials are promising biomaterials towards fostering implant interactions with body environment and as local drug delivery supports but they suffer from several issues, including their poor adhesion to the surfaces of metallic implants. This issue will be addressed by tuning the properties of the biopolymer chitosan through different deposition techniques, and metallic substrate properties through surface deformation and removal techniques - i.e. milling, grit blasting and electrical discharge machining.

3. Surface properties not only affect tissue response but also the response of bacterial pathogens: the previously mentioned techniques, with additional laser texturing experiments, will be employed to analyze the effect of surface modification techniques and features on *in vitro* bacterial response.

To help understanding the structure of this work, Figure 3 shows a flow chart of the dissertation outline.

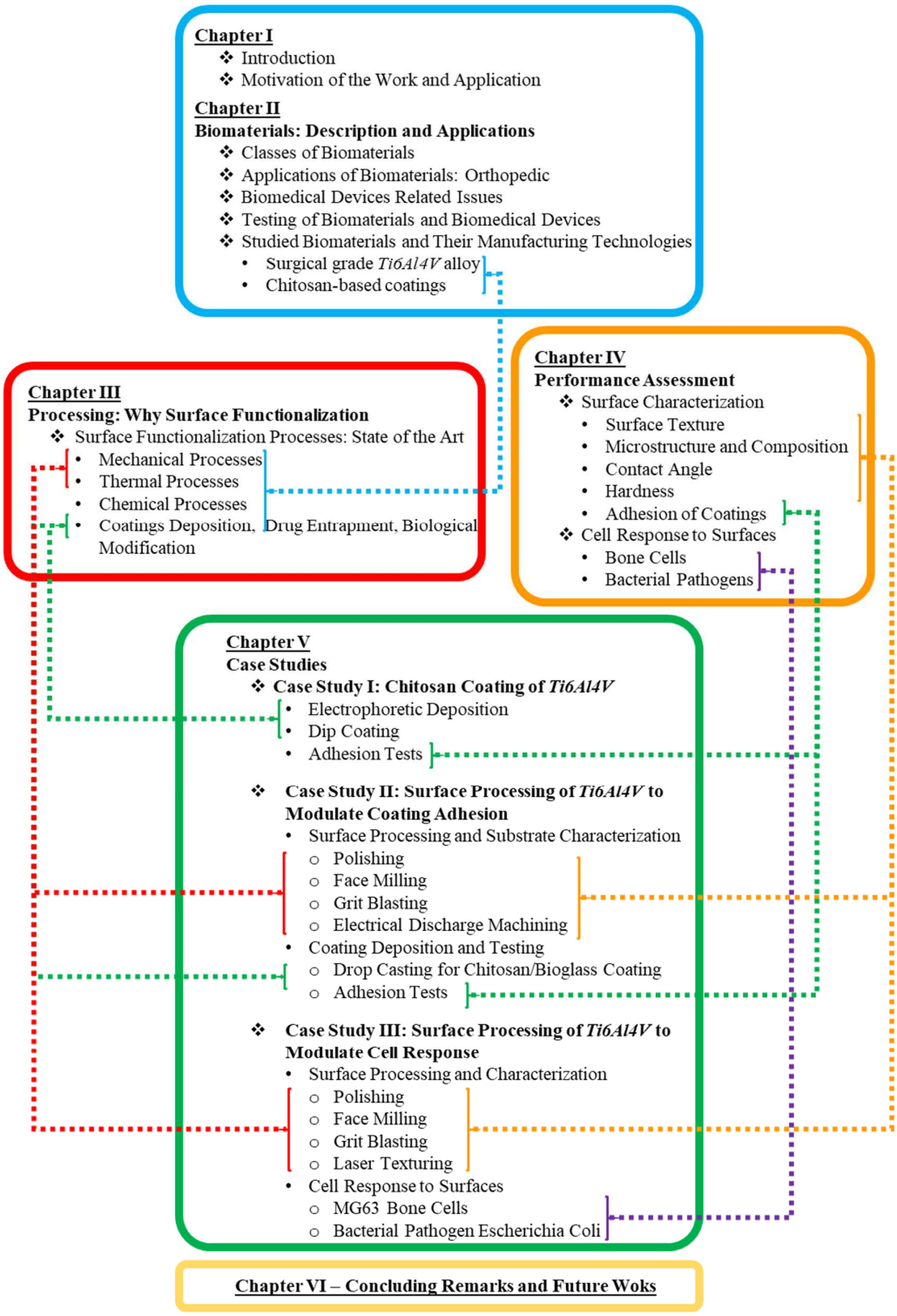

Figure 3. Dissertation outline flow chart.

CHAPTER I

BIOMATERIALS: DESCRIPTION AND APPLICATIONS

This chapter provides a brief state of the art on the most commonly used materials in medical applications. A few definitions will be provided in the next lines to clarify the terminology employed throughout the dissertation:

1. According to a consensus of experts, the definition of the term *biomaterial* is "*a nonviable material used in a medical device, intended to interact with biological systems*" [8]. These materials are now required to strictly comply with composition, purity, and further constraints that would make them suitable for medical use [9] like the ones developed by the ISO Technical Committee 194 with a family of guidelines on the biological evaluation of medical devices [10].
2. A biomedical device has been defined by the Global Harmonization Task Force [11] and adopted by the World Health Organization [12] as "*any instrument, apparatus, implement, machine, appliance, implant, reagent for in vitro use, software, material, or other similar or related article, intended by the manufacturer to be used, alone or in combination, for human beings, for one or more specific medical purpose {…} and does not achieve its primary intended action by pharmacological, immunological, or metabolic means, but which may be assisted in its intended function by such means*".
3. Biocompatibility has been defined as "*the ability of a material to perform with an appropriate host response in a specific application*". Yet, biocompatibility can either be referred to a biomaterial or a device and in certain cases, the "biocompatible" label can only be assigned to an overall device and not to a specific biomaterial. This definition is mostly related to an operational point of view and in the future it will be necessary to provide more insight into the design of devices to define biocompatibility measurement in strict correlation to a specific application. This is also because each area of the body possesses different properties, e.g. local pH, which then require the biomaterial to be designed to withstand specific conditions during use.

What is clear is that biocompatibility is negatively affected by: (i) materials leaching from biomaterials, (ii) reactions triggered by microorganisms (e.g. bacteria) colonizing the biomaterial, (iii) mechanical effects like local rubbing, irritation, stiffness mismatch with local tissue, (iv) interaction between cells/tissues and the biomaterial, including inflammatory cells [9].

Herein, the term "biomedical device" will be used to indicate altogether medical implants, prostheses, instrumentation, etc., and parts thereof. When in text reference is made to devices that are implanted in, or in direct contact with, patient's tissue or organs the terms "implants" and "prostheses/sis" shall be preferred.

For the proper design of a biomedical device, as it happens for the design of devices intended for different fields of application, the different tasks to be taken up by the device need to be clearly defined. The part of the body to be replaced requires a deep knowledge of the functionalities to be provided by its substitute and of the stress conditions related to the area of application in an aggressive environment such as the human body.

As highlighted in the definition of biocompatibility, a favorable bioresponse – another term to define biological reaction to a material/device – is dictated by the specific application and location in the body and, as a consequence, the design constraints on the above mentioned engineering properties. As an example, under certain circumstances, it is necessary for a device to remain in the human body for a limited amount of time (e.g. resorbable screws [13]) while in other applications the capability of the device to preserve its properties over the long-term is of pivotal importance (e.g. load bearing applications like artificial joints). The engineering properties of materials, of general interest within biomedical devices are: elastic modulus, ductility, yield strength, ultimate tensile strength, work hardening, hardness, resilience, toughness and fracture toughness, fatigue, corrosion, and wear resistance, in certain cases also thermal and optical properties.

Within the classes of biomaterials, four main categories[1] can be identified:

- Metals;
- Polymers;
- Ceramics and glasses;
- Engineered natural materials.

For visualization purposes and as introduction to the next paragraphs, the following material properties charts show a scatter plot of Young's Modulus vs Density (Figure 4),

[1] Further categories exist but their features are outside the scope of this work and will not be reported.

Strength vs Density (Figure 5), and Fracture Toughness vs Young's Modulus (Figure 6) for different classes of engineering materials. As can happen with other fields of applications, the previously mentioned classes of biomaterials can be combined to obtain composites and multi-material devices to accommodate multiple application-specific requirements.

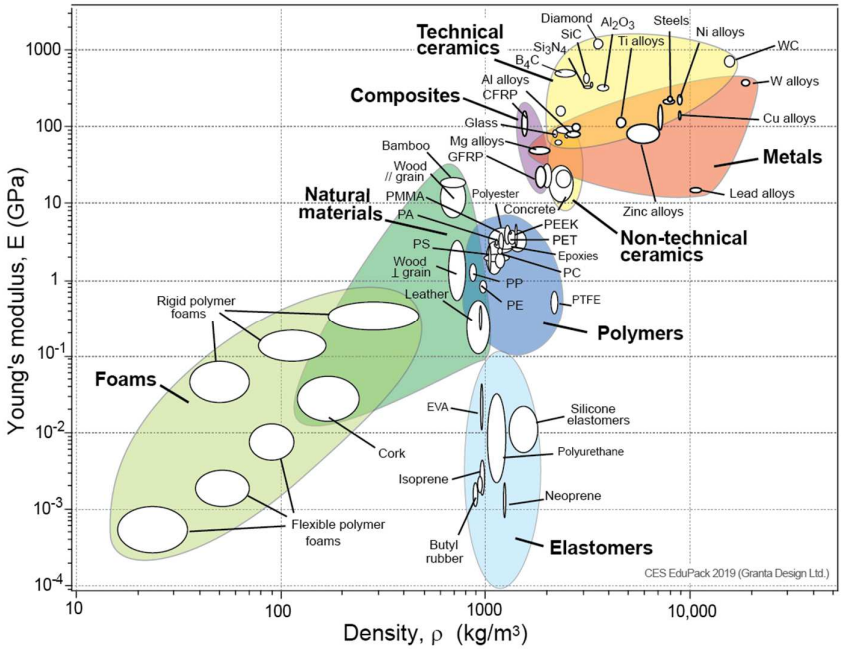

Figure 4. Ashby's chart – Young Modulus vs Density [14].

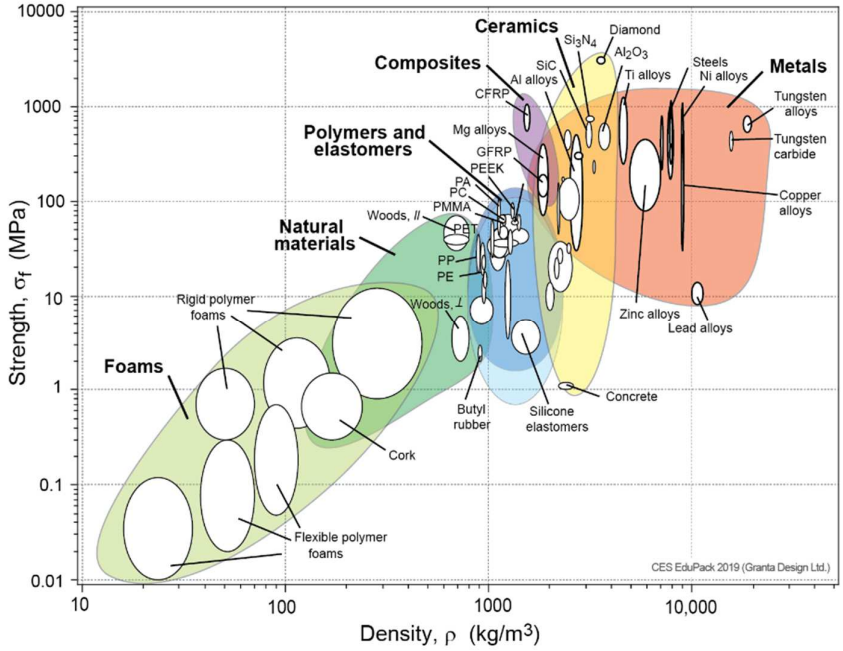

Figure 5. Ashby's chart – Strength vs Density [14].

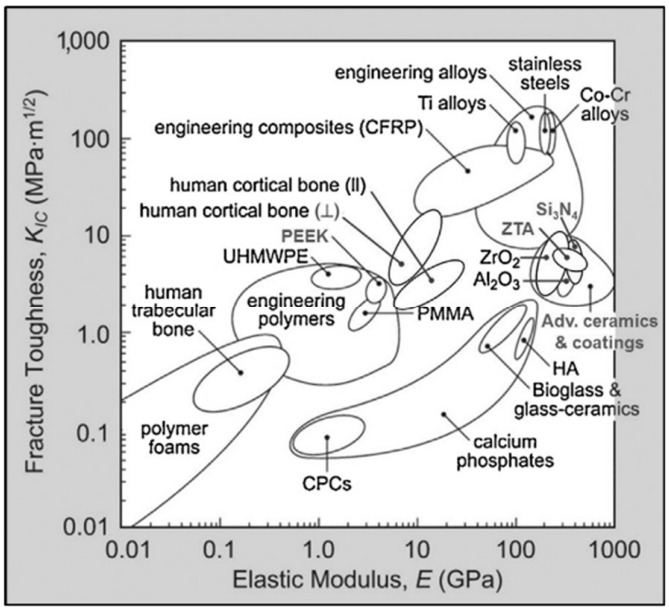

Figure 6. Ashby's chart – Fracture Toughness vs Elastic Modulus [15].

CLASSES OF BIOMATERIALS

METALS

Metals are widely used for medical devices where load bearing capacity is a requirement. The most used within the non-resorbable metallic alloys are:

- Stainless Steels
- Cobalt alloys
- Titanium and its alloys
- Nickel-titanium alloys

STAINLESS STEELS

Stainless steels are iron-carbon alloys with a Chromium content generally above wt% 10.5 as an alloying element, allowing the formation of a Chromium-based protective oxide layer enhancing their corrosion resistance. Austenitic stainless steels – mainly with Nickel as an alloying element in wt% 8-22 to stabilize the austenitic phase – are the most used for biomedical devices, being also non-magnetic and safe for diagnostic imaging

techniques. Most recently, adverse reactions triggered in patients due to Nickel sensitization brought the development of low Ni content stainless steels, substituting Manganese to Nickel as a stabilizer for the austenitic phase. Table 1 shows a summary of the most common implantable stainless steels, their composition, and used nomenclature according to different standards.

Table 1. Composition of common implantable stainless steels (wt%) [16].

Alloy	Cr	Ni	Mn	Mo	C	N	Nb	V	Si	Cu	P	S
316L	17.00–19.00	13.00–15.00	<2.00	2.25-3.00	<0.03	0.10	-	-	<0.75	<0.50	<0.025	<0.010
ASTM F138 ISO 5832-1												
22-13-5	20.50-23.50	11.50-13.50	4.00-6.00	2.00-3.00	<0.03	0.20-0.40	0.10-0.30	0.10-0.30	<0.75	<0.50	<0.025	<0.010
ASTM F1314												
Rex 734	19.50-22.00	9.00-11.00	2.00-4.25	2.00-3.00	<0.08	0.25-0.50	0.25-0.80	-	<0.75	<0.25	<0.25	<0.010
Ortron 90 ASTM F1586 ISO 5832-9												
BioDur® 108	19.00-23.00	<0.050	21.00-24.00	0.50-1.50	<0.08	0.85-1.10	-	-	<0.75	<0.25	<0.03	<0.010
ASTM F2229												

COBALT-BASED ALLOYS

Cobalt-based alloys were introduced in the biomedical field right after stainless steels and are sometimes preferred to those because of their higher corrosion and wear resistance and strength. The currently most used cobalt-based alloys mainly contain Chromium and Molybdenum elements (*Co-28Cr-6Mo* is dominant for joint replacements), but also Nickel and Tungsten elements, although the Nickel release in the body for applications involving surface wear is raising concern. Novel cobalt-based alloys are currently under development to reduce Nickel contents. Table 2 reports the composition of the most common implantable cobalt-based alloys.

Table 2. Composition of common implantable cobalt-based alloys (wt%) [17], [18].

Alloy	Cr	Mo	Ni	Fe	C	Si	Mn	W	P	S	Other
Co-28Cr-6Mo	27-30	5.0-7.0	1.0	0.75	0.35 max	1.00	1.00	0.2	0.020	0.01	*
ASTM F75 (cast)											
Co-35Ni-20Cr-10Mo	19-21	9.0-10.5	33.0-37.0	1.00	0.025	0.15	0.15	-	0.015	0.01	*
ASTM F562 (wrought)											
Co-20Cr-15W-10Ni-1.5Mn	19-21	-	9.0-11.0	3.00	0.05-0.15	0.40	1.00-2.00	14-16	0.040	0.03	*
ASTM F90 (wrought)											

*See [17] for other elements.

TITANIUM AND ITS ALLOYS

Titanium and its alloys are non-ferrous materials featuring a high strength-to-weight ratio (Figure 5), which makes them appealing to manufacture load bearing lighter parts. Table 3 reports the composition of the most common implantable titanium alloys. Innovative titanium alloys are currently being developed to substitute potentially toxic alloying elements currently used in standard of care alloys, e.g. Vanadium in *Ti6Al4V*, although the biomedical devices market is still dominated by this alloy in orthopedic applications and commercially pure Titanium (*CPTi* – %wt 99 of *Ti*) in dental applications. Titanium alloys are advantageous for their lower stiffness (Figure 4), higher corrosion resistance and improved bioresponse with respect to Cobalt-Chromium alloys and Stainless Steels, although their poor wear and frictional properties represent an issue for applications such as artificial joints [18].

Table 3. Composition of common implantable titanium alloys [17].

Alloy	Al	V	Nb	Mo	Zr
Ti6Al4V ELI F136	5.50-6.50	3.50-4.50	*	*	*
Ti6Al4V F1472	5.50-6.75	3.50-3.50	*	*	*
Ti6Al7Nb F1295	5.50-6.50	*	6.50-7.50	*	*
Ti15Mo F2066	*	*	*	14.00-16.00	*
Ti12Mo6Zr2Fe F1813	*	*	*	10.00-13.00	5.00-7.00
Ti3Al2.5V F2146	2.50-3.50	2.00-3.00	*	*	*

*See [17] for alloying elements in amounts higher than wt% 2 (average of specified range).

NICKEL-TITANIUM ALLOYS

Nickel-Titanium alloys based on the presence of the equiatomic intermetallic nickel-titanium compound have become popular in the past due to their shape-memory and superelasticity properties, related to the austenite-to-martensite reversible phase transformation. Their composition is typically based on atomic percentage of Nickel and Titanium elements around 49%–51%, involving sometimes the partial substitution of Nickel or Titanium with elements such as Palladium, Hafnium or Platinum [19]. They already have several clinical applications for non-load bearing devices such as

orthodontic arch wires and vascular stents but they recently became of interest for orthopedic applications due to their low Young's Modulus. In fact, it can be tuned to reach values below 70 GPa [17], [20] which could help reducing the bone stress-shielding phenomena. Despite the advantages related to the utilization of these alloys, the presence and release of the allergenic Nickel into the body is still a concern so that major effort is being devoted to the development of surface treatments for their successful passivation [18].

POLYMERS

Polymers are organic compounds obtained by repeated patterns of monomers via a controlled polymerization reaction and they feature a wide range of appealing macroscopic properties including good toughness (Figure 6). Based on their molecular weight, degree of polymerization, crystallinity and other processing factors their properties are subjected to a high variability. These materials are widely employed in medical applications including orthopedics and tissue replacements, sometimes combined with metals and ceramics in multimaterial devices, to compensate for their lower load-bearing capacity (Figure 5) (e.g. in joint prostheses). The most used polymers for the biomedical devices include Poly(methyl methacrylate) (PMMA) used for bone cement, high-density Polyethylene (HDPE) for prosthetic joints, Poly(ethylene terephthalate) (PET) for ligaments reconstruction, Polydimethylsiloxane (PDMS) for finger joints.

CERAMICS AND GLASSES

Ceramics and glasses encompass a wide range of inorganic/non-metallic compositions and a just as wide range of properties. They are widely used as scaffolds and tissue defect fillers. Some of them show a high chemical inertness which, if the implant is properly designed, contributes to a low inflammatory response from the body. Examples of these ceramic materials are aluminum oxide (Al_2O_3), zirconium oxide (ZrO_2) and silicon nitride (Si_3N_4). Conversely, other materials within this group show high interaction with tissues and bond-forming capabilities at the interface like calcium phosphates and bioactive glasses, making these materials appealing to foster implants integration with surrounding tissues. Ceramics and glasses have a great drawback i.e. their high brittleness (Figure 6)

accompanied by low impact resistance, which makes their stand-alone use appropriate only under certain loading conditions involving a compression stress state.

ENGINEERED NATURAL MATERIALS

Naturally occurring materials have recognized advantages since the body can break down and use these materials through physiological processes like e.g. the enzymatic one. However, these materials suffer from high batch-to-batch variability and generally have poor mechanical properties. While these features may not be good for long term load bearing implants, they can be helpful when the body needs to naturally absorb the material over time, like in drug delivery systems. Another common issue with natural materials is the immune response: even if the implanted materials are similar to the body's components (e.g. extracellular matrix), they can cause a significant immune reaction. Several research studies have to date demonstrated the possibility to overcome those challenges by modifying and purifying naturally occurring materials and few of them are currently being used to treat patients. Some of the most used natural materials are: alginate having origin from algae, chitosan from crustacean exoskeletons, collagen and hyaluronic acid from natural tissues or bacterial fermentation. [18]

APPLICATIONS OF BIOMATERIALS: ORTHOPEDIC

The applications of biomaterials span a wide range based on the functionality to be restored in the patient, including: cardiovascular, orthopedic, and dental applications, ophthalmic, extracorporeal artificial organs, wound healing, drug delivery, and diagnostics. Several material types as polymers, glass, and ceramics are involved but metals continue to play a main role in the framework of biomaterials, as most implants contain at least one metallic part [16]. The main use of orthopedic biomaterials is to replace or improve the function of bones, joints, tendons, cartilage, or ligaments (Table 4) as bone and joint wear or trauma and arthritis affect millions of people worldwide.

Table 4. Summary of the main orthopedic applications [16].

Fracture fixation devices	Joint replacement
Spinal fixation devices	Arthroplasty of:
Fracture plates	Hip
Wires	Knee
Pins	Spine
Screws	Ankle
Intramedullary devices	Shoulder
Artificial ligaments	Elbow
	Wrist
	Finger

The focus of this work will be on orthopedic applications of metals, in particular bone fixators. It is necessary to highlight that although these applications involve bone-contacting and anchoring of implants, different considerations are involved in the final development of these devices based on the properties of the implantation site, requested duration, and load-bearing capacity of the implant. This will be a necessary step to be addressed in the future developments of the current work.

ORTHOPEDIC DEVICES-RELATED ISSUES

The majority of load bearing metallic implants is made up of titanium alloys, which represent now the clinical "gold standard" since they generally elicit better bioreaction as compared to other available metallic alloys. Still, the presence of a biomedical implant inside the body increases the susceptibility to infection as it stimulates the reaction of the immune system and it also increases the risk of implant failure due to the aggressive body environment conditions. Despite the systemic antibiotic prophylaxis and the operating procedures, which are as aseptic as possible, the issue is not completely solved. In fact, orthopedic implant infections might not develop until months after the implant, they are difficult to detect and not always completely solved by systemic antibiotic delivery, but might also often require implant revision surgery.

Within this context, biomaterials-tissue interactions largely affect implant operation as these are related to the alteration of physiological processes. In general, a few types of implant-tissue responses for non-resorbable materials may be identified, which affect tissue attachment: (i) surrounding tissue death because of material toxicity; (ii) fibrous

tissue formation for non-toxic nearly inert materials, bringing to the absence of osteointegration, sometimes coupled with implant mobilization and wear debris release, which contributes to fibrous capsule thickening and further potential complications; (iii) interfacial bonding, i.e. direct bone attachment without interposed soft tissue, between implant and tissue in absence of toxicity and bioactive behavior of the material surface. [16]

There is an evident need for developing surfaces provided in anti-bacterial properties to hinder the development of infection and antibiotic resistance, but also able to successfully integrate with the surrounding tissues without affecting the overall load bearing capacity of the device. Implant detachment from the surrounding bone, its migration and, in cascade, pain and inflammation in the patient still represent an issue. Furthermore, understanding the relationship between biomaterial composition, device design, and biological response in complex living organisms is challenging. *In vivo* tests, which are essential in establishing the biological safety of a medical device (Figure 7) raise many ethical concerns, thus providing a drive towards the improvement of *in vitro* predictive models. *In vitro* methods are recognized for their value, but they have visible constraints, also due to the absence of the systemic immune and inflammatory responses. Currently available characterization techniques do not allow the prediction of *in vivo* performance for biomaterials and devices, and contradictive results are often obtained. There is a potential for multivariate statistical algorithms to generalize data into useful correlations and trends in biomaterials and medical device design but this goal is still a work in progress.

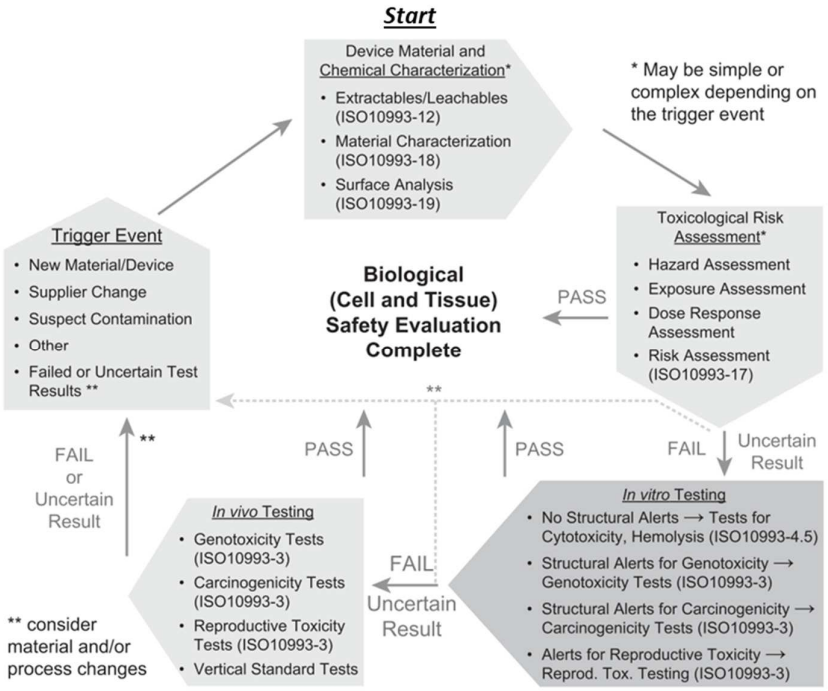

Figure 7. Schematic showing the process to establish the preclinical biological safety of a medical device material. Source: [18].

STUDIED BIOMATERIALS

SURGICAL GRADE TI6AL4V ALLOY

Titanium exhibits two allotropic structures, with an allotropic phase transformation occurring at 882 °C. Below this temperature, it assumes a closed-pack hexagonal crystal structure known as the alpha phase, and above it transforms into a body-centered cubic crystal structure referred to as the beta phase (Figure 8). The hexagonal crystal structure of the alpha phase displays anisotropic behavior, influencing the elastic and plastic deformation characteristics of titanium and its alloys, as well as other physical properties. The transformation temperature is affected by interstitial and substitutional elements, making it dependent on the metal's purity.

This alloy consists of 6 wt% Aluminum, 4 wt% Vanadium, and the remaining percentage is titanium, with possible small amounts of other elements like Iron or Oxygen. Aluminum serves as an alpha-stabilizer, raising the stability temperature of the alpha-phase, enhancing hardness, while Vanadium acts as a beta-stabilizer, maintaining beta-temperature stability even at low temperatures and improving formability.

Classified as an alpha-beta alloy, *Ti6Al4V* features high strength, lower elastic modulus than stainless steels and cobalt-based alloys, and good corrosion resistance.

Titanium components are produced in wrought, cast, and powder metallurgy form. *Ti6Al4V's* good workability allows for the cost-effective production of numerous foundry products with consistent mechanical properties and varying sizes. Different microstructures can be obtained by heating the material above and below the beta transition temperature, along with varying cooling methods such as water quenching, air cooling, and furnace cooling (Figure 9).

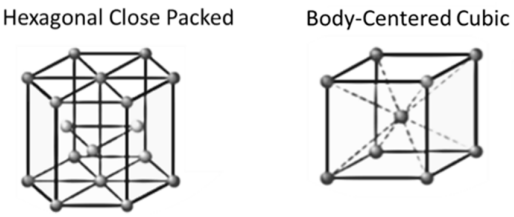

Figure 8. Hexagonal Close Packed (HCP) and Body-Centered Cubic (BCC) crystal structures.

The good corrosion characteristics of titanium alloys surface are attributed to the spontaneously formed oxide film upon exposure to air. This titanium oxide film is the primary factor contributing to the good repassivation ability of titanium alloys. In numerous applications, the device surface primarily comprises a naturally occurring oxide film and TiO_2 is the most stable within the titanium oxides, existing in different crystallographic forms. Nevertheless, this oxide film is modified once in contact with the biological environment and also repeatedly damaged when subjected to wear phenomena (e.g. when relative motion with another surface is involved, like in artificial joints) thus reducing the advantages initially featured by an intact oxide layer [22].

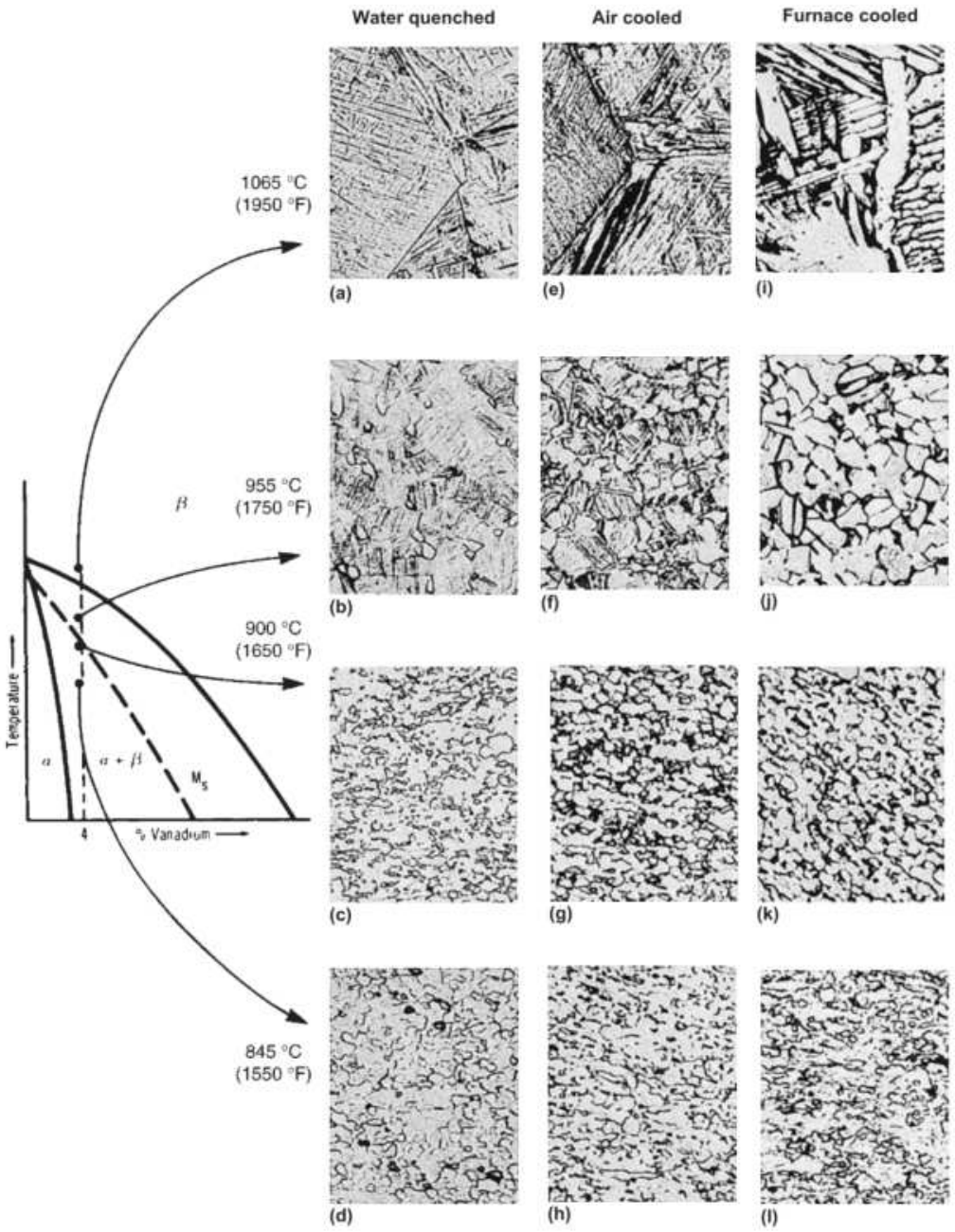

Figure 9. Effect of cooling rate on the microstructure of *Ti6Al4V*. [21]

CHITOSAN-BASED COATINGS

Chitosan, within the engineered natural materials, is a biopolymer at the heart of scientific interest in the latest years (chitosan structure in Figure 10). It is a polysaccharide, an acetylated derivative of another natural polysaccharide, chitin. The chitin is the second most abundant biopolymer in nature after cellulose and the most important component of insects' exoskeleton, crustaceans' shells, and fungi's cell walls. Chitosan has good

biodegradability, and antimicrobic and osteogenic properties able to improve the integration between implants and bone tissue [23], [24].

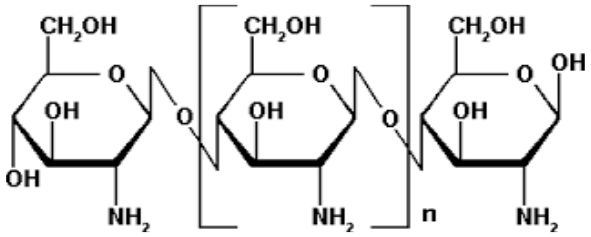

Figure 10. Structure of the chitosan [25].

Chitosan also features good versatility in manufacturing to form like films, fibers, and hydrogels. Chitosan solutions with different physicochemical properties based on the technique to be used are generally deposited on a substrate by direct casting, spraying, by the action of electrostatic interactions or by dipping the substrate into the solution and leaving the solvent to evaporate to obtain the final coating.

However, pure chitosan has poor mechanical properties, and its adhesion on metal substrates is considered weak in terms of bond interactions [26], [27]. Creating chitosan/bioactive glass composites represents a viable solution, as bioactive glass can be employed for both bonding osteogenesis and mechanical properties improvement [28]. At the same time, the tuning of the substrate properties [29], like the surface texture, chemical composition, contact angle, might significantly improve the system-coating performances in mechanical adhesion. Techniques like dip coating, drop casting, electrophoresis, electrodeposition, and electrospraying exhibit versatility in enabling the integration of bioactive and/or reinforcing substances into the coating. It is important to highlight the possibility of functionalization of chitosan, which could lead the way to the use of chitosan coatings as a means for local delivery of drugs.

CHAPTER II

PROCESSING: WHY SURFACE FUNCTIONALIZATION

For an implanted device to fulfill the purpose of its ideation, several factors must be taken into account, such as: (i) overall implant design; (ii) surgical procedure; and (iii) patient conditions. Due to the complexity of the problem and the presence of many confounding variables, reaching an optimum implant configuration is a multifaceted issue and significant effort has to be put into addressing potential inconveniences, which might eventually bring to implant failure and aggravation of patient's health.

As reported in Chapter I, several classes of materials are today employed for biomedical devices, but metals still have a major role, in particular for applications requiring immediate structural support. Unfortunately, in cases involving for example critical patient conditions, metal sensitivity [30], or invasive surgical procedures [31] the chances of failure increase dramatically. To help prevent the consequences of the above-mentioned drawbacks, an action to modify biomedical devices features is required.

Surface and subsurface properties on a macro- to nano-scale have been found to strongly affect local tissue response. In fact, it is acknowledged that the bone-implant interface can be subjected to significant changes by only modifying surface composition, texture, and energy [16].

Indeed, the surface represents the first interaction between the implants and the body environment. It controls their behavior with respect to, e.g., surface fatigue, corrosion, wear, and, as a consequence, biological reactions. Some of the parameters of interest for performance can be recognized in surface texture, composition, stiffness, charge, and, as a direct consequence, contact angle. Few of these, fall into the definition of surface integrity, introduced as condition of a surface produced by surface generation operations and often related to component response to aggressive environments [32].

In fact, mechanical failure, if arising from the surface, together with corrosion and wear are related to microstructure, residual stresses, chemical species and their stability, besides overall implant shape and geometric discontinuities [33]. Furthermore, it is acknowledged that cells and pathogens are sensitive to topographical features with which they interact and their chemical and mechanical nature [4, 5] as will be explained in Chapter III. Thus,

preliminary studying the interaction between the surface of a device and cells or tissues *in vitro* is a way to extrapolate trends to be used for device design and *in vivo* application.

Given the above, several surface modification techniques are being studied and implemented to modulate implants resistance and biological response [9]. These techniques often involve mechanical, physical, chemical, or biological alterations and can be used separately or in combination. In the broad range of available techniques, some of them involve material removal or displacement, most likely with simultaneous material modification, others involve material deposition.

Furthermore, the idea of acting on the implant's surface by introducing a coating represents one of the viable solutions to modulate the biological response to the implant by human organism without altering the load bearing capacity of the bulk of the implant.

When it comes to the deposition of a material over a substrate, both substrate and coating features dictate interface behavior and adhesion [36]. As a matter of fact, coating adhesion results in an interplay between mechanical, chemical, and physical interactions between substrate and coating, its thickness and internal stresses, coating deposition technique, and, clearly, the features of the surrounding environment. Thus, just as important as the technique employed for modification, a thorough characterization of the surface of the substrate enables to identify possible factors affecting performance during use.

STATE OF THE ART AND STUDIED PROCESSES

The higher mass ratio of titanium alloys and their general superior bioresponse with respect to the other conventionally employed alloys has been proven to not be sufficient to guarantee a good outcome of the implant. In the past years, several surface modification techniques have been developed to provide superior biomedical device performances, involving distinct mechanisms and primary sources.

In the next paragraphs, the techniques employed for surface modification applied to modulate bioresponse of titanium alloys and defined by the following mechanisms will be covered, based on the most recent research trends [37]: (i) mechanical deformation, (ii) chemical reactions, and (iii) thermal sources. Additionally, deposition techniques (which partially overlap with previously mentioned ones) and biological modification will be introduced. Categorization of techniques here will be mainly based on primary source/mechanism type. Nevertheless, each process that will be discussed may encompass

more than a single modification mechanism (sometimes involving deposition of a film on the surface) as it is hardly possible to alter e.g. surface texture without affecting local microstructure and chemistry.

MECHANICAL PROCESSES

Within mechanical-based processes, some of the most used pertain to abrasive machining. They owe their name to the utilization of a high quantity of hard and sharp, mostly irregularly shaped, particles as tools for material removal. As a result of processing, grooves or randomly distributed craters, with dimensions related to abrasive size, may be generated on the treated surface, the former for grinding and polishing, the latter for grit-blasting. [38] These techniques, together with surface texture alteration, according to processing conditions, may introduce a more or less pronounced strain hardening together with grain distortion and chemical alteration due to the elements in the abrasives. The latter applies mostly to grit-blasting, which is often performed by delivering aluminum oxide [39] particles at high speed onto part surface.

Grinding and polishing in biomedical applications are generally employed to smooth surfaces [40], which is beneficial in certain cases, for example in easing revision surgery and implant removal due to bony on growth reduction [41] but they can also be employed as a preliminary operation given further processing (e.g. chemical treatments [42]). They are also used as a reference for comparing bioresponse after applying different processing methodologies [43]–[45].

Grit-blasting is often used to roughen implant surface and increase the contact area to accommodate cells [39] but also to remove undesired surface features such as residuals of unmelted powder from additively manufactured parts. By using specific blasting media, the surface composition can be altered to some extent to purposely introduce highly biocompatible elements such as calcium phosphates [46].

Severe plastic deformation processes involve the application of high strain to the component surface, bringing to the formation of affected layers characterized by high levels of hardening, residual stresses, grain distortion, and refinement as well as modification of surface texture according to process conditions [47]. Within this category of technologies, friction stir processing (FSP) can generate ultrafine grained surface layers, beneficial to wear resistance [48] and also enable bioresponse modification, as a consequence of microstructural changes [49]. Sliding friction treatment, which involves repeated sliding of a hardened tool against a part's surface is generating interest. In fact,

it leaves plow marks on the surface and can bring surface roughness to values comparable to polished ones but simultaneously introduce grain refinement up to nano-size [50]. Furthermore, cold working superfinishing processes like burnishing alone can supply hardening, beneficial residual stresses, and superior surface finish [47].

Among material removal processes, milling, which involves a rotating cutting tool to remove layers of material, is frequently used to define the final shape of the implant starting from cast parts as in [51]. It is also involved before further processing as in [52] where grit-blasting and ion beam implantation were performed on milled parts. Nevertheless, milling alone also offers a peculiar surface texture and, according to machining conditions, the presence of a hardened layer.

THERMAL PROCESSES

Processes of interest involving thermal sources can be recognized in electrical discharge machining (EDM), laser, plasma, and electron/ion beam treatments. EDM is based on erosion of conductive surfaces through subsequent electrical discharges generated between a properly shaped conductive tool-electrode and the workpiece, submerged in a dielectric fluid and powered by a generator. It has been largely employed to machine complex shaped components and create otherwise difficult slots [38]. The process has raised interest because of the possibility, through material melting, vaporization, and removal, to obtain a wider range of microstructural and chemical variations and the creation of non-directional surface textures to provide the implant with improved performance [53]. By tuning processing parameters and environment, it is possible to obtain a wide range of surface modifications. In fact, by properly selecting tool-electrode material, an antibacterial effect might be introduced (e.g. through copper tools) but also enhanced osteointegration by processing the material with special powders mixed with the dielectric fluid (e.g. calcium phosphates).

Laser-based surface treatments make use of a coherent light beam to focus high density energy onto the workpiece surface. According to source type and processing conditions, the effects of the process on component properties may be tuned from considerable to negligible based on requirements, for instance through ultra-short pulses in the order of pico- or femtosecond [54]. It is a highly versatile process enabling the production of specific surface textures towards performance optimization e.g. the introduction of directional textures to control cell attachment and spreading [55].

Other laser-based processes like laser shock peening can be used to introduce a beneficial stress state in surface layers without involving direct tool-workpiece contact [56] as happens for plastic deformation processes. In electron beam and ion beam machining (EBM, IBM) the source of energy is a beam of electrons and ions, respectively, accelerated and focused on the surface to be treated. They may have similar applications as laser-based ones but with limitations given by the need for a vacuum chamber. Electron beam surface treatment makes it possible to modify both surface texture, microstructure, and, with it, surface energy [44]. Ion beam processes find an interesting variation in ion beam implantation which allows specific ions to penetrate part surface and modifying its mechanical and chemical properties [52]. Finally, plasma-based processes involve ionized gas used to bombard the workpiece surface, and by varying process parameters and gas type they permit the modification of surface texture and chemical composition to a different extent. In [45] rutile-dense surface layer has been generated on titanium while in [57] the effect of plasma processing was not as relevant compared to untreated samples. In fact, plasma processing can also be used to remove contaminants and obtain superhydrophilic surfaces without modifying chemical composition and texture [46].

CHEMICAL PROCESSES

Chemical processing involves the use of chemical reagents, such as acids or alkaline ones, to attack and dissolve material on surfaces in a controlled way.

These processes are frequently employed in combination with each other or mechanical/thermal processes. One typical application is to combine grit-blasting with acid etching, sometimes performing further alkaline treatment to produce a hierarchical micro-to-nano structured surface, to increase bone-implant contact area [42]. Chemical polishing and electropolishing are also employed to remove material from the surface in order to obtain a mirror-like surface finish [17].

Chemical treatment is sometimes performed as a preliminary preparation for further chemical modification or deposition. For instance in [58] titanium sheets were treated with sulfuric acid, hydrogen peroxide, ammonia, and hydrochloric acid in different combinations prior to modification with self-assembled monolayers while in [59] acid etching was used to prepare surfaces for subsequent composite coating deposition. The outcome in surface chemical alteration, apart from the reagent employed, is strongly affected by the processing atmosphere [46] and requires control.

COATINGS DEPOSITION, DRUG ENTRAPMENT, BIOLOGICAL MODIFICATION

Deposition and biological techniques are widespread and virtually unlimited, they give the possibility to anchor extra components to surfaces to tailor not only biological interactions or place a barrier between metallic implant and body environment but, in particular for coatings, to simultaneously improve mechanical and tribocorrosion behavior. Plasma-based processes such as microarc oxidation can be employed to create porous oxide coatings and hierarchical structures and decrease the surface content of toxic ions according to the processing environment and conditions. In [60] selective removal of *Al* and *V* ions was noted in produced oxide coatings while in [61] surface was coated by a multilevel porous structure and a bioactive calcium phosphate coating.

Electrochemical procedures are of interest for the deposition of porous highly biocompatible films such as chitosan/hydroxyapatite composite [59]. For example, electrophoretic deposition is a technique that allows the deposition of a coating on an electrically conductive target substrate by the application of an electric field able to move the charged particles of the coating solution toward the substrate [62], [63].

Other processes like drop casting and dip coating have been widely used to deposit polymeric films on biomaterial surfaces. Drop casting or solution casting is a relatively simple technique that consists of depositing, with a pipette, the coating solution drop-by-drop onto the substrate to be coated. Then, spread the solution on the substrate forming a layer, and let it dry until the solvent evaporates (at room temperature or other conditions). Due to its ease and fast application, drop casting has been used to assess the bioresponse of polymers on biomaterial surfaces [64]. Dip coating allows the deposition of a thin film on a solid substrate by the immersion of the substrate inside a vessel containing the solution of the material to be deposited. It is an ancient coating technique and, also, the most widely used in industrial and laboratory applications. It is widespread mainly due to the simplicity of the process and its low cost, which are both features that do not preclude, in this case, the achievement of high-quality coatings [64], [65].

Also, some techniques conventionally used to perform material removal, with proper modification, allow coating deposition such as powder mixed EDM performed using, for example, hydroxyapatite particles as additives to dielectric fluid [53]. Drug entrapment can be performed while depositing material onto the implant surface to reduce systemic delivery of pharmaceutical agents. The biological modification involves immobilization

of biological entities onto implant surfaces and it needs careful account for bond stability in aggressive environments [16].

CHAPTER III

PERFORMANCE ASSESSMENT

Surface properties are acknowledged to modulate the interactions of implantable devices with the body environment and to affect their durability. Each treatment process affects the surface properties of implants produced in a specific fashion. As mentioned in Chapter II, some of the parameters of interest for bioresponse are surface texture, microstructure, hardness, and composition, besides manufacturing defects of the implant surface and the sub-surface residual stresses. The definition of surface integrity, i.e. "inherent or enhanced conditions of a surface produced by machining processes or other surface generation operations" [5] encompasses some of them [6].

Features such as high surface roughness may worsen the mechanical performance of an implant (in particular, its fatigue life and/or wear of joints), yet surface irregularities and the presence of active sites may improve the implant biointeractions with neighboring tissues. The identification of the properties of the "ideal" surface texture is still a major challenge for the often ill-defined requirements that an implant has to meet. A good tissue-implant integration would be desirable for the implant's mechanical stability but it could be problematic in the case implant surgical revision or removal were needed. This calls for extensive supplementary experiments to gain better insight into what is happening at the site of implantation. As a result, information on the actual response of implants produced with different manufacturing techniques may only be gathered if information on geometry and mechanical properties of the overall implant is complemented with information on their surface properties. In the following paragraphs, the factors studied in this work will be introduced: surface texture, microstructure, hardness and composition, contact angle.

SURFACE CHARACTERIZATION

SURFACE TEXTURE

To characterize the surface texture of an implant, different parameters have been used expressing fluctuations in its surface from the macro- (i.e., waviness, long wavelength) to the micro- and nano-scale (i.e., micro- and nano-roughness, short wavelength). The characterization scale (and the wavelength) used depends on the required features of the surface of interest and it is generally defined in rules issued by international regulatory bodies (i.e., such as ISO 21920).

Roughness is the most commonly used parameter and it expresses the amplitude property in terms of deviations of the surface height (generally along the z-coordinate), with respect to a reference line (2D) (Figure 11) or plane (3D), from which long wavelength features have been previously filtered.

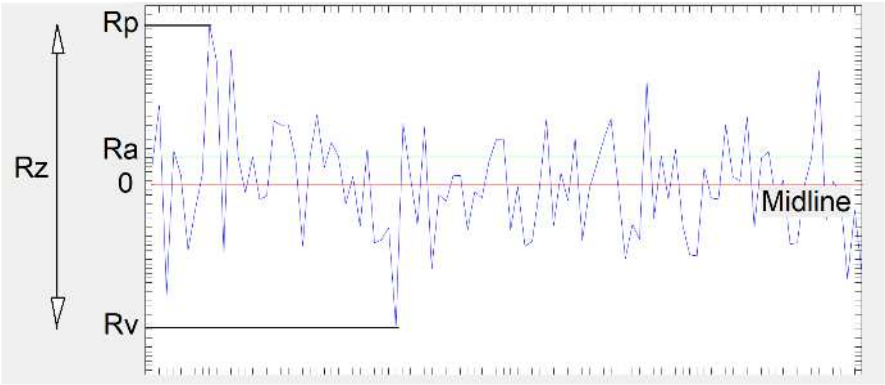

Figure 11. Schematic of various surface roughness parameters [5].

The most frequently used definitions of roughness are: the arithmetic mean deviation of the absolute z (*Ra*); the standard deviation of the height distribution (*Rq*); the sum of the maximum peak height and the maximum valley depth of the profile (*Rz*); all taken along a line and measured over a predefined reference length. Corresponding surface amplitude parameters are labeled with the capital "S", instead of capital "R" [7,8], i.e. *Sa*, *Sq* and *Sz*. Further areal surface parameters of interest are Skewness *Ssk* and Kurtosis *Sku*: the former is a measure of the asymmetry of surface deviations (height distribution) about the mean plane, the latter is a measure of the predominance of extreme peaks or pits for all measured points compared to an ideal bell curve distribution.

In conventional manufacturing processes such as forging, casting, and machining, or conventional processes involving plastic deformation, surface texture is largely dependent on the geometric and topographical features of the tool (or the die) in direct contact with the workpiece, on lubrication, if provided, and on the processing parameters.

MICROSTRUCTURE AND COMPOSITION

The surface microstructure of an implant significantly contributes to its behavior (mechanical properties, fatigue, corrosion, and similar) on typical sizes spanning various orders of magnitude. The formation of crystals in which atoms are packed (i.e., the grains) is driven by complex thermal phenomena arising during manufacturing stages and it often causes a certain degree of anisotropy in the manufactured implant. The fabrication route determines microstructural features to an extent that depends on the temperatures reached, the heating/cooling rates, and possible thermo-mechanical modifications. The microstructure is generally evaluated by sectioning representative material samples, grinding and polishing them up to a suitable finish to perform surface etching, followed by assessing the presence of various metallographic phases and the grain size via surface imaging techniques.

Conventional cast and wrought implants typically come with a highly variable distribution of metallic phases depending on alloy composition, with different crystal structures contributing to properties like oxidation resistance and formability [16, 17]. Microstructures may exhibit such features as: equiaxed (nearly equal dimensions in all directions), columnar, needle-like (acicular), or a combination of different types, depending on the thermal cycles during manufacturing.

Also, grain size reportedly affects surface reactivity, resistance to the propagation of defects in the material, and other properties [21, 22]. The chemical characterization of the surface layer in this work will be treated as complementary to the microstructural analysis.

CONTACT ANGLE

The contact angle (θ) is defined as "*the mechanical equilibrium of the drop under the action of three interfacial tensions: solid–vapor (γ_{sv}); solid–liquid, (γ_{sl}); and liquid–vapor, (γ_{lv})*" [66]. It can be explained by the balance existing between the cohesive forces

within a drop of liquid and the adhesive forces that attract the same drop to a surface. This relationship has been generally described by the equation (1):

$$\gamma_{sv} = \gamma_{sl} + \gamma_{lv} \cos\theta. \quad (1)$$

Contact angle plays an important role in the definition of the interactions between a surface and the surrounding environment either to better define, for example, the relationship between a substrate and a coating or the response of an implanted biomaterial. It can be measured through different techniques by depositing a drop on a surface (e.g. sessile drop technique in Figure 12) or by partially immersing a plate into a liquid and computing the contact angle through imaging systems, at different time frames. [16]

Contact angle measurement indirectly incorporates the effects of surface energy, texture, heterogeneity, and, if present, contamination.

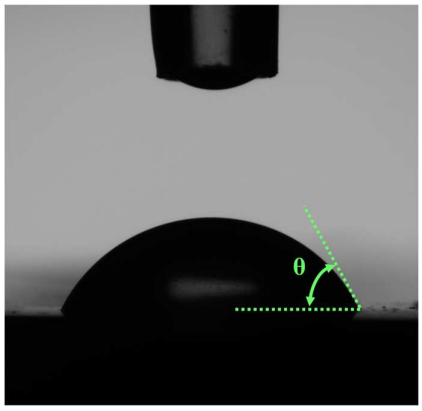

Figure 12. Example of contact angle measurement using the sessile drop technique.

HARDNESS

Hardness is generally defined as the material resistance against penetration or scratching by another body and it is strictly related to the implant microstructure. The analysis reported herein refers to hardness testing via the gradual penetration of an indenter significantly harder than the material to be tested (e.g. diamond) up to a predefined force or penetration depth.

A rectangular-based or triangular-based pyramidal indenter is typically employed to define respectively Vickers Hardness (HV) and Berkovich Hardness (HIT) as the ratio between the applied force and the projected area of the imprint (Figure 13). A conical indenter or a sphere can be used to define the Rockwell Hardness (HR) as a function of

load and penetration depth. Several other hardness scales exist depending on the tip shape, the applied load or penetration depth (i.e., macro- to nano-order characterization), and the calculation method. Rules for hardness measurement are generally defined by international standards (i.e., ISO 6507 and ISO 6508). Conversion between different hardness scales may only be approximated, because significant errors may be introduced by the inherently different measurement methodologies [9, 24]. Hardness depends on microstructural features such as alloy composition, microstructural constituents, grain size, and deformation, described in the previous paragraphs.

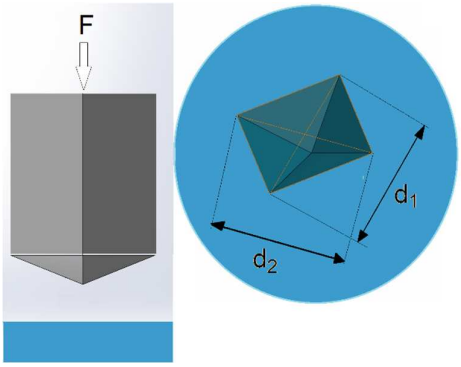

Figure 13. Schematic of Vickers Hardness test [5].

ADHESION OF COATINGS

Several methods exist to test the adhesion of coatings to substrates. Some of them like the tearing-off or the shearing-off allow measuring the load necessary to bring the coating to failure along an area of fixed size by typically gluing (or soldering) a rod on the coating and applying a normal force (tear-off) or a tangential force (shear-off) [36]. Other methods involve the quasi-static penetration of an indenter to cause coating failure, like the scratch test.

The scratch test enables quantifying the mechanical resistance of materials through the creation of a scratch of a certain length on the coating surface. The test requires the use of a tip with known geometry, called an “indenter”. During the test, the tip travels along the material surface while simultaneously applying a constant force, or an increasing force, orthogonal to the coating surface [67]–[70].

The main parameter to interpret the results of the scratch test is the critical load [71], here defined as the smallest normal load corresponding to the material failure. Indeed, this parameter depends on the mechanical strength (cohesion or adhesion strength) of the coating-substrate system. The failure point is the first point in which the coating damage

makes the coating no longer acceptable. The criterion to find this point can be twofold, for this reason, two possible critical loads can be defined [68]. The first refers to the load corresponding to the cohesive failure, while the other one is the load matched to the adhesive failure (Figure 14).

An estimation in terms of coating resistance can be made through the measure of the critical load; moreover, it is also possible to indirectly obtain an estimation of the coating thickness by detecting the penetration depth [72].

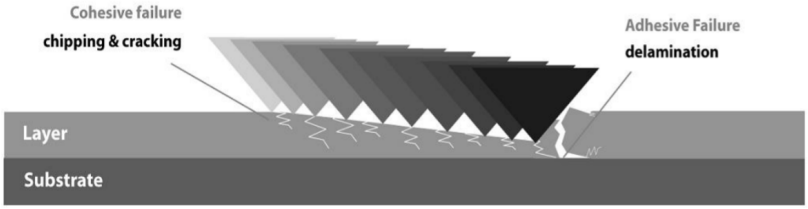

Figure 14. Principle of scratch testing. Source: [73].

CELL RESPONSE TO SURFACES

BONE CELLS

The key to a satisfactory long term implant response from the body can be identified in the initial response of cells to the material itself. Cells as basic units of living organisms are sensitive to multiple cues from the surrounding environment. In culture, substrate mechanical properties, microstructure, texture, and chemistry can affect protein adsorption (key to cell sensitivity) and cell attachment, shape, alignment, spreading, differentiation, and proliferation. As an example, the response of surface receptors of cells and protein adsorption are affected differently by different surface roughness and then exert influence on cell attachment (Figure 15). In fact, it has been demonstrated that cells can sense features above a certain cell-specific threshold starting from the nano-scale and going up to the micro-scale, also based on the size of texture's features as compared to the cell size [16]. A schematic to depict the complexity of the relationship surfaces-cell response is reported in Figure 16, with cell response affected by its type and culturing conditions.

Each of the processes covered in previous paragraphs potentially introduces more than one variation into implant surface and subsurface layers thus identification of affected

properties is the core of a proper reading of results from biological tests, as will be discussed in the next chapter.

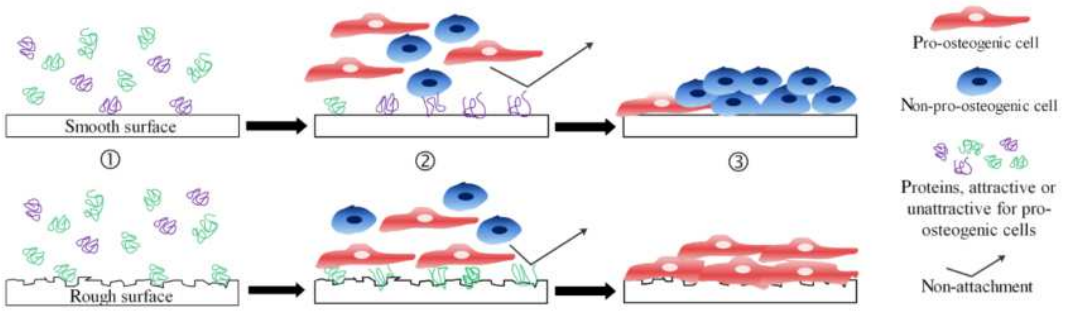

Figure 15. Example of different cell responses based on the surface texture of the biomaterial. Source: [74].

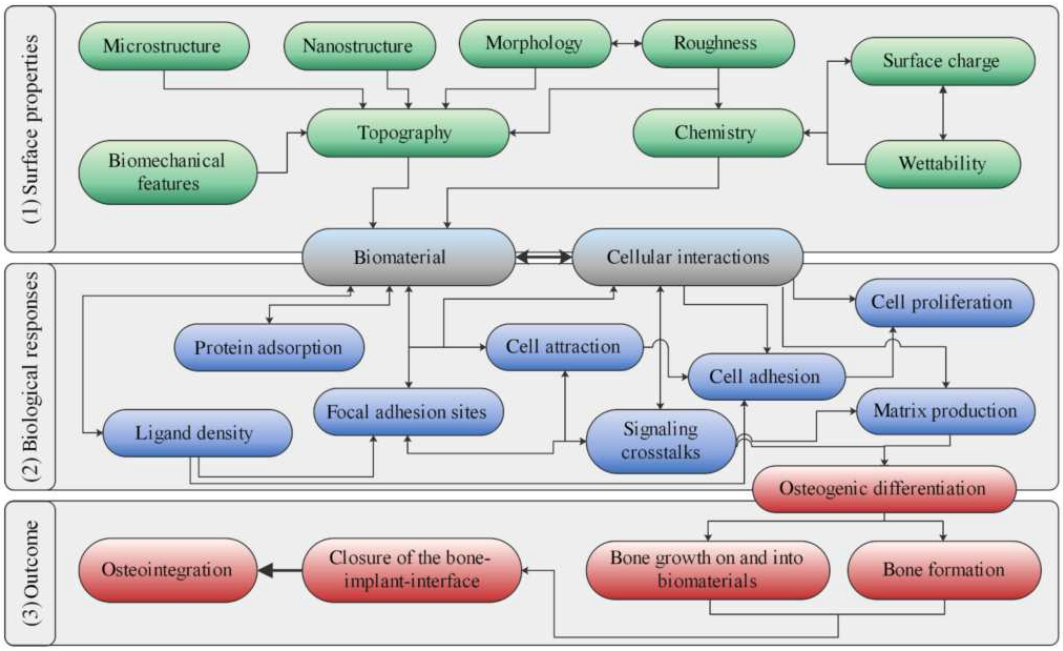

Figure 16. Visualization of the interrelationship of surface characteristics of a biomaterial and cell response. Source: [74].

BACTERIAL PATHOGENS

The surface modification enables tuning up biological interactions of the prosthesis with neighboring tissue, including the response of possible pathogens [9]. Bacterial pathogens, as other microorganisms, are sensitive to the surface features to which the try to attach and, when they succeed in attachment, the formation of biofilms starts. Biofilms are "structured microbial communities" [75] that, when formed, determine a strong adhesion

and a high survival of the pathogens on the surfaces of implants. Inhibition of bacterial adhesion and biofilm formation remain major issues, often approached by doping the biomaterial with antibacterial (bio)chemicals, which in the long term might bring an improved bacterial resistance to those substances. Thus, a proper surface modification from the nano- to the micro-scale can be the key to inhibiting biofilm formation [76]. Multiple elements have been recognized to affect bacterial response to surfaces, including roughness, stiffness, wettability, and charge [75] as exemplified in Figure 17: the interaction of these factors and their effect is specific to the type of bacteria.

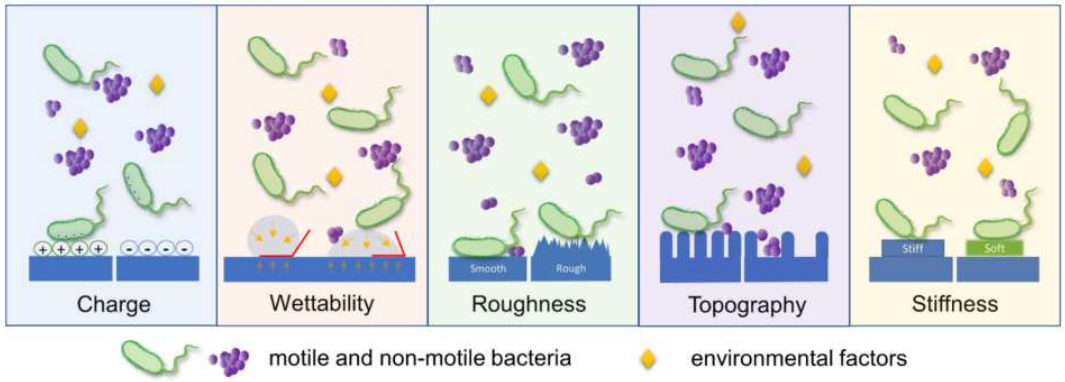

Figure 17. Example of response from different types of bacteria to surface parameters. Source: [75].

CHAPTER IV

CASE STUDIES

CASE STUDY I: CHITOSAN COATING OF TI6AL4V

In this work, the analysis is focused on the mechanical adhesion, thickness, and uniformity of pure chitosan coatings to the substrates based on different deposition techniques.

METHODOLOGY

CHITOSAN COATING DEPOSITION

The experimental tests were carried out by depositing the chitosan dissolved in solution on *Ti6Al4V* alloy sheets (annealed – ASTM B265). The sheets (substrates) have the following length, width, and thickness: 7.5 x 2.5 x 1.0 mm^3. Depending on the chosen methodology the coating will have different features in terms of: microstructure, surface morphology, mechanical properties, and micro-porosity [77].

The deposition techniques were executed on the substrates in as-manufactured conditions - surface properties of the substrates are not a subject of this case study- , under the same solution concentration, so that the mixture had fixed chemical-physical characteristics to obtain comparable results. The concentration of solutions, hence, is not part of the variables explored in this case study. After choosing the type of chitosan and the composition of the solution, the other suspension-related parameters are automatically set. Consequently, in these conditions, the final properties of coatings can be controlled through processing parameters only.

Before coating deposition, the sheets were treated with two sonication cycles using two different solutions of acetic acid and methanol, respectively. The aqueous solution for the deposition tests had the following composition: 1% (w/w) of chitosan with 700kDa molecular weight and DD 95% (Molekula Group, France); 1% (w/w) of acetic acid (Sigma Aldrich, USA); 98% (w/w) of distilled water [64], [78].

These proportions ensured the realization of a Newtonian solution to work with constant viscosity, thus eliminating a further degree of complexity. The pH of the solution was approximately 4.5 (monitored using litmus paper). Before the deposition, the solution was magnetically stirred to ensure the correct mixing, dispersion, and stabilization of the chitosan.

The coatings were realized through two different kinds of deposition methods: Electrophoretic Deposition and Dip Coating.

ELECTROPHORETIC DEPOSITION

The Electrophoretic Deposition (EPD) took place on horizontally positioned sheets to prevent the dripping from causing variation in the thickness along the length of the sample (Figure 18). Proper insulated sheet holders have been designed and 3D printed (Figure 19).

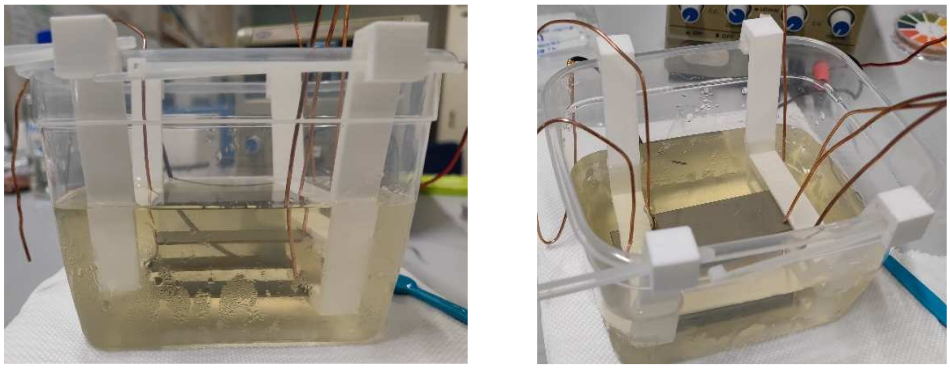

Figure 18. Electrophoretic deposition setup.

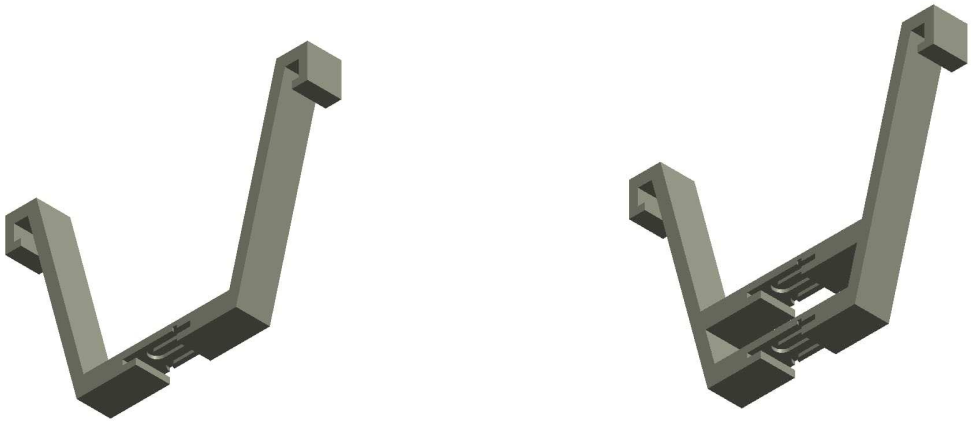

Figure 19. 3D printed sheets holders for EPD process.

To analyze the effect on the coatings quality, the parameters that were investigated during the EPD were the difference in potential applied and the processing time. The choices of numeric values of the processing parameters investigated are based on previous studies in the literature [62]–[64], [79].

As regards the applied voltage, the values of 5 V and 15 V were examined. Although each case study has specific differences in the choices of operating conditions, the previously mentioned values are within the range of values used in several experimental campaigns [64], [80]. No value above 15 V was used because exceeding this threshold, the formation of cracks and conglomerates is usually promoted [64]. The values of voltages chosen also allow to better appreciate the variation of coating thickness and properties by exploring the farthest conditions.

As concerns the processing time, the values of 1 min and 5 min were examined. The tests lasted no more than 5 minutes since, based on current literature, the deposition under similar conditions has a linear trend with the time until a maximum time of approximately 400 s; past that threshold, the growth of the deposit decreases owing to the shield that the coating thickness itself creates acting as an electrical resistance [79].

Moreover, several sources in the literature report ranges of analysis included between 30 s and 5 min, with optimum conditions around the time of 1 min processing [80].

An experimental campaign was realized by combining the two factors of applied voltage (V) and processing time (t). Using two values for the voltage and two values for processing time a matrix of tests was obtained (Table 5). The execution sequence of the tests was randomized to minimize the systematic errors.

Table 5. Parameters values used during the electrophoretic deposition tests.

t / V	5 V	15 V
1 min	1 min/ 5V	1 min/ 15V
5 min	5 min/5 V	5 min/ 15 V

DIP COATING

The dip coating tests (Dip) were performed by setting the substrates in a vertical position and by immersing each of them into a plastic vessel containing the solution to be deposited. The withdrawal speed was kept as constant as possible below 10 mm/s [65] to not introduce further processing variables. The investigated parameter in this case was the immersion time. The choice was to examine the time values of 1 minute and 5

minutes. No investigation was done under 1 minute to make sure that the substrate was completely wet from the chitosan solution. The choice of the value of 5 minutes comes from the willingness to check for a possible coating thickness increase while remaining within the range of analysis of literature studies [80], [81].

After the deposition phase, the samples were dried at room temperature for 24 hours, in dry air. This drying time is adequate to ensure the removal of the liquid phase and the formation of a coating with invariant features during the rest of the trial. For each processing condition, three replications were realized. The nomenclature of the tests is reported in Table 6.

Table 6. Nomenclature of the tests.

Technique	Nomenclature	Processing time [min]	Voltage applied [V]
EPD	EPD_Xmin_YV	X = 1, 5	Y = 5, 15
Dip	Dip_Xmin		-

As an example EPD_1min_5V stands for: sample coated through the Electrophoretic Deposition technique with 1 minute of processing time and 5V of applied voltage.

COATING ADHESION TESTING

Adhesion tests have been performed utilizing a micro-scratch tester (Anton Paar GmbH, Austria) through a Rockwell C tip (120°, 100 μm radius). Scratch testing, although qualitative, is considered an advantageous test means relating to usage conditions, in particular for orthopedic implants [82]. Coatings have been tested in a controlled laboratory environment (25°C temperature, 60% relative humidity). Each type of sample has been replicated three times to ensure statistical robustness. A number of 10 scratches, spaced at least by 5 times the scratch width, has been performed on each sample. The parameters selection was supported by a thorough campaign of preliminary tests, following ASTM D7027-20 [71] guidelines and literature. A linearly increasing load from 10 mN to 3000 mN has been applied, with a constant growth speed about equal to 1500 mN/min and a displacement rate of 10 μm/s [83].

Scratches have been analyzed employing an optical microscope to identify different failure mechanisms and critical loads with corresponding penetration depth from computed scratch curves. Average coating thickness was estimated employing an average penetration depth value, corresponding to curve flattening as the tip reaches the substrate.

RESULTS AND DISCUSSION

As concerns the coatings surface analysis, from the observation of the coatings through the optical microscope realized by electrophoretic deposition (EPD), only the experimental tests EPD_1min_5V (1 min of time processing and 5 V of voltage applied) produced free from bubbles homogeneous and uniform coatings. In almost all the other tests, which come from electrophoretic depositions performed with other time and voltage combinations, the formation of bubbles of different sizes occurred (Figure 20). Because of the presence of bubbles on the other types of samples, the EPD_1min_5V was the only combination screened through scratch tests. Most likely, the worsening of the EPD coating uniformity is due to the value of voltage equal to 15 V, which could have been an excessively high value affecting coating homogeneity [80], [84], despite its frequent use. As regards Dip coated samples, no defects were detected via optical observation but an improved quality of the coating was detected for 1 min of processing time, thus the 5 min processing time condition was screened out for scratch testing.

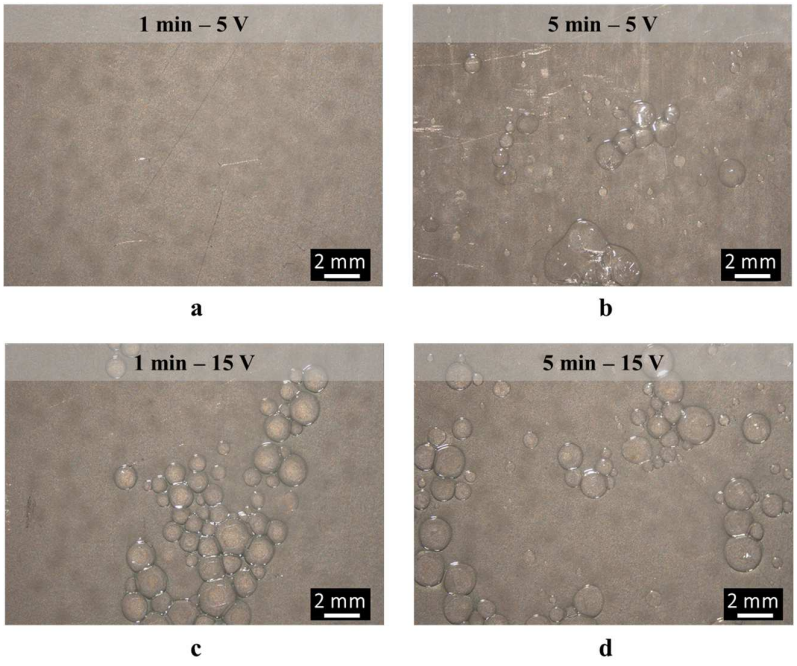

Figure 20. Macrographs of EPD coated *Ti6Al4V* for tests conducted at a) 1 min, 5 V, b) 5 min, 5 V, c) 1 min, 15 V, d) 5 min, 15 V.

Dealing with the scratch tests, the focus was on the trends of the normal load and the penetration depth. Specifically, the determinations from computed scratch curves were about (i) the critical normal load (L_c) at failure for the resistance estimation; and (ii) the

penetration depth at failure for the thickness estimation (t). By coupling the image of the scratch from the optical microscope and the graph produced by the instrument, it was possible to identify the point of failure and the corresponding values of load and penetration (Figure 21).

From the analysis of the realized scratch, the average values and the standard deviations of load and penetration depth at failure were calculated (Table 7). The percentage errors were estimated by computing the ratio between the standard deviation and the average value.

For each test, average values and the corresponding standard deviations were represented through histograms (Figure 22). As can be seen from the measurement results, current electrophoretic deposition conditions allow the realization of thicker coatings.

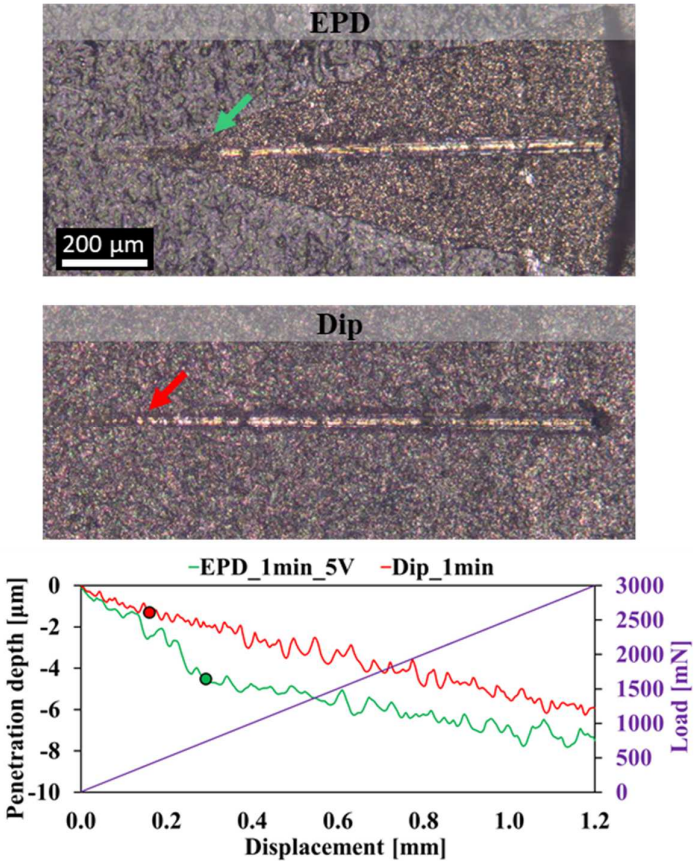

Figure 21. Scratch with the related graphs from tests EPD_1min_5V and Dip_1min. Coating failure onset is highlighted by arrows. Penetration depths at failure are denoted by markers.

Table 7. Results for the two deposition techniques: average values of the Critical Load (L_c) and the thickness (t) estimated via the Penetration Depth, with standard deviations in parentheses.

Technique	L_c [mN]	L_c % error	Estimated t [µm]	Estimated t % error
EPD	936 (43)	4.6 %	5.50 (0.47)	8.5 %
Dip	284 (17)	6.0%	0.99 (0.08)	8.1 %

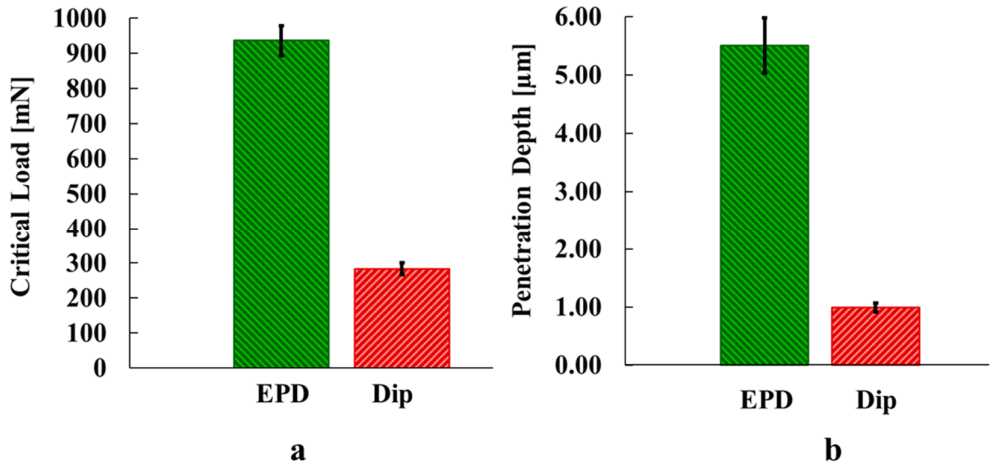

Figure 22. Results for the two deposition techniques: (a) average values of normal load at net adhesive failure and (b) average values of penetration depth at the point of net adhesive failure. The error bars represent the standard deviation.

During the scratch test, different phases and mechanisms of coating damage can be recognized (Figure 2): in the first stage there is the "elastic deformation"; when the load increases, the irreversible deformations of the "plastic deformation" stage start; the irreversible deformations culminate with the phenomena of coating cracking and chipping (cohesive failure of the coating material) but generally remaining adherent to the substrate. Later the propagation of cracks causes the full failure of the material which breaks up to detach from the substrate (adhesive failure) [29].

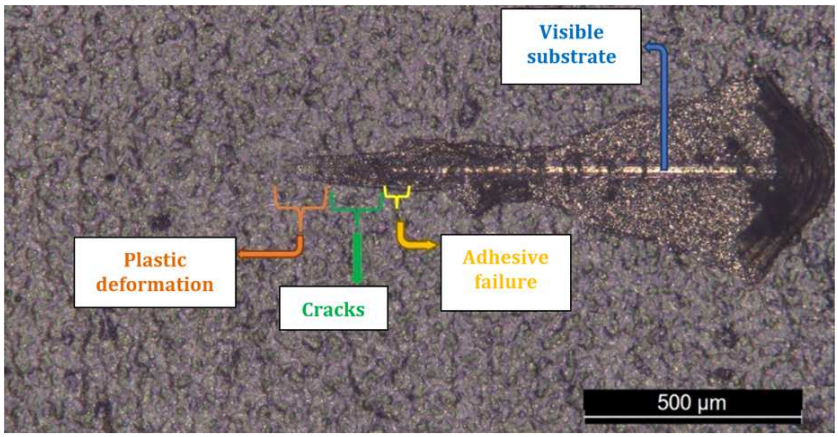

Figure 23. Identification of failure phases in a scratch test [85].

For the samples made by the Dip coating deposition technique, the visual identification of the scratches upon the sheets and the clear distinction of phases at the optical microscope were not as immediate. In the Dip samples, the cracking area was smaller than in the EPD samples and it was often almost indistinguishable from the plastic deformation zone. In some cases, the coating uncovered the substrate only for a very short distance; then the coating continued to compact again until the net and actual and continuous adhesive failure happened.

Another observation can be made by analyzing the numerical errors calculated and shown in Table 7. These errors facilitate the display of the weight that each standard deviation has compared to its average values. More in detail, the errors of the EPD and Dip coatings were of the same magnitude both for the critical load measure and for the estimated thickness. The scratch test results showed that, in these operation conditions, the EPD films are more resistant and thicker than the ones realized by Dip coating. On the one side, the different resistance may depend in some ways on the different thickness [29]. Previous studies in literature tried to correlate coating thickness and resistance; some of them found that the critical load of delamination increases as the thickness increases [33], which could be a reasonable motivation even looking at the results of the current study. But generally, since the coupled effect between the substrate and the coating in a thin layer introduces a great deal of complexity in the stress field [29], the precise relationship between the resistance of the coating and its thickness requires further investigation.

CASE STUDY II: SURFACE PROCESSING OF TI6AL4V TO TUNE COATING ADHESION

This case study describes a methodology to improve *Ti6Al4V* surface quality with different mechanical and thermal surface processes to get a reliable chitosan/bioglass composite coating. The overall treatments modified the surface roughness, texture, and chemical characteristics to a different extent influencing the coating adhesion probed via scratch test.

METHODOLOGY

SURFACE MODIFICATION

The material used in this work is the Titanium Grade 5 *Ti6Al4V* alloy (forged, rolled, and annealed – ASTM B348) in the shape of discs (20 mm diameter, 6 mm thickness) extracted from a round bar. The microstructure of the starting samples consists of α grains with intergranular β. Four preparation processes were studied, namely face milling, grit-blasting, electrical discharge machining, and polishing to study the effects of different surface processing techniques on the coating-substrate system behavior (published results in ref. [72]). All samples were previously ground up to F2000 grit size to reduce the variability in initial surface conditions before further surface processing.

FACE MILLING

The face milling process has been conducted on a CNC Mazak vertical machining center, employing a commercial carbide milling cutter coated with *TiAlSiN*, 16 mm diameter – D (Product code WZF 126486 - Meusburger Georg GmbH & Co KG, Austria) and four cutting edges (Z – number of cutting edges).

To differentiate between the high surface finish obtained by polishing and try to introduce mechanical interlocking effects with the coating, roughing conditions have been chosen for milling. As per the manufacturer's advice for the specific cutting tool and following the recommendations in [38], the parameters were chosen as: cutting speed V_c = 60 m/min, depth of cut a_p = 0.1 mm, table feed V_f = 250 mm/min (Table 8). Flood lubrication was employed.

A single pass was performed to not introduce surface texture alterations caused by the interaction of multiple passes and a fresh tool was used for each test. To confirm process repeatability and the absence of chattering effects, milling forces were monitored through a six-components piezoelectric dynamometer (Kistler© 9257 - *Kistler*, Switzerland), as shown in the experimental setup in Figure 2.

Table 8. Experimental test conditions for milling.

Milling parameter	**Roughing**
Cutting speed – V_c [m/min]	60
Depth of cut – a_p [mm]	0.10
Table feed – V_f [m/min]	250
Sample name	**R**

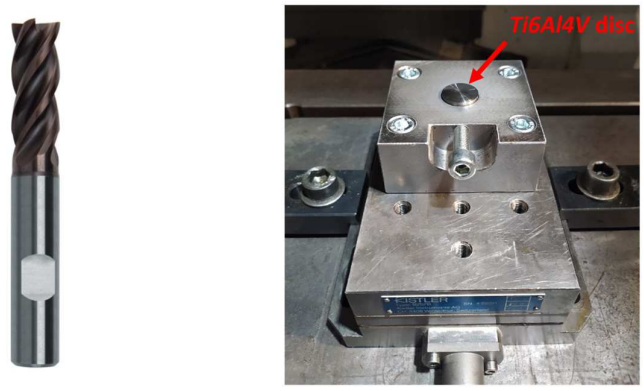

a **b**

Figure 24. Images of the (a) cutting tool and (b) the experimental setup for face milling.

GRIT BLASTING

Grit blasting (GB) was performed using a Fervi 0687 (Fervi, Italy) sandblaster and aluminum oxide Al_2O_3 particles (F36 grit size), performing two passes of 10 s each, with a 90° angle. Air pressure was set to 0.3 MPa [86], while the sample-nozzle distance was set to 60 mm.

ELECTRICAL DISCHARGE MACHINING

For electrical discharge machining (EDM), a die sinking process (AEG ELOTHERM ELBOMAT 303) was selected, using a flat copper electrode and a commercial dielectric fluid specific for EDM (Electroflux TE), with fully submerged electrodes and side flushing (Figure 25). According to preliminary tests, manufacturer's advice, and literature [87], pulse duration (tON) and pulse interval (tOFF) were set respectively equal to 25 µs and 16 µs, while a voltage of 135 V was employed, reaching a discharge current up to 2 A.

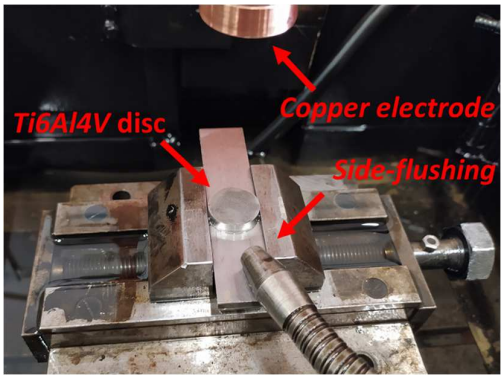

Figure 25. Experimental setup for die sinking Electrical Discharge Machining.

CHITOSAN/BIOGLASS COATING DEPOSITION

The experimental tests were carried out by depositing a Chitosan/Bioglass in solution on the treated *Ti6Al4V* discs (substrates). Tested substrates were subjected to different surface modification processes to assess the effects of substrate surface properties on the overall substrate-coating system.

A 0.7% solution of chitosan (medium molecular weight, 75-85% degree of deacetylation, Sigma Aldrich, USA) in 1% acetic acid was prepared. The solution was kept under magnetic stirring in an oil bath, at 40°C overnight [88]. It was then centrifuged, adding to the supernatant 0.3% of bioactive glass nanoparticles (nBG - 77 wt% SiO_2, 14 wt% CaO, 9 wt% P_2O_5, particle size below 100 nm). The mixture was kept under agitation overnight and then sonicated at 40°C for 20 minutes [89].

2 ml of solution was used to coat each *Ti6Al4V* support by the solution casting method. Substrates were previously sonicated in distilled water and ethanol bath for 15 minutes, for 3 times respectively. The process of coating consisted of measuring 2 ml of solution

using a pipette and then dropping and gently stretching the solution to cover the surface of the substrates. The coated discs were then dried in an oven at 80°C for 7 hours [90].

SUBSTRATE – COATING CHARACTERIZATION

SUBSTRATE CHARACTERIZATION

Each type of processed *Ti6Al4V* sample was cut perpendicularly to the treated face, embedded on a black bakelite mounting resin, and mechanically polished up to 0.5 μm grade. Nano-hardness was probed along the depth below the surface (10 replications for each depth value) through an NH^2 CSM Nanoindentation Platform (*Anton Paar GmbH*, Austria) equipped with a Berkovich diamond tip. Indentations were performed at a maximum load of 50 mN with 10 s of dwell time [29], [91]. For microstructural analysis, the polished samples have been etched employing Kroll's reagent (100 ml H_2O, 3 ml HF, 6 ml HNO_3) and analyzed through an optical microscope.

Furthermore, a Confovis structured light profilometer connected to a Nikon Eclipse LV150N microscope was employed to obtain areal surface texture parameters (scanned area size: 0.5 mm x 0.5 mm, four replications). The analyzed parameters are recalled in Table 9.

The images of the non-sectioned surfaces were taken using a scanning electron microscope (ESEM Quanta-200 - Fei Oxford Instruments), equipped with the detector for EDS analysis (X-EDS Oxford INCA-350), which was performed on different areas of the samples (area size: 400 μm x 520 μm) to confirm the surfaces' composition. The EDS analysis was combined with μRaman spectroscopy (LabRam - Jobin-Yvon, France) employing a 532 nm wavelength and 40 mW power laser (3 replications for each scan, each of 10 s duration, in the region 100 - 1600 cm^{-1}).

Contact angle (CA) was quantified employing the sessile drop technique (DSA30S – Krüss Scientific, Germany): drops of 1 μl of the chitosan/bioglass solution used for coating were delivered on substrate surfaces performing five repetitions for each sample. For milled surfaces, due to texture anisotropy, five measurements were made for each of the two directions: direction 1 (D1) and direction 2 (D2) parallel and orthogonal to the machining direction, respectively.

Table 9. Areal height surface parameters analyzed in this case study, their classification and meaning according to current standards [92], [93], [94].

Symbol	Units	Description
Sa	[µm]	The arithmetic mean height of the surface, aka average roughness. An overall measure of the texture comprising the surface.
Sz	[µm]	Maximum height: distance between the highest peak and the lowest valley within the data. Maximum height, Sum of the largest peak height value and the largest pit depth value. Each value is generated from two single points and is often unrepeatable.
Sq	[µm]	Root Mean Square (RMS) height: standard deviation of the surface height. The RMS height of all data points from the mean surface height, aka RMS roughness. An overall measure of the texture comprising the surface.
Ssk	[-]	Skewness is a measure of the asymmetry of surface deviations (height distribution) about the mean plane. Figuratively, the shift of the heights of all measured points to lower or higher values compared in an ideal bell curve distribution. Higher skewness values indicate higher protruding spikes on the surface.
Sku	[-]	Kurtosis of the height distribution relative to *Sq* is a measure of the predominance of extreme peaks or pits for all measured points compared to an ideal bell curve distribution. Higher Kurtosis values correspond to a surface with more spikes while lower Kurtosis values are related to a surface with bumps.

COATING ADHESION TESTING

Adhesion tests have been performed utilizing a micro-scratch tester (Anton Paar GmbH, Austria) through a Rockwell C tip (120°, 100 µm radius). Coatings have been tested in a controlled laboratory environment (25°C temperature, 60% relative humidity). Each type of sample, that is polished (P), face milled (M), grit blasted (GB) and EDM treated (EDM) coated with the chitosan-based material has been replicated three times to ensure statistical robustness.

A number of 10 scratches, spaced at least by 5 times the scratch width, has been performed on each sample. Additional tests were performed on milled surfaces to assess the anisotropy in adhesion. The parameters selection was supported by a thorough campaign of preliminary tests, following ASTM D7027-20 [71] guidelines and literature. A linearly increasing load from 10 mN to 5000 mN has been applied, with a constant growth speed about equal to 1500 mN/min and a displacement rate of 10 µm/s [83].

Scratches have been analyzed employing an optical microscope and a SEM ZEISS Crossbeam 350, to identify different failure mechanisms and critical loads with corresponding penetration depth from computed scratch curves. Average coating

thickness has been estimated employing an average penetration depth value, corresponding to curve flattening as the tip reaches the substrate.

RESULTS AND DISCUSSION

SURFACE PROPERTIES AFTER PROCESSING

Processing of samples, as expected, brought a wide range of surface modification mechanisms as seen in the top row of Figure 25 showing the processed surface (magnifications in red rectangles). The microstructure of the P, R, and GB samples is unchanged with α equiaxed grains and intergranular β. Surface grain distortion distinctive of the plastic deformation processes is highlighted with dotted lines in Figure 26 of cross-sectioned P, R, and GB samples.

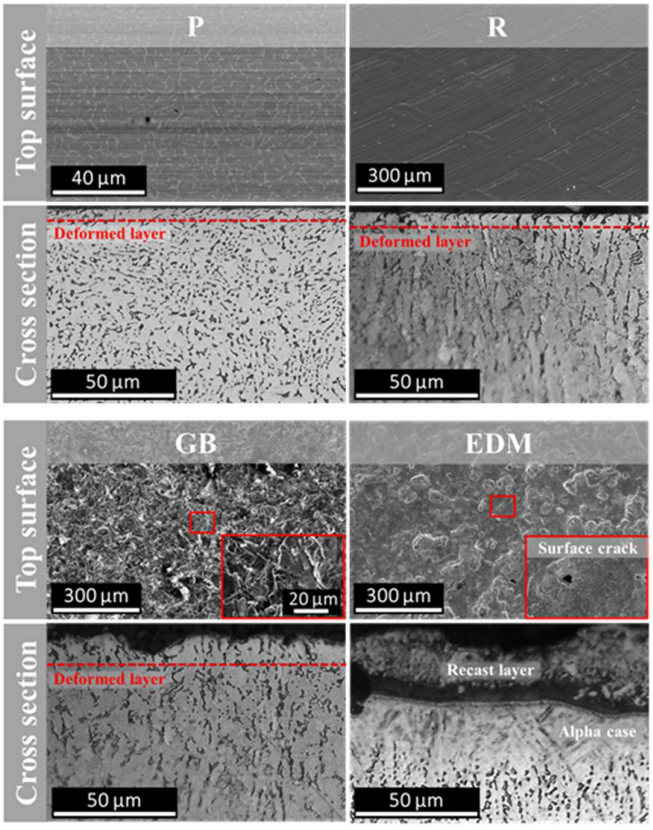

Figure 26. Images of *Ti6Al4V* substrates after processing: SEM images of the worked surface in the top rows and micrographs of cross-sectioned and etched samples in the bottom rows [72].

The significant cold working after the face milling process is confirmed by the nano-hardness profile, reaching values up to 5.8 GPa below the surface. The hardness profile

for P and GB samples is nearly unaffected, except for a few µm thick layer, not detected by the instrument (Figure 27) although the deformed portion of GB is larger.

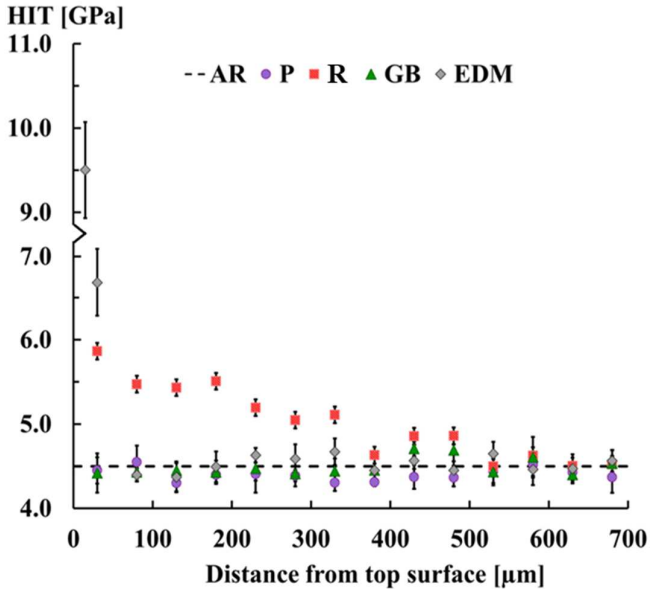

Figure 27. Nano-hardness profiles of *Ti6Al4V* substrates after processing, compared to as received (AR) conditions. Reported error bars represent the standard deviation [72].

Concerning EDM samples, the formation of a thick recast layer of hard and fragile titanium oxide with an average thickness of 19.0 ± 2.9 µm was detected. A transformation zone (alpha case) is confirmed by the presence of acicular alpha and the layer has an average thickness of 16.8 ± 1.4 µm. The presence of surface and subsurface cracks is recognizable in the rectangle magnification in Figure 26 and Figure 28 as pointed by the arrows.

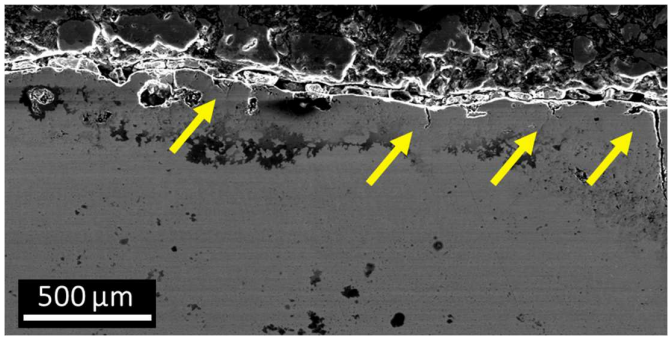

Figure 28. SEM image of *Ti6Al4V* after EDM processing: cross-section of the substrate with subsurface cracks [72].

The combination of EDS analysis and μRaman spectroscopy was used to better assess the surface of the samples in terms of chemical alteration and oxide formation. More in detail, Figures 29 to 32 show the analysis in areas of interest of samples P, M, GB, and EDM, respectively. The EDS mapping of polished samples displays, as expected, a negligible presence of oxygen, and, connected to this result, the Raman spectrum shows no signal, thus evidencing the absence of rutile titanium dioxide [95]. The same results were obtained for the milled surface.

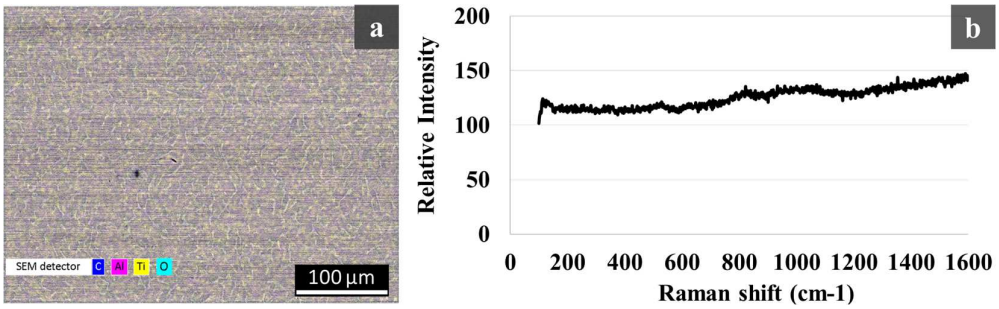

Figure 29. Polished *Ti6Al4V* surface (a) EDS mapping (b) Raman spectra [72].

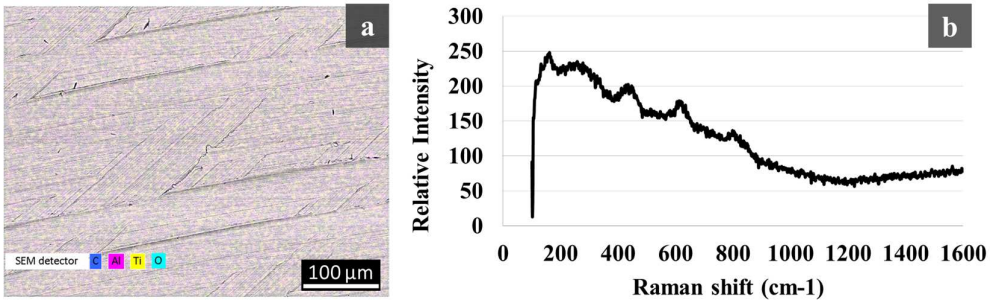

Figure 30. Milled *Ti6Al4V* surface (a) EDS mapping (b) Raman spectra [72].

Instead, from EDS mapping of the GB sample, a great amount of oxygen was detected (Figure 31a), confirmed by the Raman spectrum with the peak of alumina [96], [97], an oxide present in the sample as a processing residue. To confirm this, it is worth noting that the percentage of aluminum in the grit-blasted sample was doubled to the standard value for *Ti6Al4V* obtained in both polished and milled ones. From EDS mapping of the EDM-treated surface (Figure 32b), copper and oxygen residuals have been detected because of tool-electrode material and rapid oxidation on contact with air, respectively. The Raman spectrum detected the three peaks of rutile in good agreement with the findings of the literature about the characterization of the recast layer of titanium samples processed with EDM [98].

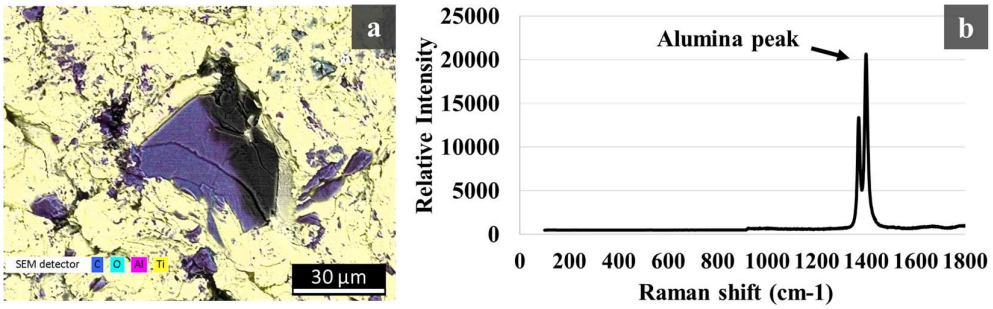

Figure 31. Grit-blasted *Ti6Al4V* surface (a) EDS mapping (b) Raman spectra [72].

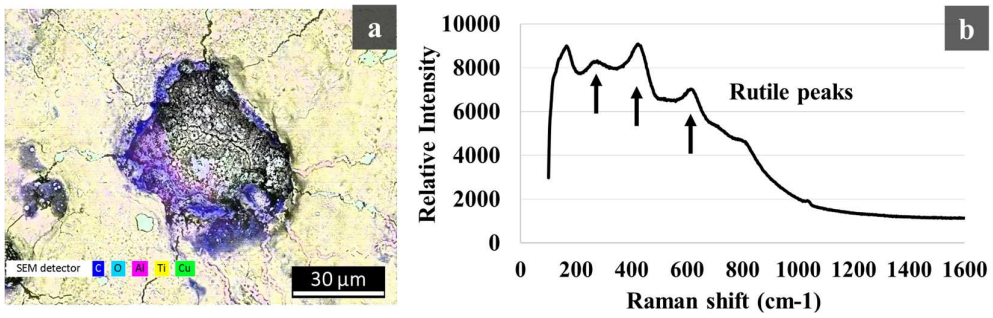

Figure 32. EDM treated *Ti6Al4V* surface (a) EDS mapping (b) Raman spectra [72].

Surface morphology after sample processing is shown in Figure 33 and the main parameters are reported in Table 10. As reasonably expected, the lowest and most regular distribution is found for polished ones, followed by the grid-like texture for milling. Surface unevenness finds a maximum for EDM-treated surfaces, together with the highest maximum height. The high standard deviation found for polished surfaces in terms of *Sz*, *Sku*, and *Ssk* depended on random imperfections and notched areas that strongly influenced their calculation. On the contrary, the values of *Sa* and *Sq*, less influenced by these random imperfections, showed an acceptable standard deviation, confirming the regular distribution and the low roughness of the polished surface.

Regarding the contact angle (Figure 34), the lowest value was found for GB samples, obtaining 26°. P and EDM samples show comparable values, 50° and 53° respectively. The lowest wettability was found for R samples, showing contact angles above 60° in the direction parallel to tool passes (D1), values further increased in the direction orthogonal to tool passes (D2).

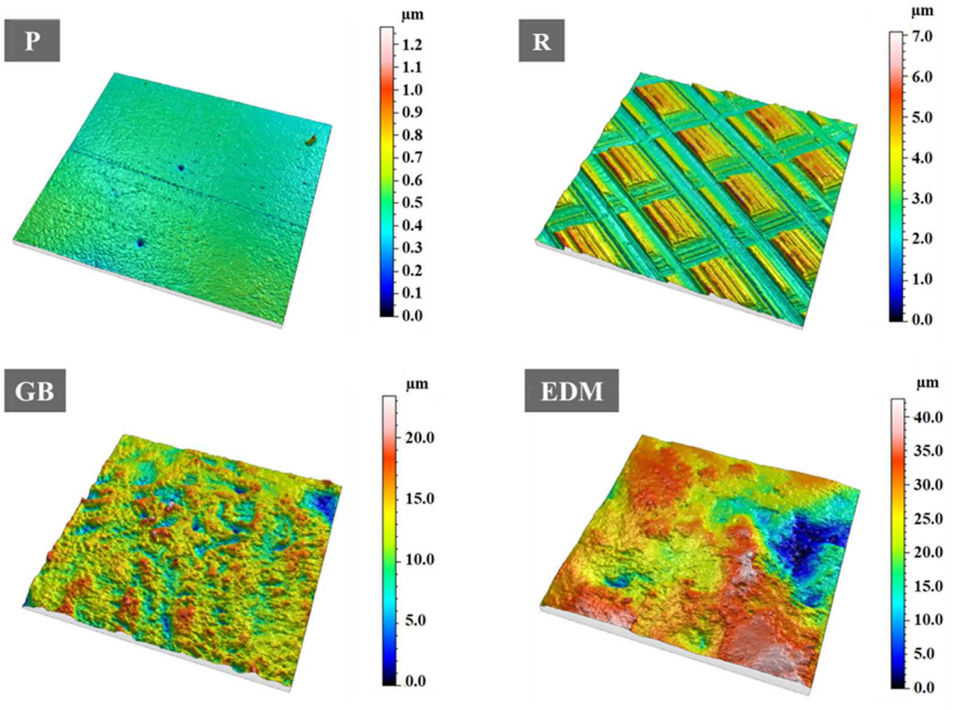

Figure 33. Surface roughness distribution for processed *Ti6Al4V* samples, scanned area size: 0.5 mm x 0.5 mm [72].

Table 10. Surface roughness parameters for processed samples - height parameters following ISO 25178: *Sa* Arithmetical mean height, *Sz* Maximum height, *Sq* Root Mean Square height, *Ssk* Skewness, *Sku* Kurtosis [72]. The standard deviation is reported in parentheses.

Roughness parameter	**P**	**R**	**GB**	**EDM**
Sa [µm]	0.05 (0.01)	0.68 (0.04)	2.26 (0.16)	5.97 (1.09)
Sz [µm]	1.51 (0.79)	6.82 (0.37)	26.72 (1.21)	46.12 (5.67)
Sq [µm]	0.06 (0.01)	0.80 (0.04)	2.95 (0.18)	7.47 (1.28)
S_{sk} [-]	-0.32 (0.66)	0.80 (0.07)	-0.45 (0.17)	-0.58 (0.40)
S_{ku} [-]	11.18 (12.18)	2.22 (1.00)	3.91 (0.19)	3.27 (0.85)

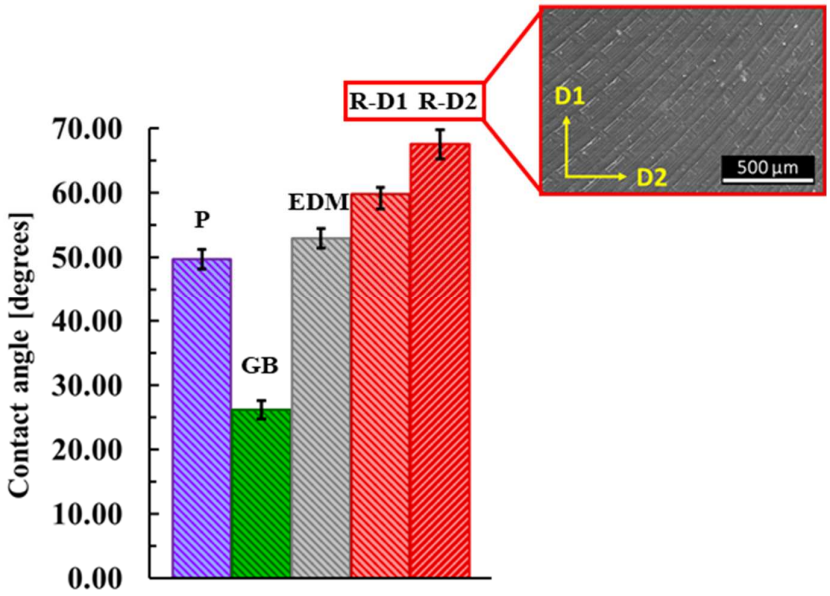

Figure 34. Chitosan/bioglass solution contact angle for treated surfaces measured in a controlled laboratory environment (25°C temperature, 60% relative humidity). Reported error bars represent the standard deviation [72].

COATING ADHESION

Coating failure mechanisms are the same for each type of pretreated substrate, apart from variations in critical loads: (i) initial plastic deformation and plowing, (ii) cohesive failure, showing transversal and longitudinal cracks that interconnect at a critical load, (iii) adhesive failure, with formerly surface cracks reaching the substrate and complete detachment of the coating. An example of results from a scratch test is reported in Figure 35, showing the pile-up phenomenon from the onset of plastic deformation to the end of the scratch from the SEM image. Peaks in the penetration depth plot indicate accumulation of coating debris during the test. Due to a partial elastic recovery after the test, the metallic substrate is not readily visible from the SEM image, its damage has been assessed optically after the complete removal of the coating.

Coating thickness reaches a value of 45.00 ± 2.15 µm, computed based on scratch test results obtained from each sample. Thickness results from scratch tests were validated by analyzing the cross-section of the coated samples.

A low amount of variation of thickness occurs from one sample to another but, to consider this factor, critical loads for cohesive and adhesive failure have been normalized for the estimated coating thickness of each sample.

Polished (P) and milled (R) coated samples show similar behavior and, in the ending phase of testing, the coating is easily detached and raised from the substrates; milled ones perform better, due to the peculiar surface morphology of the process but failure load was not affected by the direction of the texture as opposed to contact angle. The best case is represented by grit-blasted (GB), of which normalized critical loads exceed EDM by 36% and polished by 18% (Figure 36). Also, coatings on P, R, and EDM samples were gradually completely detached from substrates under vacuum conditions required for SEM analysis, below $2 \cdot 10^{-3}$ Pa. The same did not happen for GB samples.

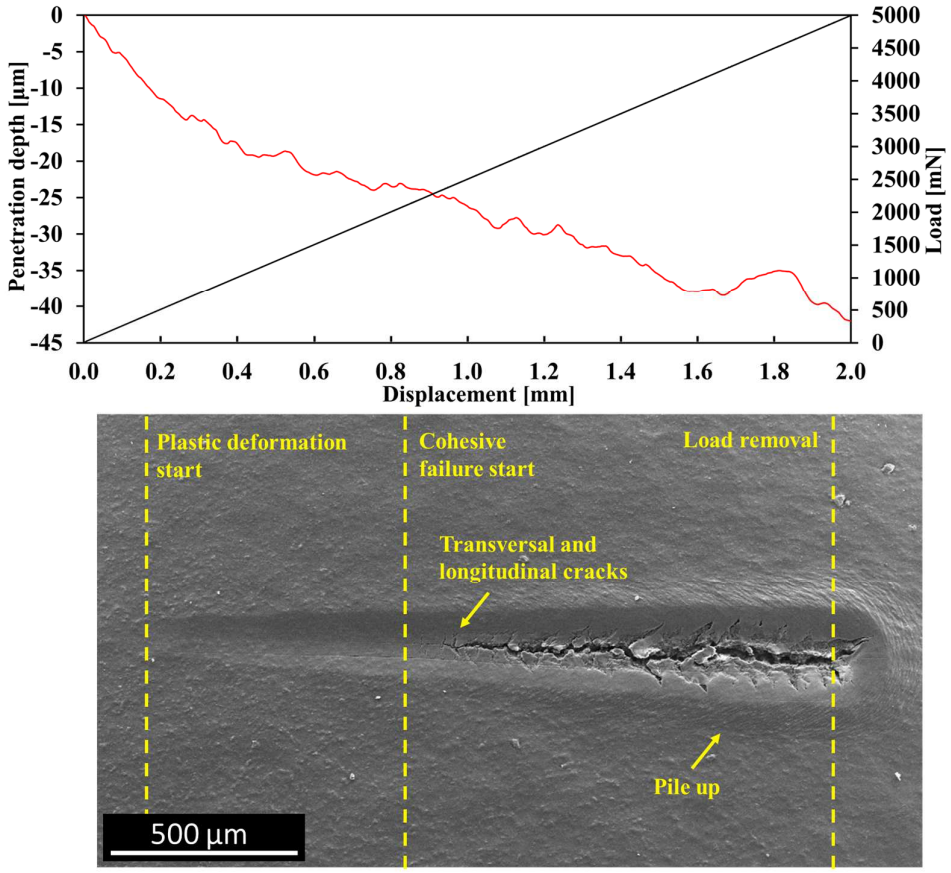

Figure 35. SEM image of a GB sample coated with Chitosan/Bioactive glass nanoparticles after scratch testing, different failure mechanisms are highlighted, and the representation is combined with load/penetration depth graphs plotted against tip displacement [72].

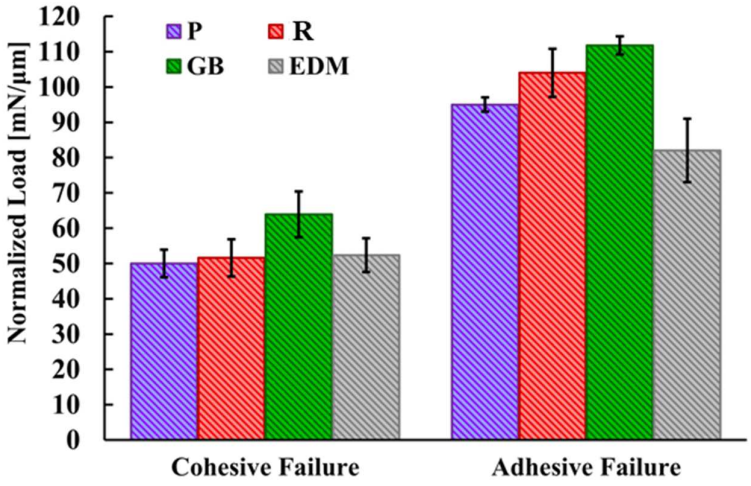

Figure 36. Critical scratch loads for different failure mechanisms of Chitosan/Bioactive glass nanoparticles coating, normalized to coating thickness. Reported error bars represent the standard deviation [72].

Ideally, cohesive failure i.e., the onset of cracking of the coating, is expected to be unrelated to substrate surface characteristics, however, slight changes in coating thickness can lead to a change in the cohesive critical load. Also, the coating used herein was, by nature, inhomogeneous in terms of slight changes in bioactive glass particles distribution in the layer, causing possible variation in the cohesive failure.

Analyzing adhesive failure, the worst behavior is given by the presence of EDM-treated substrates as processing conditions bring the growth of a surface oxide layer with poor mechanical properties, resulting in multiple crack formation on both coating and substrate, indicating the unsuitability of the EDM process parameters to properly treat the samples for the specific application. This layer can be easily detached together with the coating, nullifying the effects of mechanical interlocking provided by the higher surface roughness and surface area.

The improved behavior of GB samples can be due to a combination of factors. The grit blasting process was able to more effectively generate a surface prone to make intimate contact with the coating due to mechanical interlocking given by the peculiar surface texture and is demonstrated to be effective in improving coating adhesion [86]. Also, scratch results partially follow the trend of contact angle values, having GB surfaces with a good capability to be wetted by coating solution. The grit blasting process, due to its easy and inexpensive implementation has several upsides and its combination with chemical etching can bring the generation of a well-performing surface but care should be taken in terms of the presence of debris from the blasting medium [22].

Polished samples exhibited a low adhesion strength as the poor chemical affinity of *Ti6Al4V* and the low surface energy usually displayed by the mirrored surface together with no mechanical interlocking effect lead to unsuccessful coating adhesion.

The overall results for milling and EDM show a slight increase in strength compared to polishing, due to a more effective texturing of the surface. In fact, in both cases, mechanical texturing is the driving effect for the coating adhesion so that the delamination load is similar. However, the randomized texture obtained by grit blasting leads to better results since it allows to increase the energy needed for an open crack in the coating to propagate faster. In fact, grit blasted samples showed 18% and 36% higher normalized critical load with respect to polished and EDM treated samples, respectively.

CASE STUDY III: SURFACE PROCESSING OF TI6AL4V TO TUNE CELL RESPONSE

This case study reports an analysis of the response of osteoblastic cells and gram negative bacteria to different surface modification processes. The material used is the *Ti6Al4V* alloy (forged, rolled, and annealed – ASTM B348) in the shape of discs (20 mm diameter, 6 mm thickness) extracted from a round bar. The microstructure of the starting samples consists of α grains with intergranular β. Different outcomes in terms of response to surfaces might be attributed to the different physical properties of specific bone cell types and bacterial species, and thus the focus of this work will be on: MG63 osteoblast-like bone cells and a Gram-negative bacterial species, the Escherichia Coli (strain K-12). Three preparation processes were studied for bone cells response, namely face milling with surface finishing parameters, grit-blasting, and polishing. For the Escherichia Coli response, the selected processes were face milling with roughing parameters, laser texturing, and polishing [99]. In fact, laser treatments of biomaterial surfaces are appealing as they permit effective patterning and the production of hierarchical surface textures [75][100].

BONE CELLS: MG63

METHODOLOGY

SURFACE PROCESSING OF TI6AL4V

Each processing condition was replicated five times. All samples were previously ground up to F2000 grit size to reduce the variability in initial surface conditions before further surface processing. As regards the polishing samples, they were polished up to 0.5 μm grade.

FACE MILLING

The face milling process has been conducted on a CNC Mazak vertical machining center, employing a commercial carbide milling cutter coated with *TiAlSiN*, 16 mm diameter –

D (Product code WZF 126486 - Meusburger Georg GmbH & Co KG, Austria) and four cutting edges (Z – number of cutting edges).

Finishing parameters have been chosen as per the manufacturer's advice on optimum conditions for the specific cutting tool: cutting speed V_c = 120 m/min, depth of cut a_p = 0.05 mm, table feed V_f = 600 mm/min.

Tests with a cutting speed of V_c = 60 m/min were additionally made, with other parameters fixed, to compare their effects on the obtained surface features (Table 11). Flood lubrication was employed.

A single pass was performed to not introduce surface texture alterations caused by the interaction of multiple passes and a fresh tool was used for each test. To confirm process repeatability and the absence of chattering effects, milling forces were monitored through a six-components piezoelectric dynamometer (Kistler© 9257 - *Kistler*, Switzerland), as shown in the experimental setup in for Case Study II in Chapter IV.

Table 11. Experimental test conditions for milling.

Milling parameter	**Finishing**	
Cutting speed – V_c [m/min]	60	120
Depth of cut – a_p [mm]	0.05	
Table feed – V_f [m/min]	600	
Sample name	**F60**	**F120**

GRIT BLASTING

Grit blasting (GB) was performed using a Fervi 0687 (Fervi, Italy) sandblaster and aluminum oxide Al_2O_3 particles (F36 grit size), performing five passes of 10 s each, with a 90° angle. Air pressure was set to 0.3 MPa [86], while the sample-nozzle distance was set to 50 mm.

CHARACTERIZATION OF SURFACE PROCESSED TI6AL4V

Each type of processed *Ti6Al4V* sample was cut perpendicularly to the treated face, embedded on a black bakelite mounting resin, and mechanically polished up to 0.5 μm grade. Nano-hardness was probed along the depth below the surface (10 replications for each depth value) through an NH^2 CSM Nanoindentation Platform (*Anton Paar GmbH*,

Austria) equipped with a Berkovich diamond tip. Indentations were performed at a maximum load of 50 mN with 10 s of dwell time [29], [91]. For microstructural analysis, the polished samples have been etched employing Kroll's reagent (100 ml H_2O, 3 ml HF, 6 ml HNO_3) and analyzed through an optical microscope.

To study the surface texture, a Sensofar S neox 3D optical profilometer (*Sensofar*, Spain) was used in confocal mode, scanning three different areas on each processed sample, with five replications for each processing condition (scanned area: 1.7 x 1.3 mm^2). The data have been filtered according to ISO 25178 adopting a S-filter of 2.5 µm and a L-filter of 80 µm to obtain areal roughness parameters. Areal parameters investigated are reported in Table 12.

Backscattered Scanning Electron Microscopy (BSD-SEM) and Energy Dispersive X-ray (EDX) analysis were performed using a Phenom ProX SEM (*Thermo Fisher Scientific*, US) to assess compositional variations due to processing.

Contact angle (CA) was measured through the sessile drop technique via a Drop Shape Analyzer (DSA30S – *Krüss Scientific*, Germany): drops of 1 µl of distilled water were gently placed on *Ti6Al4V* treated surfaces performing five measurements for each sample and five replications for each processing condition.

Table 12. Areal height surface parameters analyzed in this work, their classification and meaning according to current standards [92], [93], [94].

Symbol	Units	Description
Sa	[µm]	The arithmetic mean height of the surface, aka average roughness. An overall measure of the texture comprising the surface.
Sq	[µm]	Root Mean Square (RMS) height: standard deviation of the surface height. The RMS height of all data points from the mean surface height, aka RMS roughness. An overall measure of the texture comprising the surface.
Sz	[µm]	Maximum height: distance between the highest peak and the lowest valley within the data. Maximum height, Sum of the largest peak height value and the largest pit depth value. Each value is generated from two single points and is often unrepeatable.
Ssk	[-]	Skewness is a measure of the asymmetry of surface deviations (height distribution) about the mean plane *Sq*. Figuratively, the shift of the heights of all measured points to lower or higher values compared in an ideal bell curve distribution. Higher skewness values indicate higher protruding spikes on the surface.

The *Sa* is used for machined surfaces, while the *Sq* is typically used to characterize optical surfaces. Together these parameters are used to take into account, without loss of

information, the effects of the different mechanical processes performed on the samples. The *Sz* is exploited to bring out if the cell proliferation is hindered by high peaks or deep valleys. The *Ssk* is typically useful in specifying honed surfaces and monitoring for different types of wear conditions, as well as lubricants and tribological tests. In this application, this parameter is reported to verify how surface asymmetry and protruding spikes affect cell adhesion and proliferation and cell shapes when attached to the surfaces.

CELL CULTURES

Ti6Al4V samples were immersed in absolute ethanol for 24 hours, then they were steam autoclaved and UV dried before cell culture.

The osteoblast-like osteosarcoma MG63 cell line was used for the in vitro tests. Cells were cultured in Dulbecco's Modified Eagle Medium (DMEM – *Euroclone*, Italy) with 10% heat-inactivated fetal bovine serum (FBS – *Euroclone*, Italy). *Ti6Al4V* samples were entered into a 12-well cell polystyrene culture plate (*Corning*, US) and $5x10^4$ cells in 200 µl of culture medium were seeded onto the surface of processed *Ti6Al4V* discs. Samples were left to sit for 2 hours, using well plates of the same size as the control.

After this first stage, further culture medium was added to ensure the whole coverage of the samples into a 12-well cell culture plate (final volume 1 ml). Samples were then incubated at 37°C in a 5% CO_2/95% air-humidified atmosphere for 48 hours. Subsequently, Cell Counting Kit - 8 (CCK8 – *Elabscience*, US) for quantification of viable cell number in proliferation was used, coupled with absorbance measurement at 450 nm (Infinite 200 Pro - *Tecan Trading AG*, Switzerland). Three replications were performed.

May Grunwald-Giemsa staining (MGG QUICK STAIN – *Bio Optica*, Italy) was performed to visualize the cells on *Ti6Al4V* discs and control them using an optical microscope.

RESULTS AND DISCUSSION

SURFACE PROPERTIES AFTER PROCESSING

As concerns microstructural properties after processing, the presence of a plastic deformed layer can be seen in Figure 37b and 37c, remarked by grain distortion. The base material microstructure was preserved during processing.

Nano-indentation performed on the cross-section provides a reliable trend on hardness modifications induced by the processes. The variation of nano-hardness below the surface (Figure 38) shows a more marked effect of the milling process on material hardening compared to grit blasting, with a maximum HIT increase of 11% compared to bulk hardness. Nano-hardness of milled samples (F) gradually decreases with increasing depth below the surface, reaching the average reference value of 4.0 GPa denoted as the hardness of the as-received material (AR). The variation between the samples milled at 120 m/min (F120) and 60 m/min (F60) shows a marked effect of higher cutting speed on HIT.

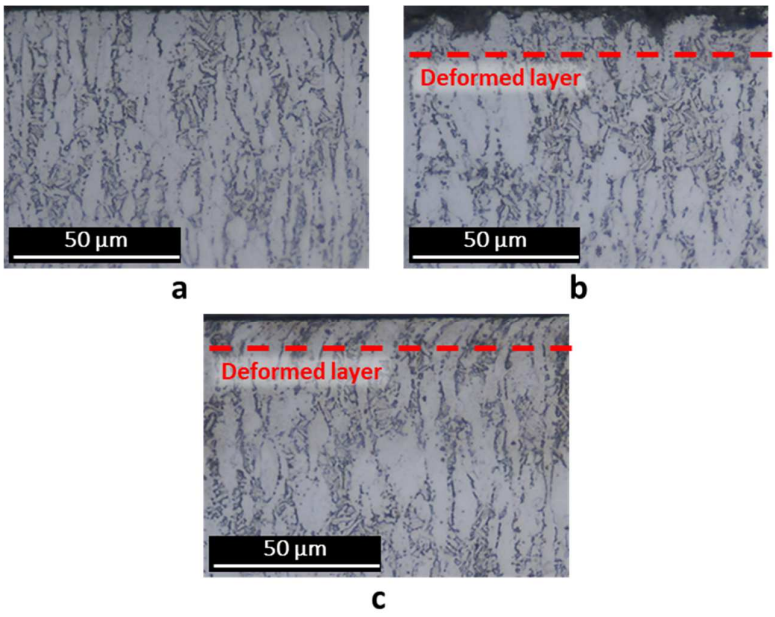

Figure 37. Cross-section and microstructure of *Ti6Al4V* samples: (a) polished – P, (b) grit-blasted – GB and (c) milled – F.

Grit-blasting induced texture of random craters and plastic deformation marks due to the impact of abrasive particles, as shown in Figure 39b. Milled samples exhibit a grid-like and periodic surface texture with rectangular ridges of varying size, originating from the roto-translational motion of the cutting tool.

On the milled samples two main areas, each with a peculiar texture shape, were identified and reported in Figure 40.

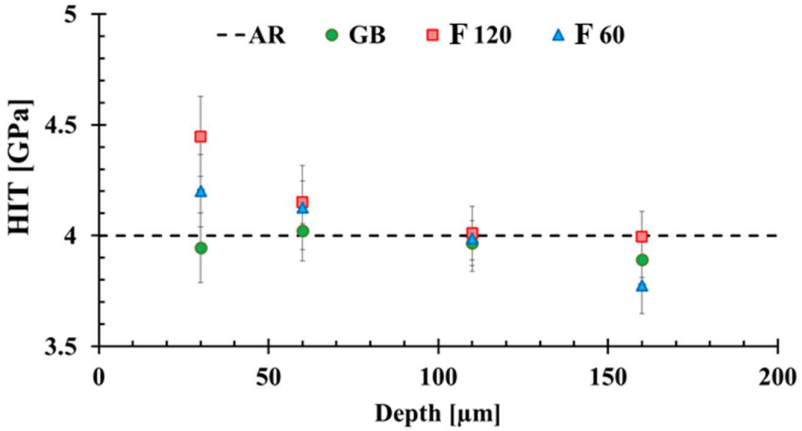

Figure 38. Nano-indentation hardness measured along the cross-section of treated samples compared to as received (AR) bulk hardness. Error bars represent the standard deviation.

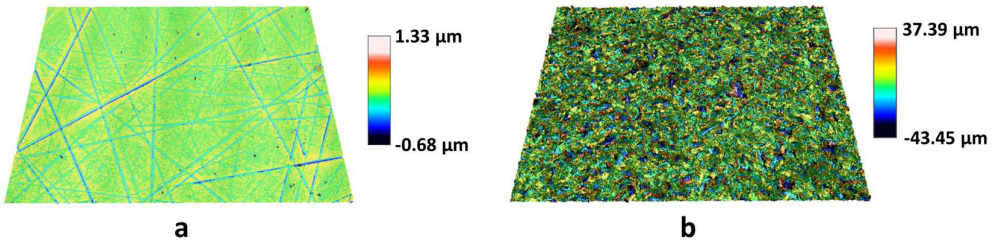

Figure 39. 3-D surface maps of *Ti6Al4V* treated samples: (a) polished – P, (b) grit-blasted – GB. Scanned area size: 1.70 mm x 1.30 mm.

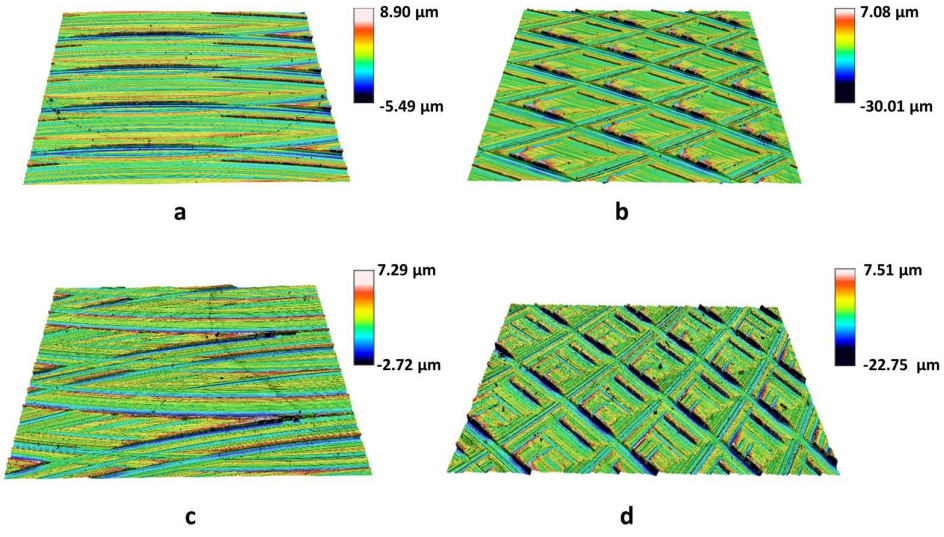

Figure 40. 3-D surface maps of *Ti6Al4V* treated samples: (a, b) F120 and (c, d) F60 on different areas of the same sample. Scanned area size: 1.70 mm x 1.30 mm.

Height parameters in Table 13 and Figure 41, span three orders of magnitude, and as such, they can provide a wide range of surface finish to compare. In particular, the above concerns *Sa* and *Sq*, for which the minimum is given by P as expected, with *Sa* 0.02 µm and *Sq* 0.03 µm, increasing with milled samples and then GB (Table 13).

The growing trend is reflected in *Sz*, further confirmed by the high dispersion between sample replications. Nevertheless, it is useful to note that the maximum height of the features in F (*Sz* 20.69 µm) and GB (*Sz* 72.45 µm) is in the same order of magnitude as the studied cells and then it is able to exert an influence on their behavior [101].

As regards the F120 and F60 mean areal surface height parameters are higher for F60.

Table 13. Surface roughness parameters for processed samples - height parameters following ISO 25178: *Sa* Arithmetical mean height, *Sq* Root Mean Square height, *Ssk* Skewness, *Sz* Maximum height. The standard deviation is reported in parentheses.

Roughness parameter	P	GB	F120	F60
Sa	0.02 (0.00)	1.73 (0.01)	0.43 (0.01)	0.44 (0.01)
Sq	0.03 (0.00)	2.29 (0.02)	0.59 (0.02)	0.63 (0.02)
Ssk	-1.83 (0.23)	-0.25 (0.04)	0.17 (0.22)	0.28 (0.14)
Sz	0.57 (0.06)	72.45 (4.84)	18.10 (3.31)	20.69 (2.79)

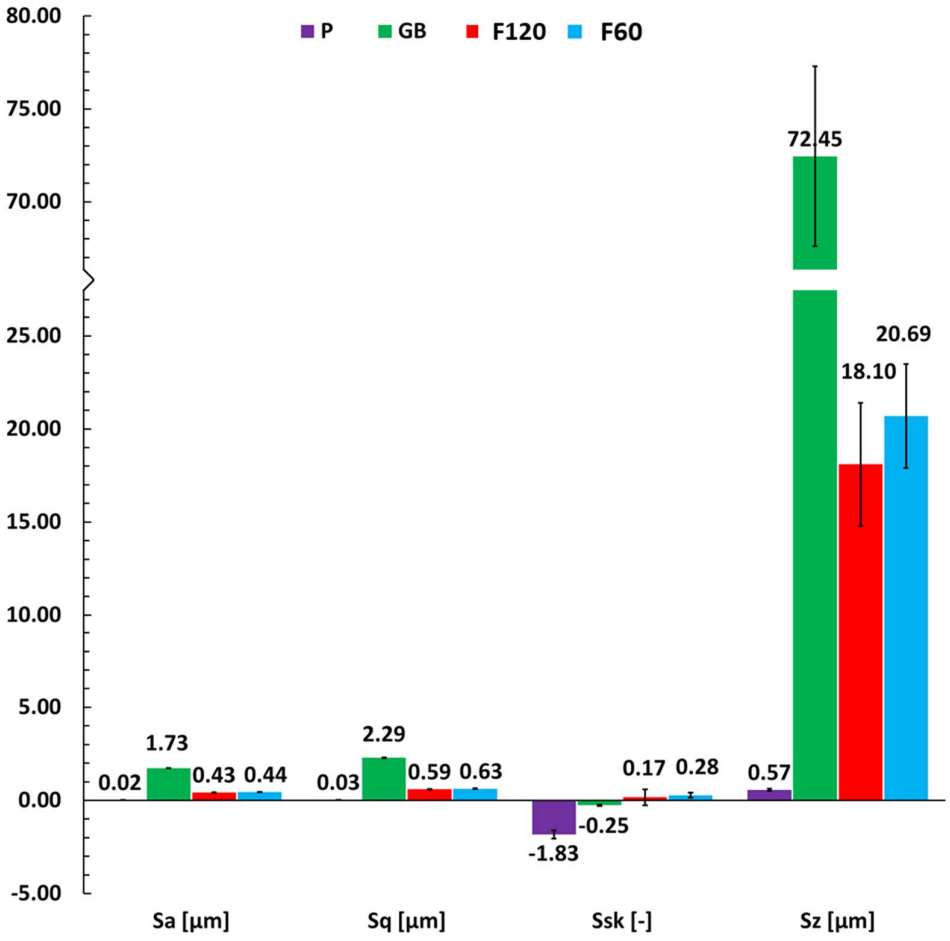

Figure 41. Areal surface height parameters for processed samples: *Sa*, *Sq*, *Ssk*, *Sz*. Error bars represent the standard deviation.

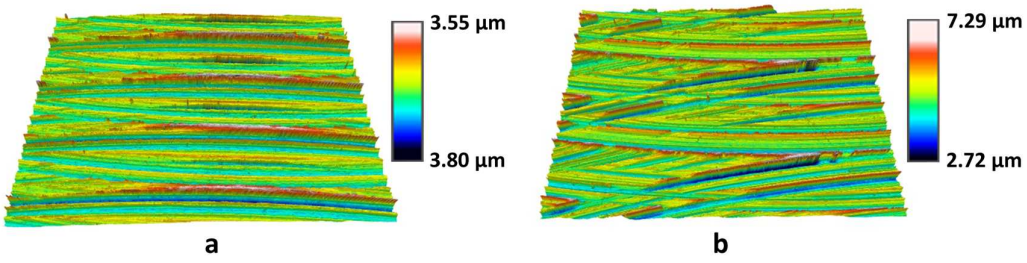

Figure 42. 3D surface maps on similar areas for (a) F120 and (b) F60. Scanned area size: 1.70 mm x 1.30 mm.

To further analyze cell response, it is important to notice that if the feed per tooth *fz* parameter used for the two different milling conditions is computed[2], it amounts to 0.063

[2] $f_z = (\pi \cdot D \cdot V_f) / (Z \cdot V_c \cdot 1000)$

mm/tooth for F120 and 0.126 mm/tooth for F60, determining a different profile shape on which cells can attach (Figure 42).

The values of parameters *Sa* and *Sq* confirm the surface finishing resulting from mechanical processes executed on samples. *Ssk* parameter serves as a confirmation of the presence of higher protruding spikes on GB (*Ssk* -0.25) and F (*Ssk* 0.17 and 0.28 for F120 and F60, respectively) compared to P (*Ssk* -1.83), the latter rich in flat areas and few shallow valleys.

The positive values of *Ssk* reveal that milled samples have higher occurrences of peaks than others. The polished sample P exhibits values of *Ssk* typical of a flat surface and negligible deviations.

Similarly, as reported in [72] and in Case Study II Chapter IV, being processing conditions similar, the composition mapping of P and F showed a negligible presence of oxygen, and the composition of the base alloy was confirmed. From EDX of the GB sample, a great amount of oxygen was detected with Al and O proportions recalling the presence of aluminum oxide from the blasting media, fragmented on impact, and embedded in the base material, as shown in Figure 43.

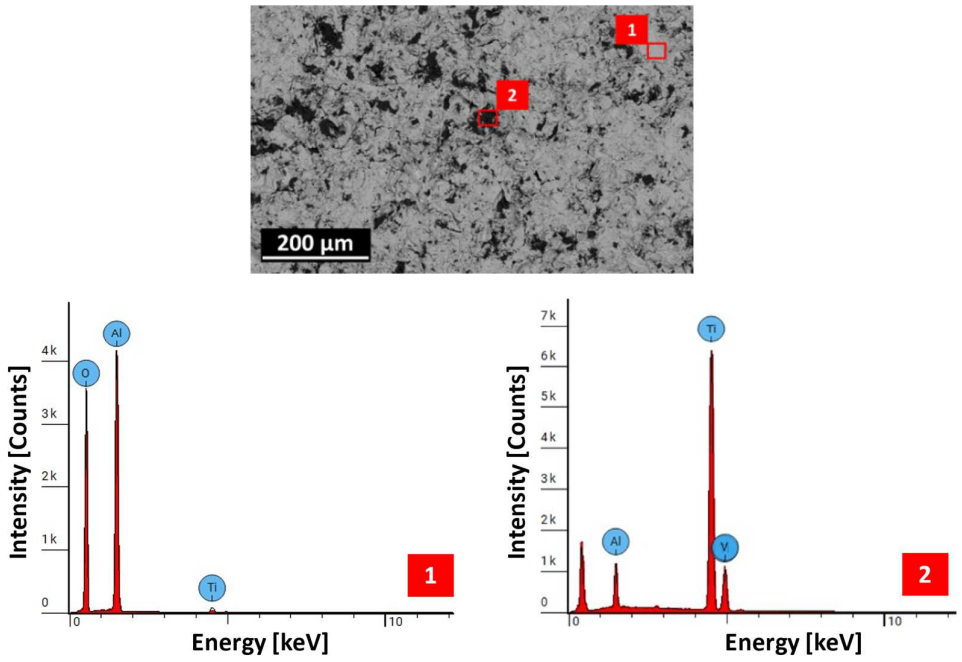

Figure 43. BSD-SEM image of the grit-blasted (GB) sample and EDX results from analyzed areas.

Due to the different surface textures, water contact angle results were significantly different between samples (Figure 44). Compared to P, GB samples showed a 57% higher

contact angle. For F120 and F60 samples the contact angle is +12% and +21% higher than P, respectively.

The above-stated, related to drop behavior and air entrapment when it is placed upon surface asperities might act on cell adhesion mechanisms mediated by proteins as discussed in [9], and affect their overall behavior in contact with the titanium alloy.

As a means of comparison, the typical average roughness of culture plates amounts to a few nanometers [9] while the water contact angle of multiwell plates varies generally between 50° and 80°, for the polystyrene multiwell plates used in this work as control it is reported to be approximately 50° [102].

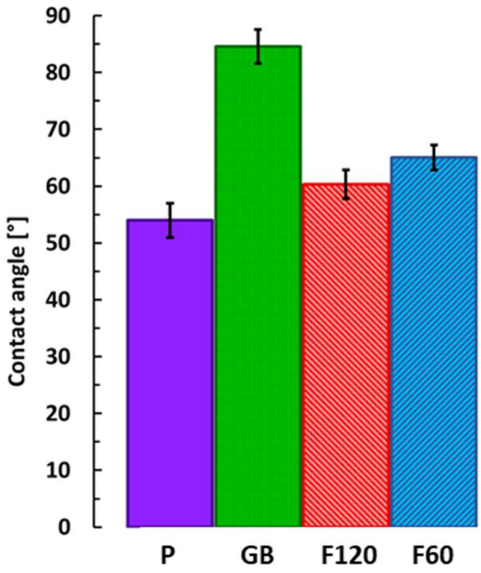

Figure 44. Water contact angle measured on surface-treated *Ti6Al4V* samples.

CELL RESPONSE: PROLIFERATION OF MG63 BONE CELLS

Cell proliferation on the surfaces processed through polishing (P), face milling with finishing parameters (F60 and F120), and grit-blasting (GB) was compared to that obtained on polystyrene cell culture plates with flat bottom and size similar to *Ti6Al4V* samples, given this kind of support is optimized for in vitro culturing of adherent cell lines, such as MG63.

From the absorbance measurement (Table 14), the cell number detected at 48 hours in all samples was higher than the number of seeded cells (> $5.0x10^4$) indicating the ability of MG63 cells to adhere to the different surfaces. The results of the CCK-8 assay show a proliferation on grit blasted (GB) and milled at 60 m/min (F60) samples, with a cell number 13% and 4% higher than the polystyrene plate used as control, respectively. In

contrast, proliferation is slowed down on the polished (P) samples and the ones milled at 120 m/min (F120), with cell numbers 13% and 16% lower than the control, and the worst behavior given by the polished. It can be then deduced that this type of cells prefers the polystyrene over the *Ti6Al4V*, being the roughness of P and F120 comparable.

In contrast, the higher spikiness of M60, and the slightly higher contact angle might have improved the proliferation bringing up the effect of the roughness on cell behavior, given their relative positive difference of 25% in proliferation.

Table 14. Number of viable MG63 cells after 48h incubation, measured through absorbance method.

	P	**GB**	**F120**	**F60**	**Culture Plate**
N° of cells	$5.9 \cdot 10^4$	$7.7 \cdot 10^4$	$5.7 \cdot 10^4$	$7.1 \cdot 10^4$	$6.8 \cdot 10^4$

The above findings on proliferation are partially in accordance with those reported in [74] on bone cells preferring surfaces with an average roughness in the order of a few microns. Indeed, roughening is often reported to produce an enlarged surface area on which cells can adhere and, for the MG63 cell line, some studies confirm this trend [55].

In Figure 45, micrographs of cells cultured on *Ti6Al4V* surfaces are reported paired to magnified 3D surface maps to provide an overview of cell spread and alignment on different topographies.

The micrographs show how cells tend to elongate and align along the texture of the F samples, trying to go around the higher parts of the ridges to link with each other or flatten on top of the ridges (Figure 45f and h). On GB samples they tend to spread and cover the asperities and better link with each other, due also to the smaller asperities compared to F samples, bringing to a consequently higher proliferation (Figure 45b). On P samples no specific direction is followed in cells alignment (Figure 45a). In each case, most of them show a flattened morphology to try and form intimate contact with the surface.

This behavior can be due to asperities and topographical features within the same order of magnitude and thus the cells are forced to orient themselves [101].

The treatments altered the surface and sub-surface properties of the samples at different levels, each in a distinctive fashion. This allows the comparison of extreme behavior both from a strictly mechanical point of view and cell response.

The in vitro tests performed herein provide a first comparison in a simplified model involving osteoblast-like cells. Surface irregularities such as craters or ridges change the interactions with the body environment further tuned by the presence of different

chemical species. In general, the evaluation of cell response to multiple cues is of high complexity since the separation of the effects (morphological, chemical, etc.) is difficult to perform when properties derive from a manufacturing chain.

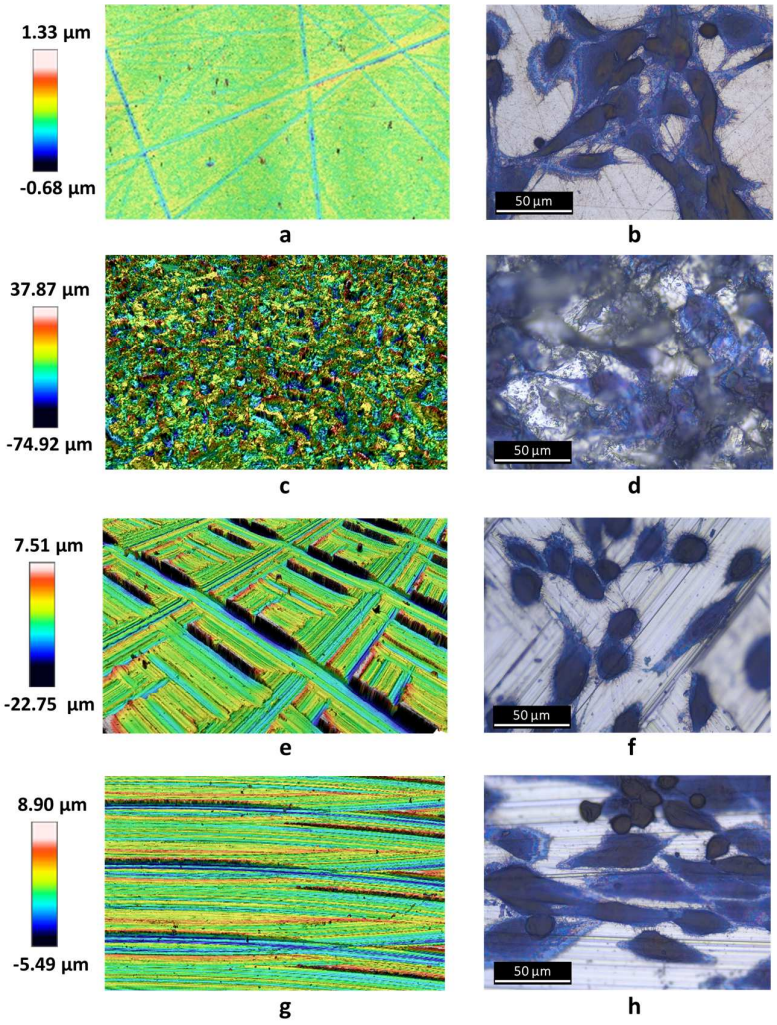

Figure 45. Magnified 3D surface maps coupled with stained adhered cells for samples: (a, b) P, (c, d) GB, (e, f, g, h) F120 on two different areas.

The analysis reported herein provides the guidelines for a wide experimental campaign with a limited quantity of factors and an explicit study of the interactions on a longer inspection interval. In particular, milling process parameters can strongly affect cell behavior and, to a greater extent, have the potential to improve bone-implant interdigitation.

In fact, despite the higher cell proliferation on grit blasted samples, this process can introduce blasting media particles that might be released in the body environment and

need to be removed a priori by chemical treatment. The milling process does not bring such issue, also, it is already part of the manufacturing chain of most of the implantable metallic devices.

BACTERIAL PATHOGENS: ESCHERICHIA COLI K-12

METHODOLOGY

SURFACE PROCESSING OF TI6AL4V

FACE MILLING

The face milling process has been conducted on a CNC Mazak vertical machining center, employing a commercial carbide milling cutter coated with *TiAlSiN*, 16 mm diameter – D (Product code WZF 126486 - Meusburger Georg GmbH & Co KG, Austria) and four cutting edges (Z – number of cutting edges).

Roughing parameters have been chosen as per the manufacturer's advice on optimum conditions for the specific cutting tool: cutting speed V_c = 60 m/min, depth of cut a_p = 0.1 mm, table feed V_f = 250 mm/min (Table 15). Flood lubrication was employed.

A single pass was performed to not introduce surface texture alterations caused by the interaction of multiple passes and a fresh tool was used for each test. To confirm process repeatability and the absence of chattering effects, milling forces were monitored through a six-components piezoelectric dynamometer (Kistler© 9257 - *Kistler*, Switzerland), as shown in the experimental setup for Case Study II in Chapter IV.

Table 15. Experimental test conditions for milling.

Milling parameter	**Roughing**
Cutting speed – V_c [m/min]	60
Depth of cut – a_p [mm]	0.10
Table feed – V_f [m/min]	250
Sample name	**R**

LASER TEXTURING

Ultra-short laser texturing was performed using a picosecond GR laser source (Ekspla Atlantic 5, Lithuania) using a wavelength of 532 nm, a frequency of 100 kHz, and a power of 1.22 W. A grid texture with 50 µm x 50 µm laser pitch was created by performing 100 passes with a laser speed of 2000 mm/min with the aim to study bacterial response on a multi-scale level.

CHARACTERIZATION OF SURFACE PROCESSED TI6AL4V

Each type of processed *Ti6Al4V* sample was cut perpendicularly to the treated face, embedded on a black bakelite mounting resin, and mechanically polished up to 0.5 µm grade. Nano-hardness was probed along the depth below the surface (10 replications for each depth value) through an NH^2 CSM Nanoindentation Platform (*Anton Paar GmbH*, Austria) equipped with a Berkovich diamond tip. Indentations were performed at a maximum load of 50 mN with 10 s of dwell time [29], [91]. For microstructural analysis, the polished samples have been etched employing Kroll's reagent (100 ml H_2O, 3 ml HF, 6 ml HNO_3) and analyzed through an optical microscope.

Furthermore, a Confovis structured light profilometer connected to a Nikon Eclipse LV150N microscope was employed to obtain real surface texture parameters (scanned area size: 0.5 mm x 0.5 mm, four replications).

Additionally, the images of the non-sectioned surfaces were taken using a scanning electron microscope (ESEM Quanta-200 - Fei Oxford Instruments), equipped with the detector for EDS analysis (X-EDS Oxford INCA-350), which was performed on different areas of the samples (area size: 400 µm x 520 µm) to confirm the surfaces' composition. The EDS analysis was combined with µRaman spectroscopy (LabRam - Jobin-Yvon, France) employing a 532 nm wavelength and 40 mW power laser (3 replications for each scan, each of 10 s duration, in the region 100 - 1600 cm^{-1}).

Contact angle (CA) was measured through the sessile drop technique via a Drop Shape Analyzer (DSA30S – *Krüss Scientific*, Germany): drops of 1 µl of distilled water were gently placed on *Ti6Al4V* treated surfaces performing five measurements for each sample and five replications for each processing condition.

CELL CULTURES

Ti6Al4V samples were immersed in absolute ethanol for 24 hours, then they were steam autoclaved and UV dried before cell culture. For the culture experiments, approximately 10^5 cells from an overnight culture in Luria Bertani (LB) broth of Escherichia coli JM109, K-12 strain, were suspended in sterile 1:500 LB/PBS solution and seeded on the sample discs. Cells were cultured at 37°C for 7 days. After incubation, the discs were rinsed, transferred to tubes containing sterile LB/PBS, and vortexed to remove bacteria from the disc surface. Cells were then plated on an LB agar medium and incubated overnight to estimate the number of viable cells. Cells were visualized under the optical microscope after Gram staining.

RESULTS AND DISCUSSION

SURFACE PROPERTIES AFTER PROCESSING

Periodic structures of square protruding areas (Figure 456), about 35 x 35 μm^2, separated by channels less than 10 μm wide were generated on laser textured samples by controlling laser motion (LT). Grid-like structures made up of rectangular ridges with varying size and pitch were manufactured by milling (R) (Figure 46). The typical feature size of R texture is about 70 x 90 μm^2 with a broader dispersion in size and spacing due to the roto-translational motion of the tool. No significant microstructural variations were detected along the depth below the treated surface, apart from the presence of a plastic deformed layer and grain distortion due to plastic deformation processes (Figure 46). No relevant variations in nanoindentation hardness (HIT) (Figure 47) along the cross-section were detected between LT and P samples, with respect to the bulk of as received bar (AR). The core concept of ultrashort laser modification is the reduced impact of the treatment on microstructure and composition, which can be expressed in terms of the reduced affected zone [103] in the order of a few microns below the surface: from the analysis performed, confirmation of the above can be provided as no significant microstructural alterations have been detected along the depth below treated surface, according to the resolution of employed techniques. Strain hardening was detected for R samples (+28% HIT compared to P).

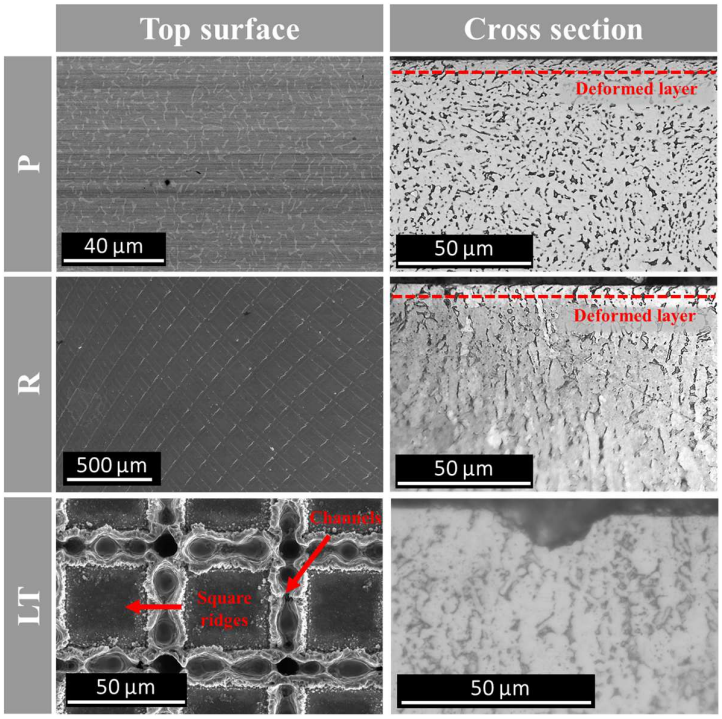

Figure 46. Images of *Ti6Al4V* substrates after processing: SEM images of the worked surface on the left and micrographs of cross-sectioned and etched samples on the right.

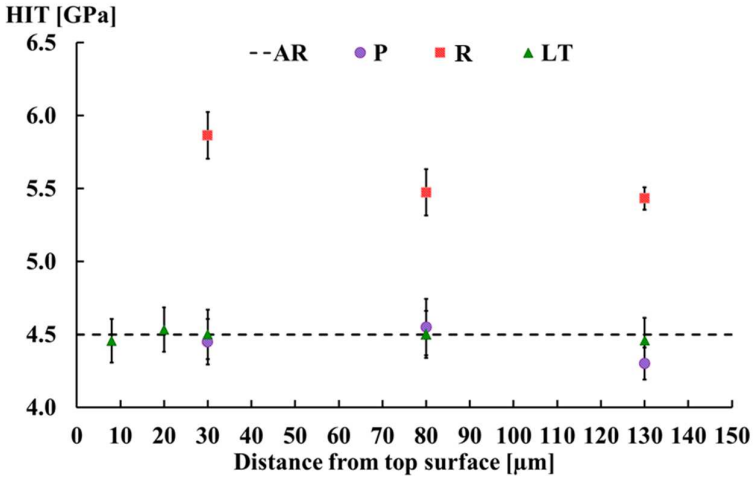

Figure 47. Nano-indentation hardness measured along the cross-section of treated samples compared to as received (AR) bulk hardness. Error bars represent the standard deviation.

Surface morphology after samples processing is shown in Figure 48 and the main parameters are reported in Table 16. As reasonably expected, the lowest and most regular distribution is found for polished ones, followed by the grid-like texture for milling. Surface unevenness finds a maximum for laser textured surfaces, together with the highest maximum height: the maximum height, *Sz,* of surface profiles is 1.51 µm, 6.82 µm, and

25.33 µm for the polished P, milled R, and laser textured LT samples, respectively. The high standard deviation found for polished surfaces in terms of *Sz*, *Sku*, and *Ssk* depended by random imperfections and notched areas that strongly influenced their calculation. On the contrary, the values of *Sa* and *Sq*, less influenced by these random imperfections, showed lower standard deviation, confirming the regular distribution and the low roughness of the polished surface.

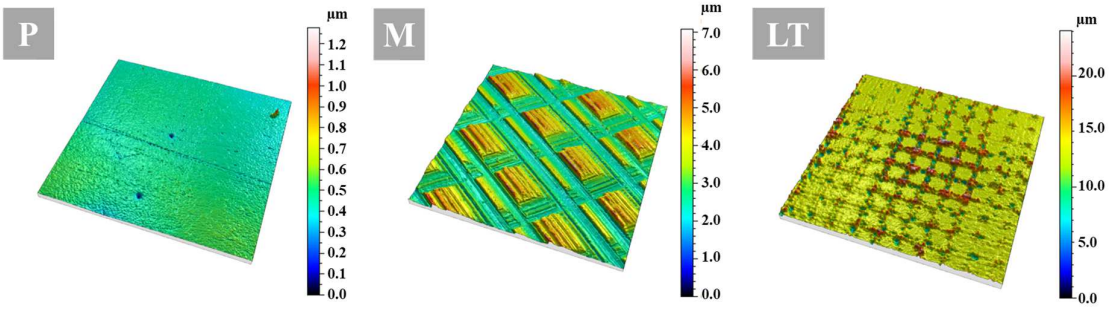

Figure 48. Surface roughness distribution for processed *Ti6Al4V* samples, scanned area size: 0.5 mm x 0.5 mm.

Table 16. Surface roughness parameters for processed samples - height parameters following ISO 25178: *Sa* Arithmetical mean height, *Sz* Maximum height, *Sq* Root Mean Square height, *Ssk* Skewness, *Sku* Kurtosis. The standard deviation is reported in parentheses.

Roughness Parameter	P	R	LT
Sa [µm]	0.05 (0.01)	0.68 (0.04)	1.39 (0.02)
Sz [µm]	1.51 (0.79)	6.82 (0.37)	25.33 (0.91)
Sq [µm]	0.06 (0.01)	0.80 (0.04)	2.33 (0.02)
Ssk [-]	-0.32 (0.66)	0.80 (0.07)	-0.13 (0.09)
Sku [-]	11.18 (12.18)	2.22 (1.00)	6.56 (0.14)

Raman spectroscopy detected the presence of rutile along the edges of the square flat ridges of the LT grid structure, as highlighted in Figure 49 a and b. The Raman spectrum of polished and milled samples shows no signal (Figure 49 a), evidencing the absence of rutile titanium dioxide [95].

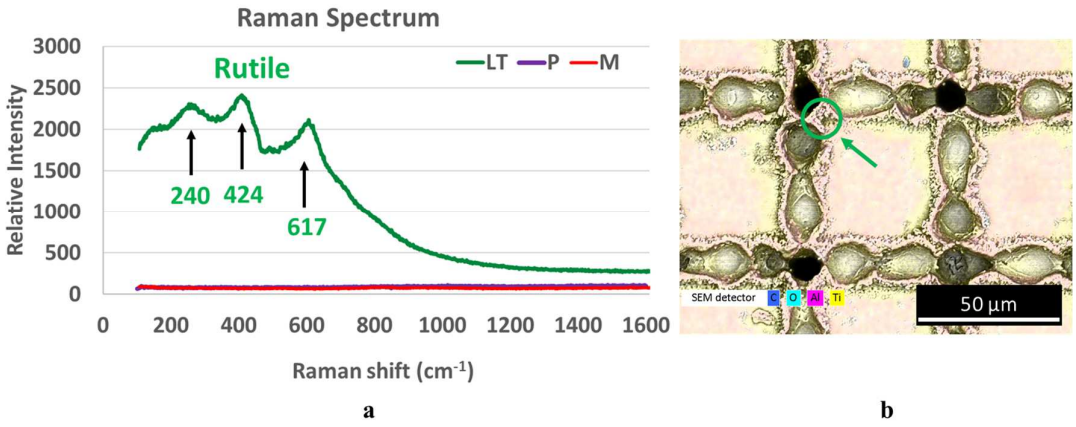

Figure 49. *Ti6Al4V* surface processed samples: (a) Raman spectra of Polished (P), milled (R), and laser textured samples (LT) and (b) EDS of LT sample, highlighted in green the area where rutile was located.

Due to the different surface textures, the water contact angle results are significantly different between samples (Figure 50). The lowest value was found for R samples, obtaining 37°, 30% lower than P. Compared to P, LT samples showed a 41% and 6% higher contact angle along D1 and D2, respectively.

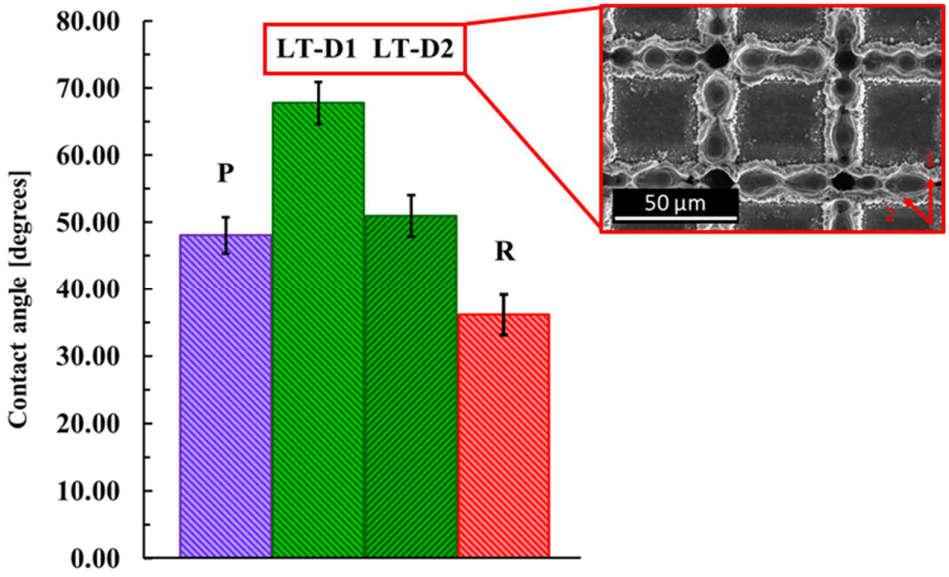

Figure 50. Water contact angle measured on *Ti6Al4V* modified surfaces.

CELL RESPONSE: PROLIFERATION OF ESCHERICHIA COLI

Preliminary culture experiments suggest that surface wettability (Figure 50) correlates with cell proliferation and colonization (Figure 51). The lowest wettability of LT discs

apparently yielded the highest proliferation (+987% compared to P), with an accumulation of bacteria in the channels of the texture. The highest wettability of R discs hindered cell proliferation (-95% compared to P), cells did not adhere thus biofilm formation was prevented. These findings are partially in accordance with the literature [104] but further assessment is necessary to deepen the correlation between bacterial proliferation and colonization with respect to surface texture, contact angle and chemistry of the surfaces.

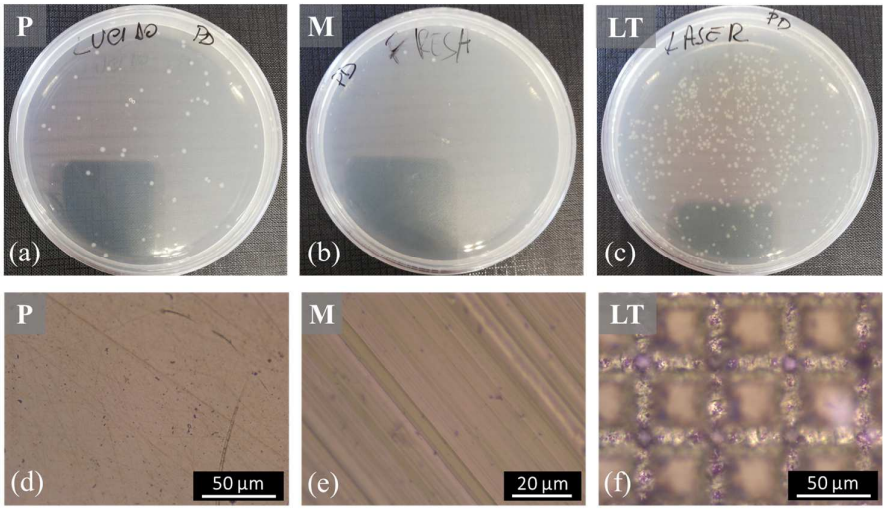

Figure 51. Material interaction with E. Coli: (a)-(c) proliferation, (d)-(f) colonization after Gram staining – bacterial colonies in violet coloration [99].

CONCLUDING REMARKS AND FUTURE WORKS

This dissertation covered a wide range of surface modification techniques applied to the *Ti6Al4V* alloy to address current issues of skeletal fixation devices with a multi-level goal:

1. Modulate the integration of the implants with surrounding bone tissues by acting on surface properties, employing material deformation and removal techniques, and studying the effects on *in vitro* cell response.

The long-term goal of the study on cell response to different surface cues is to locate a processing window for the modulation of the osteointegration of *Ti6Al4V* implants, as this alloy currently keeps on being the clinical standard of care for bone contacting implants.

The work carried out confirmed an influence of surface processing on osteoblast-like cell behavior and paves the way for a broad investigation, to deepen the relationship between bone cells behavior and surface processed implantable material. Future developments will cover a thorough analysis of the studied surface modification techniques, in particular milling, taking into account all the underlying phenomena that correlate surface texture, microstructure, composition, contact angle. Also, a systematic analysis of these complex phenomena using not only osteosarcoma cell lines but also primary cells might increase the translational power of this study.

2. Improve the poor adhesion of coatings made by engineered natural materials like chitosan by: tuning film properties through different deposition techniques, coating composition, and substrate properties through material deformation and removal techniques.

The results on pure chitosan coating suggest the electrophoretic deposition as the deposition technique with better results as regards the resistance of coating. The long-term goal of the study on chitosan is to prevent coatings from early failure during handling and surgical procedures, addressing also its different behavior after exposure to body fluids and performance as drug release support. In future works, a deeper investigation of thickness effects on coating resistance will be included. Further insights will be necessary to a large scale implementation of these processes.

As concerns surface modification applied to *Ti6Al4V* substrates towards improved coating adhesion, the tests demonstrated a strong influence of texture on adhesion parameters (contact angle, scratch test). The best performance is given by grit blasted

substrates while the others show markedly inferior coating adhesion. The overall results contribute to the insight into surface modification of *Ti6Al4V* to improve coating performance by focusing on mechanical and thermal processes, as the current state of the art does not allow to properly correlate adhesion and texture.

On the one side, depending on the type of prosthesis or implant at issue, it will be necessary to determine the forces that the implant must be able to face during usage and on the other side, further research in the medical and biochemical fields should be added to identify the requirements of the films - and thus develop a pass or fail criteria for the coating performance.

3. Preliminary analyze the effect of surface modification techniques on *in vitro* bacterial response.

The impact of surface properties on bacterial adhesion and biofilm formation was preliminary explored and demonstrated. As also confirmed in literature, increased surface roughness enlarges the available surface area for bacterial attachment and proliferation. Furthermore, rough surfaces can offer protection to bacteria against shear forces generated by body fluids. But surface contact angle affects bacterial behavior and correlates in a complex fashion with other surface features. It has been observed that higher roughness positively influences the response of bone cells, leading also to improved implant interdigitation with bone. Consequently, further research is required to find a common solution to address both issues. Investigating combinations of surface properties may offer more meaningful insights into bacterial adhesion and biofilm formation, as surface parameters are inherently interdependent, and different bacterial species show different response: while the potential dominance of some surface properties over others is plausible, it is essential to concurrently assess multiple surface parameters and extrapolate interdependencies.

ACKNOWLEDGMENTS

The author gratefully acknowledges @STAR laboratories, for providing the equipment for indentation and scratch measurements ("PROGETTO STAR 2 – PIR01-00008" – MUR) and Ing. Giuseppe Romeo from Meusburger Georg GmbH & Co KG (Austria) for providing advice on milling operations.

LIST OF FIGURES

Figure 49. *Ti6Al4V* surface processed samples: (a) Raman spectra of Polished (P), milled (R), and laser textured samples (LT) and (b) EDS of LT sample, highlighted in green the area where rutile was located.

Figure 50. Water contact angle measured on *Ti6Al4V* modified surfaces.

Figure 51. Material interaction with E. Coli: (a)-(c) proliferation, (d)-(f) colonization after Gram staining – bacterial colonies in violet coloration [99].

LIST OF TABLES

Table 16. Surface roughness parameters for processed samples - height parameters following ISO 25178: *Sa* Arithmetical mean height, *Sz* Maximum height, *Sq* Root Mean Square height, *Ssk* Skewness, *Sku* Kurtosis. The standard deviation is reported in parentheses.

REFERENCES

[1] World Organization Health, Health Promotion Glossary of Terms 2021. (2021).

[2] Pabinger, C., H. Lothaller, N. Portner, A. Geissler, Projections of hip arthroplasty in OECD countries up to 2050, HIP Int., 28(5), 498–506, (2018), doi: 10.1177/1120700018757940.

[3] Henkel, J. *et al.*, Bone Regeneration Based on Tissue Engineering Conceptions — A 21st Century Perspective, Bone Res., 1(3), 216–248, (2013), doi: 10.4248/BR201303002.

[4] Zanetti, E. M. *et al.*, Additive Manufacturing of Metal Load-Bearing Implants 1: Geometric Accuracy and Mechanical Challenges, Chemie Ing. Tech., 96, (4), (2024) (In Press). doi: https://doi.org/10.1002/cite.202300171.

[5] Zanetti, E. M. *et al.*, Additive Manufacturing of Metal Load-Bearing Implants 2: Surface Modification and Clinical Challenges, Chemie Ing. Tech., 96, (4), (2024) (In Press). doi: https://doi.org/10.1002/cite.202300172.

[6] K-Synth Srl, Bibliometrix: an R-tool for comprehensive science mapping analysis (Version 4.1.2), *2023*. https://www.bibliometrix.org.

[7] Aria, M., C. Cuccurullo, bibliometrix: An R-tool for comprehensive science mapping analysis, J. Informetr., 11(4), 959–975, (2017), doi: 10.1016/j.joi.2017.08.007.

[8] Williams, D. F., Definitions in Biomaterials, in Proceedings of a Consensus Conference of the European Society for Biomaterials (Chester, England, March 3-5 1986), 4, New York: Elsevier, (1987).

[9] Ratner, B. D., A. S. Hoffman, F. J. Schoen, J. E. Lemons, Biomaterials science: an introduction to materials in medicine, Third Ed. (2013).

[10] ISO 10993-1:2018 Biological evaluation of medical devices: Part 1: Evaluation and testing within a risk management process, (2018).

[11] Study Group 1 of the Global Harmonization Task Force, Definition of the Terms “Medical Device” and “In Vitro Diagnostic (IVD) Medical Device”. Global Harmonization Task Force (revision of GHTF/SG1/N29:2005), (2012).

[12] Word Health Organization, What are medical devices?, 2023. https://www.who.int/teams/health-product-policy-and-standards/assistive-and-medical-technology/medical-devices (accessed 2023).

[13] Biomatlante SAS, Osteotwin Interference Screws, 2023. https://biomatlante.com/en/products/osteotwin (accessed 2023).

[14] Ansys Granta, Material property charts, 2024. https://www.grantadesign.com/education/students/charts/ (accessed 2024).

[15] McEntire, B. J., B. S. Bal, M. N. Rahaman, J. Chevalier, G. Pezzotti, Ceramics and ceramic coatings in orthopaedics, J. Eur. Ceram. Soc., 35(16), 4327–4369, (2015), doi: 10.1016/j.jeurceramsoc.2015.07.034.

[16] Ratner, B. D., A. S. Hoffman, F. J. Schoen, J. E. Lemons, Eds., Biomaterials Science: An Introduction to Materials in Medicine, Third Edit. Academic Press, (2013).

[17] Narayan, R. J., Ed., ASM Handbook - Volume 23: Materials for Medical Devices. ASM

International, (2012).

[18] Wagner, W. R., S. E. Sakiyama-Elbert, G. Zhang, M. J. Yaszemski, Biomaterials Science: An Introduction to Materials in Medicine. (2020).

[19] Susan, D. *et al.*, Confirming the Composition of Shape Memory Alloys by Microstructural Characterization, 2014. https://www.osti.gov (accessed 2014).

[20] Chmielewska, A., D. Dean, The role of stiffness-matching in avoiding stress shielding-induced bone loss and stress concentration-induced skeletal reconstruction device failure, Acta Biomater., 173, 51–65, (2024), doi: 10.1016/j.actbio.2023.11.011.

[21] Donachie, M. J., Titanium - A Technical Guide, Second Ed. ASM International, (2000).

[22] Brunette, D. M., P. Tengvall, M. Textor, P. Thomsen, Titanium in Medicine: Material Science, Surface Science, Engineering, Biological Responses and Medical Applications., (3). Springer-Verlag Berlin Heidelberg GmbH, (2001).

[23] Leedy, M. R., H. J. Martin, P. A. Norowski, J. A. Jennings, W. O. Haggard, J. D. Bumgardner, Use of chitosan as a bioactive implant coating for bone-implant applications, Adv. Polym. Sci., 244(1), 129–166, (2011), doi: 10.1007/12_2011_115.

[24] Hallmann, L., M. D. Gerngroß, Chitosan and its application in dental implantology, J. Stomatol. Oral Maxillofac. Surg., 123(6), e701–e707, (2022), doi: 10.1016/j.jormas.2022.02.006.

[25] Chatterjee, R., M. Maity, M. S. Hasnain, A. K. Nayak, Chitosan: source, chemistry, and properties, in Chitosan in Drug Delivery, Elsevier, (2022), 1–22.

[26] Bumgardner, J. D. *et al.*, Chitosan: Potential use as a bioactive coating for orthopaedic and craniofacial/dental implants, J. Biomater. Sci. Polym. Ed., 14(5), 423–438, (2003), doi: 10.1163/156856203766652048.

[27] Greene, A. H., J. D. Bumgardner, Y. Yang, J. Moseley, W. O. Haggard, Chitosan-coated stainless steel screws for fixation in contaminated fractures, Clin. Orthop. Relat. Res., 466(7), 1699–1704, (2008), doi: 10.1007/s11999-008-0269-5.

[28] Sergi, R., D. Bellucci, V. Cannillo, A review of bioactive glass/natural polymer composites: State of the art, Materials (Basel)., 13(23), 1–38, (2020), doi: 10.3390/ma13235560.

[29] Rotella, G., M. Alfano, S. Candamano, Surface modification of Ti6Al4V alloy by pulsed Yb-laser irradiation for enhanced adhesive bonding, CIRP Ann. - Manuf. Technol., 64(1), 527–530, (2015), doi: 10.1016/j.cirp.2015.04.042.

[30] Yao, Z., T. H. Lin, J. Pajarinen, T. Sato, S. Goodman, Host Response to Biomaterials: The Impact of Host Response on Biomaterial Selection. Elsevier Inc., (2015).

[31] Jain, S., B. A. Haughton, C. Brew, Intramedullary fixation of distal fibular fractures: a systematic review of clinical and functional outcomes, J. Orthop. Traumatol., 15(4), 245–254, (2014), doi: 10.1007/s10195-014-0320-0.

[32] Jawahir, I. S. *et al.*, Surface integrity in material removal processes: Recent advances, CIRP Ann. - Manuf. Technol., 60(2), 603–626, (2011), doi: 10.1016/j.cirp.2011.05.002.

[33] Ashby, M. F., D. R. H. Jones, Engineering Materials 1: An Introduction to Properties, Applications, and Design, Fourth Ed. Elsevier B.H., (2012).

[34] Chang, H.-I., Y. Wang, Cell Responses to Surface and Architecture of Tissue Engineering Scaffolds, Regen. Med. Tissue Eng. - Cells Biomater., (2011), doi: 10.5772/21983.

[35] Zheng, S. *et al.*, Implication of Surface Properties, Bacterial Motility, and Hydrodynamic Conditions on Bacterial Surface Sensing and Their Initial Adhesion, Front. Bioeng. Biotechnol., 9(February), 1–22, (2021), doi: 10.3389/fbioe.2021.643722.

[36] Menčík, J., Mechanics of Components with Treated or Coated Surfaces, First Ed. Springer, Dordrecht, (1996).

[37] Sanguedolce, M., G. Rotella, L. Filice, F. Micari, Ti6Al4V Surface Modification Techniques to Modulate Bone Cell Response: A Review, Procedia CIRP, 110(C), 41–46, (2022), doi: 10.1016/j.procir.2022.06.010.

[38] Kalpakjian, S., Manufacturing Engineering & Technology, Sixth Edit. Prentice Hall, (2009).

[39] Szymczyk-Ziółkowska, P. *et al.*, The impact of ebm-manufactured ti6al4v eli alloy surface modifications on cytotoxicity toward eukaryotic cells and microbial biofilm formation, Materials (Basel)., 13(12), 1–21, (2020), doi: 10.3390/ma13122822.

[40] Abar, B. *et al.*, Effect of surface topography on in vitro osteoblast function and mechanical performance of 3D printed titanium, J. Biomed. Mater. Res. - Part A, 109(10), 1792–1802, (2021), doi: 10.1002/jbm.a.37172.

[41] Hayes, J. S., U. Seidenglanz, A. I. Pearce, S. G. Pearce, C. W. Archer, R. G. Richards, Surface polishing positively influences ease of plate and screw removal, Eur. Cells Mater., 19(0), 117–126, (2010), doi: 10.22203/eCM.v019a12.

[42] Yang, Y., T. Zhang, M. Jiang, X. Yin, X. Luo, H. Sun, Effect of the immune responses induced by implants in a integrated three-dimensional micro-nano topography on osseointegration, J. Biomed. Mater. Res. - Part A, 109(8), 1429–1440, (2021), doi: 10.1002/jbm.a.37134.

[43] Vilardell, A. M., P. Krakhmalev, I. Yadroitsava, I. Yadroitsev, N. Garcia-Giralt, In vitro characterization of in situ alloyed Ti6Al4V(ELI)-3 at.% Cu obtained by laser powder bed fusion, Materials (Basel)., 14(23), (2021), doi: 10.3390/ma14237260.

[44] Nikolova, M. . P., M. Ormanova, V. Nikolova, M. D. Apostolova, Electrochemical, tribological and biocompatible performance of electron beam modified and coated ti6al4v alloy, Int. J. Mol. Sci., 22(12), (2021), doi: 10.3390/ijms22126369.

[45] Bayrak, Ö., H. Ghahramanzadeh Asl, A. Ak, Protein adsorption, cell viability and corrosion properties of Ti6Al4V alloy treated by plasma oxidation and anodic oxidation, Int. J. Miner. Metall. Mater., 27(9), 1269–1280, (2020), doi: 10.1007/s12613-020-2020-5.

[46] Berger, M. B., K. B. Bosh, D. J. Cohen, B. D. Boyan, Z. Schwartz, Benchtop plasma treatment of titanium surfaces enhances cell response, Dent. Mater., 37(4), 690–700, (2021), doi: 10.1016/j.dental.2021.01.026.

[47] Schulze, V., F. Bleicher, P. Groche, Y. B. Guo, Y. S. Pyun, Surface modification by machine hammer peening and burnishing, CIRP Ann. - Manuf. Technol., 65(2), 809–832, (2016), doi: 10.1016/j.cirp.2016.05.005.

[48] Li, B., Y. Shen, W. Hu, L. Luo, Surface modification of Ti-6Al-4V alloy via friction-stir processing: Microstructure evolution and dry sliding wear performance, Surf. Coatings Technol., 239, 160–170, (2014), doi: 10.1016/j.surfcoat.2013.11.035.

[49] Hoseini, M., P. Bocher, A. Shahryari, F. Azari, J. A. Szpunar, H. Vali, On the importance of crystallographic texture in the biocompatibility of titanium based substrate, J. Biomed. Mater. Res. - Part A, 102(10), 3631–3638, (2014), doi: 10.1002/jbm.a.35028.

[50] Huo, W. T., L. Z. Zhao, W. Zhang, J. W. Lu, Y. Q. Zhao, Y. S. Zhang, In vitro corrosion behavior and biocompatibility of nanostructured Ti6Al4V, Mater. Sci. Eng. C, 92(June), 268–279, (2018), doi: 10.1016/j.msec.2018.06.061.

[51] Achtelik-franczak, A., J. Dobrza, Application Solid Laser-Sintered or Machined Ti6Al4V Alloy in Manufacturing of Dental Implants and Dental Prosthetic Restorations According to Dentistry 4.0 Concept, (2020).

[52] Jörg, F., K. A. Betül, M. Heiner, K. Gerhard, B. R. Erwin, Effects of ti6al4v surfaces manufactured through precision centrifugal casting and modified by calcium and phosphorus ion implantation on human osteoblasts, Metals (Basel)., 10(12), 1–20, (2020), doi: 10.3390/met10121681.

[53] Yaar, H., B. Ekmekci, The effect of micro and nano hydroxyapatite powder on biocompatibility and surface integrity of Ti6Al4V (ELI) in powder mixed electrical discharge machining, Surf. Topogr. Metrol. Prop., 9, (2021).

[54] Schnell, G., S. Staehlke, U. Duenow, J. Barbara Nebe, H. Seitz, Femtosecond laser nano/micro textured Ti6Al4V surfaces-effect on wetting and MG-63 cell adhesion, Materials (Basel)., 12(13), (2019), doi: 10.3390/ma12132210.

[55] Rafiee, K., H. Naffakh-Moosavy, E. Tamjid, The effect of laser frequency on roughness, microstructure, cell viability and attachment of Ti6Al4V alloy, Mater. Sci. Eng. C, 109(December 2019), (2020), doi: 10.1016/j.msec.2020.110637.

[56] Kalentics, N., E. Boillat, P. Peyre, S. Ćirić-Kostić, N. Bogojević, R. E. Logé, Tailoring residual stress profile of Selective Laser Melted parts by Laser Shock Peening, *Additive Manufacturing*, 16. 90–97, 2017, doi: 10.1016/j.addma.2017.05.008.

[57] Alemán-Domínguez, M. E. *et al.*, Comparison of low-pressure oxygen plasma and chemical treatments for surface modifications of Ti6Al4V, Bio-Design Manuf., 2(2), 65–75, (2019), doi: 10.1007/s42242-019-00036-9.

[58] Hasan, A., L. M. Pandey, Surface modification of Ti6Al4V by forming hybrid self-assembled monolayers and its effect on collagen-I adsorption, osteoblast adhesion and integrin expression, Appl. Surf. Sci., 505(November 2019), 144611, (2020), doi: 10.1016/j.apsusc.2019.144611.

[59] Zhang, T., X. Zhang, M. Mao, J. Li, T. Wei, H. Sun, Chitosan/hydroxyapatite composite coatings on porous Ti6Al4V titanium implants: In vitro and in vivo studies, J. Periodontal Implant Sci., 50(6), 392–405, (2020), doi: 10.5051/jpis.1905680284.

[60] Guan, S., M. Qi, C. Wang, S. Wang, W. Wang, Enhanced cytocompatibility of Ti6Al4V alloy through selective removal of Al and V from the hierarchical micro-arc oxidation coating, Appl. Surf. Sci., 541(September 2020), 148547, (2021), doi: 10.1016/j.apsusc.2020.148547.

[61] Huang, L. *et al.*, Comparative Study on 3D Printed Ti6Al4V Scaffolds with Surface Modifications Using Hydrothermal Treatment and Microarc Oxidation to Enhance Osteogenic Activity, ACS Omega, 6(2), 1465–1476, (2021), doi: 10.1021/acsomega.0c05191.

[62] Avcu, E., F. E. Baştan, H. Z. Abdullah, M. A. U. Rehman, Y. Y. Avcu, A. R. Boccaccini, Electrophoretic deposition of chitosan-based composite coatings for biomedical applications: A review, Prog. Mater. Sci., 103, 69–108, (2019), doi: 10.1016/j.pmatsci.2019.01.001.

[63] Frederichi, D., M. H. N. O. Scaliante, R. Bergamasco, Structured photocatalytic systems: photocatalytic coatings on low-cost structures for treatment of water contaminated with

micropollutants—a short review, Environ. Sci. Pollut. Res., 28(19), 23610–23633, (2021), doi: 10.1007/s11356-020-10022-9.

[64] Ramos Avilez, H. V., D. A. Castilla Casadiego, A. L. Vega Avila, O. J. Perales Perez, J. Almodovar, Production of chitosan coatings on metal and ceramic biomaterials, in Chitosan Based Biomaterials Volume 1, Elsevier, (2017), 255–293.

[65] Schneller, T., R. Waser, M. Kosec, D. Payne, Eds., Chemical solution deposition of functional oxide thin films, in Chemical Solution Deposition of Functional Oxide Thin Films, Vienna: Springer, (2014), 1–796.

[66] Sonia, T. A., C. P. Sharma, Experimental techniques involved in the development of oral insulin carriers, in Oral Delivery of Insulin, Elsevier, (2014), 169–217.

[67] Browning, R. L., G. T. Lim, A. Moyse, H. J. Sue, H. Chen, J. D. Earls, Quantitative evaluation of scratch resistance of polymeric coatings based on a standardized progressive load scratch test, Surf. Coatings Technol., 201(6), 2970–2976, (2006), doi: 10.1016/j.surfcoat.2006.06.007.

[68] Sangermano, M., M. Messori, Scratch resistance enhancement of polymer coatings, Macromol. Mater. Eng., 295(7), 603–612, (2010), doi: 10.1002/mame.201000025.

[69] Holmberg, K., A. Laukkanen, H. Ronkainen, K. Wallin, S. Varjus, J. Koskinen, Tribological contact analysis of a rigid ball sliding on a hard coated surface. Part I: Modelling stresses and strains, Surf. Coatings Technol., 200(12–13), 3793–3809, (2006), doi: 10.1016/j.surfcoat.2005.03.040.

[70] Wirasate, S., F. J. Boerio, Effect of Adhesion, Film Thickness, and Substrate Hardness on the Scratch Behavior of Poly(carbonate) Films, J. Adhes., 81(5), 509–528, (2005), doi: 10.1080/00218460590944954.

[71] ASTM International, ASTM D7027-20 - Standard Test Method for Evaluation of Scratch Resistance of Polymeric Coatings and Plastics Using an Instrumented Scratch Machine, (2020), doi: 10.1520/D7027-20.

[72] Sanguedolce, M. *et al.*, Effects of Ti6Al4V mechanical and thermal surface modification on the adhesion of a chitosan - bioactive glass coating, Int. J. Adv. Manuf. Technol., 125, 4621–4629, (2023), doi: 10.1007/s00170-023-10943-y.

[73] Nanovea Inc., Understanding Coating Failures Using Scratch Testing, 2013. https://nanovea.com/ (accessed 2013).

[74] Stich, T., F. Alagboso, T. Křenek, T. Kovàřík, V. Alt, D. Denitsa, Implant-bone-interface: Reviewing the impact of titanium surface modifications on osteogenic processes in vitro and in vivo, Bioeng. Transl. Med., 7(1:e10239), (2022), doi: https://doi.org/10.1002/btm2.10239.

[75] Zheng, S. *et al.*, Implication of Surface Properties, Bacterial Motility, and Hydrodynamic Conditions on Bacterial Surface Sensing and Their Initial Adhesion, Front. Bioeng. Biotechnol., 9(February), 1–22, (2021), doi: 10.3389/fbioe.2021.643722.

[76] Jang, Y. *et al.*, Inhibition of Bacterial Adhesion on Nanotextured Stainless Steel 316L by Electrochemical Etching, ACS Biomater. Sci. Eng., 4(1), 90–97, (2018), doi: 10.1021/acsbiomaterials.7b00544.

[77] Leedy, M. R., H. J. Martin, P. A. Norowski, J. A. Jennings, W. O. Haggard, J. D. Bumgardner, Use of chitosan as a bioactive implant coating for bone-implant applications, Adv. Polym. Sci., 244(1), 129–166, (2011), doi: 10.1007/12_2011_115.

[78] Kazi, G. A. S., T. Yamanaka, Y. Osamu, Chitosan Coating an Efficient Approach to Improve the Substrate Surface for In Vitro Culture System, J. Electrochem. Soc., 166(9), B3025–B3030, (2019), doi: 10.1149/2.0051909jes.

[79] Laska, A., M. Bartmański, Parameters of the Electrophoretic Deposition Process and Its Influence on the Morphology of Hydroxyapatite Coatings. Review, Inżynieria Mater., 1(1), 20–25, (2020), doi: 10.15199/28.2020.1.3.

[80] Heise, S. *et al.*, Electrophoretic deposition and characterization of chitosan/bioactive glass composite coatings on Mg alloy substrates, Electrochim. Acta, 232, 456–464, (2017), doi: 10.1016/j.electacta.2017.02.081.

[81] Simchi, A., F. Pishbin, A. R. Boccaccini, Electrophoretic deposition of chitosan, Mater. Lett., 63(26), 2253–2256, (2009), doi: 10.1016/j.matlet.2009.07.046.

[82] Barnes, D., S. Johnson, R. Snell, S. Best, Using scratch testing to measure the adhesion strength of calcium phosphate coatings applied to poly(carbonate urethane) substrates, J. Mech. Behav. Biomed. Mater., 6, 128–138, (2012), doi: 10.1016/j.jmbbm.2011.10.010.

[83] Mishra, S. K., S. Kannan, Development, mechanical evaluation and surface characteristics of chitosan/polyvinyl alcohol based polymer composite coatings on titanium metal, J. Mech. Behav. Biomed. Mater., 40, 314–324, (2014), doi: 10.1016/j.jmbbm.2014.08.014.

[84] Ramos Avilez, H. V., D. A. Castilla Casadiego, A. L. Vega Avila, O. J. Perales Perez, J. Almodovar, Production of chitosan coatings on metal and ceramic biomaterials, 1. Elsevier, (2017).

[85] Sanguedolce, M., M. Latino, G. Coppola, On the Polymeric Coating Deposition Techniques to Increase Body Acceptance and Allow Drug Delivery in Smart Bio-devices, Procedia Comput. Sci., (4th International Conference on Industry 4.0 and Smart Manufacturing (ISM 2023)), (2023).

[86] Guo, Y., J. Guan, H. Peng, X. Shu, L. Chen, H. Guo, Tightly adhered silk fibroin coatings on Ti6Al4V biometals for improved wettability and compatible mechanical properties, Mater. Des., 175, 107825, (2019), doi: 10.1016/j.matdes.2019.107825.

[87] Gupta, V., B. Singh, R. K. Mishra, Machining of titanium and titanium alloys by electric discharge machining process: A review, Int. J. Mach. Mach. Mater., 22(2), 99–121, (2020), doi: 10.1504/IJMMM.2020.105661.

[88] Caridade, S. G., E. G. Merino, N. M. Alves, V. de Z. Bermudez, A. R. Boccaccini, J. F. Mano, Chitosan membranes containing micro or nano-size bioactive glass particles: Evolution of biomineralization followed by in situ dynamic mechanical analysis, J. Mech. Behav. Biomed. Mater., 20, 173–183, (2013), doi: 10.1016/j.jmbbm.2012.11.012.

[89] Mota, J. *et al.*, Chitosan/bioactive glass nanoparticle composite membranes for periodontal regeneration, Acta Biomater., 8(11), 4173–4180, (2012), doi: 10.1016/j.actbio.2012.06.040.

[90] Caridade, S. G., E. G. Merino, G. M. Luz, N. M. Alves, J. F. Mano, Bioactivity and viscoelastic characterization in physiological simulated conditions of chitosan/Bioglass® composite membranes, Mater. Sci. Forum, 636–637, 26–30, (2010), doi: 10.4028/www.scientific.net/MSF.636-637.26.

[91] Lucca, D. A., K. Herrmann, M. J. Klopfstein, Nanoindentation: Measuring methods and applications, CIRP Ann. - Manuf. Technol., 59(2), 803–819, (2010), doi: 10.1016/j.cirp.2010.05.009.

[92] ISO 25178-2: 2012. BSI Standards Publication Geometrical product specifications (GPS

) — Surface texture : Areal Part 2 : Terms , definitions and surface texture parameters. BSI Standards, 2012.

[93] ISO 25178-3: 2012. Geometrical product specifications (GPS) — Surface texture : Areal Part 3 : Specification operators. BSI Standards, 2012.

[94] Sensofar Metrology (Spain), SensoVIEW Software version: 1.9 - User Manual. .

[95] Frank, O., M. Zukalova, B. Laskova, J. Kürti, J. Koltai, L. Kavan, Raman spectra of titanium dioxide (anatase, rutile) with identified oxygen isotopes (16, 17, 18), Phys. Chem. Chem. Phys., 14(42), 14567–14572, (2012), doi: 10.1039/c2cp42763j.

[96] Krishnan, S. V. *et al.*, Chemical synthesis and characterization of nano alumina, nano composite of carbon-alumina and their comparative studies, Zeitschrift fur Phys. Chemie, 232(12), 1827–1842, (2018), doi: 10.1515/zpch-2017-1075.

[97] Aminzadeh, A., Excitation frequency dependence and fluorescence in the Raman spectra of Al2O3, Appl. Spectrosc., 51(6), 817–819, (1997), doi: 10.1366/0003702971941331.

[98] Rahman, S. S., M. Z. I. Ashraf, M. S. Bashar, M. Kamruzzaman, A. K. M. Nurul Amin, M. M. Hossain, Crystallinity, surface morphology, and chemical composition of the recast layer and rutile-TiO2 formation on Ti-6Al-4V ELI by wire-EDM to enhance biocompatibility, Int. J. Adv. Manuf. Technol., 93(9–12), 3285–3296, (2017), doi: 10.1007/s00170-017-0772-5.

[99] Sanguedolce, M. *et al.*, Texturing Ti6Al4V surfaces with hierarchical structures on the micro/nano scale by ultra-short laser: effect on pathogen adhesion and colonization, 32nd Annu. Conf. Eur. Soc. Biomater. Bordeaux, (2022).

[100] Lutey, A. H. A. *et al.*, Towards laser-textured antibacterial surfaces, Sci. Rep., 8(1), 1–10, (2018), doi: 10.1038/s41598-018-28454-2.

[101] Sola-Ruiz, M. F., C. Perez-Martinez, C. Labaig-Rueda, C. Carda, J. J. Martín De Llano, Behavior of human osteoblast cells cultured on titanium discs in relation to surface roughness and presence of melatonin, Int. J. Mol. Sci., 18(4), (2017), doi: 10.3390/ijms18040823.

[102] Zeiger, A. S., B. Hinton, K. J. Van Vliet, Why the dish makes a difference: Quantitative comparison of polystyrene culture surfaces, Acta Biomater., 9(7), 7354–7361, (2013), doi: 10.1016/j.actbio.2013.02.035.

[103] Kong, M. C., J. Wang, Surface quality analysis of titanium and nickel-based alloys using picosecond laser, Procedia CIRP, 13, 417–422, (2014), doi: 10.1016/j.procir.2014.04.071.

[104] Lorenzetti, M. *et al.*, The influence of surface modification on bacterial adhesion to titanium-based substrates, ACS Appl. Mater. Interfaces, 7(3), 1644–1651, (2015), doi: 10.1021/am507148n.